OPTIMIZATION FOR POWER SYSTEM PLANNING AND STATE ESTIMATION WITH STOCHASTIC EV USER BEHAVIOR

NIE YONGQUAN

Ph.D

The Hong Kong Polytechnic University

2017

The Hong Kong Polytechnic University
Department of Electrical Engineering

OPTIMIZATION FOR POWER SYSTEM PLANNING AND STATE ESTIMATION WITH STOCHASTIC EV USER BEHAVIOR

NIE YONGQUAN

A thesis submitted in partial fulfillment of the requirements for the Degree of Doctor of Philosophy

July 2016

CERTIFICATE OF ORIGINALITY

I hereby declare that this thesis is my own work and that, to the best of my knowledge and belief, it reproduces no material previously published or written, nor material which has been accepted for the award of any other degree or diploma, except where due acknowledgement has been made in the text.

_______________________(Signed)

_____NIE Yongquan_____(Name of student)

To my family

Abstract

Environmental protection has become a global priority as people are getting increasingly aware of the importance of sustainable development. Replacing traditional internal combustion engine (ICE) vehicles with electric vehicles (EVs) is regarded as one effective way to reduce hazardous particulate matter and greenhouse gas emissions. Under the green grid paradigm, the redesigned load forecast, system state estimation and system planning methods proposed in this thesis will play an important role in monitoring, control and expansion of the future smart grid considering the increasing EV penetration with stochastic user behavior.

The stochasticity of EV user behavior mainly lies in two aspects: EV travel behavior and EV charging behavior. EV can be regarded as a kind of mobile load and this thesis first provides a general model for simulating the daily routes with multiple travel purposes considering the geographical and temporal distribution of EVs. The EV charging demand at each location is estimated by the distance traveled earlier and the distance to be traveled for the next trip. This thesis strives to make a more practical forecast of EV charging demand with realistic model and data because a reasonable forecast is the cornerstone for monitoring, control and planning of the power systems.

System monitoring is of great importance in providing useful information to regulators for fault detection and control scheme design. Compared to the complete data of travel surveys in various countries, there is no such credible statistics on EV charging preferences. As the aggregated stochastic charging power puts additional pressure to the peak load, the importance of having an accurate system state estimation (SSE) arises as the EV charging behavior can only be estimated in a range. In this thesis, an effective SSE based on quasi-

Newton (QN) method and Armijo line search (ALS) is proposed to obtain a faster, more accurate and yet more reliable state estimation under potential forecast and measurement errors. The estimation accuracy and computation time required are compared with the widespread weighted least square (WLS) method and extended Kalman Filter (EKF) method. It is shown that the QN method has the best performance under most scenarios.

Considering the increasing penetration of EVs, upgrading and reconstruction of the power system infrastructure should be planned ahead to satisfy the growth of load demand. One of the focuses is the construction of public charging stations while battery charging and battery swapping are two feasible technical options. This thesis proposes the distributed swapping and centralized charging (DSCC) battery-swap system by improving the operation and logistics among stations. Firstly, the traffic conditions are formulated such that the swapping stations and other supporting facilities can be deployed. Secondly, the real-time available batteries and demand of batteries are investigated with the improved (s, S) inventory management to guarantee adequate supply of recharged batteries. Finally, suitable optimization schemes are derived to attain the objectives of maximum battery inventory turnover or minimum impact of EV charging on power system.

This thesis also proposes the planning optimization within the scope of local distribution systems where EVs are charged at the homes of customers rather than at specialized charging or swapping stations. With vehicle to grid (V2G) technology, the increasing integration of EVs is raising the future potentials of smart grid because the residual energy stored in EV batteries can be discharged to support grid when needed. However, the stochasticity of EV user behavior poses challenges to the regulators of distribution systems. How regulators decide upon a control strategy for V2G and how EV users respond to the strategy will significantly influence the variation of load profiles in the planning horizon. In this thesis, a comprehensive cost analysis is performed to obtain the optimal planning scheme considering the variation of EV penetration, charging preference and customer damage cost (CDC). The economics and stability of the planned distribution system are assessed with real-world travel records and cost statistics to show the effectiveness of the optimization algorithm.

Acknowledgement

First of all, I would like to express my sincere appreciation to my chief supervisor, Prof. C. Y. Chung, for his continuous support and helpful suggestions throughout my PhD study. His enthusiasm, patience, rich knowledge and creative way of thinking have profoundly promoted my academic capabilities. It has been an honor to study under his guidance that every discussion with him gives me invaluable inspirations and confidence.

I reserve special gratitude to Prof. Bikash C. Pal from the Imperial College London for his patient explanation and inspiring discussion about the impact of EV penetration on power system state estimation.

I have spent four memorable and fruitful years with my research team. I really appreciate the selfless help from my colleagues and give my special thanks to Dr. N. Z. Xu, who gave me a lot of help on revising papers and encouraged me when I was depressed. Moreover, I would like to express my gratitude to my paper reviewers and thesis examiners for their precious comments to this research.

My genuine appreciation and love belong to my dear parents and wife who support me unconditionally in chasing my dreams.

Last but not least, I would like to acknowledge the support from the Hong Kong PhD fellowship awarded by RGC and the Ph.D. studentship offered by The Hong Kong Polytechnic University.

Table of Contents

Lists of Figures

Lists of Tables

Lists of Abbreviations and Symbols

Abbreviations (*in alphabetical order*)

ALS	Armijo line search
BFGS	Broyden–Fletcher–Goldfarb–Shanno formula
CDC	Customer damage cost
DG	Distributed generation
DSCC	Distributed swapping & centralized charging system
EENS	Expected energy not supplied
EKF	Extended Kalman filter
EMS	Energy Management System
EPC	Engineering, procurement and construction
EV	Electric vehicle
H	Residential areas
ICE	Internal combustion engine
MCS	Monte Carlo simulation
NRs	Normalized residuals.
NHTS	National Household Travel Survey
NYISO	New York Independent System Operator
O	Places for other family errands.
PJM	Pennsylvania-New Jersey-Maryland Interconnected system
PMU	Phasor measurement unit
RTU	Remote terminal unit
SCADA	Supervisory Control and Data Acquisition system
SE	Shopping & eating places.
SOC	State of charge
SR	Social & recreational places.

SSE	System State Estimation
SSE-QN	SSE with quasi-Newton method
SSE-WLS	SSE with Gauss-Newton method
STC	Series trip chain.
TET	Trip end time.
TWLS	Traditional weighted least square method
UKF	Unscented Kalman filter
V2G	Vehicle to grid
W	Work places

Symbols (*in order of appearance*)

Chapter II

i	Index of EVs, running from 1 to M.
k	Index of series trip chains (STC).
n	Index of buses with charging stations.
t	Index of time intervals in minutes.
N	Total number of public charging places.
R_k	Occurrence probability of the kth STC.
$T_{n,k}$	Trip end time of the kth STC at place n.
$l_{n-1,n}$	Travel distance between place $n-1$ and n.
PPM	Pearson product-moment correlation coefficient.
B_c	Total capacity of EV batteries.
E_n^i	Possible charging energy of the ith EV at place n.
ω	Energy consumption per km.
$\beta_{n,k}$, $\eta_{n,k}$, $\gamma_{n,k}$	Shape, scale and location parameters of Weibull distribution.
P_c, κ_c	Charging power and efficiency.
D_n^i	Possible charging duration of the ith bus at place n.

Chapter III

m	Index of buses.
j	Index of measurements.

q	Index of iterations in QN method.
m_b	Total number of buses.
$\widehat{P}_{m,t}, \widehat{Q}_{m,t}$	Forecast total active/reactive power at bus m, time t.
$\widetilde{P}_{m,t}, \widetilde{Q}_{m,t}$	Estimated total active/reactive power at bus m, time t.
$\Delta\widehat{P}^{base}_{m,t}, \Delta\widehat{P}^{EV}_{n,t}$	Forecast active base power load and EV charging load increment at time t.
$f^{i}_{n,k,t}, g^{i}_{n,k,t}$	Binary variables reflecting the starting and ending states of charging at place n, time t of the ith EV in STC_k.
$\widehat{V}_{m,t}, \widehat{\theta}_{m,t}$	Forecast voltage magnitude and phase angle at bus node m, time t.
$\widehat{\boldsymbol{x}}_t, \widetilde{\boldsymbol{x}}_t$	Vector of forecast and estimated system states at time t.
$\boldsymbol{z}$	Vector of measurements.
$\boldsymbol{K}$	Kalman gain
$\boldsymbol{M}$	Forecast state error covariance
$\boldsymbol{h}(\boldsymbol{x})$	Nonlinear power flow functions.
$\boldsymbol{e}$	Vector of measurement errors.
$\boldsymbol{r}$	Vector of estimation residuals.
$\boldsymbol{R}_z$	Measurement error covariance.
$\boldsymbol{H}$	System Jacobian matrix.
σ_j	Variance of the jth measurement.
$\boldsymbol{\Omega}_{jj}$	The jth diagonal entry of the residual covariance matrix.

Chapter IV

SOC^{i}_{ini}	Initial SOC of the ith EV when coming by a swapping station.
$th\%$	Alarming threshold that users must charge their battery.
ζ	Vehicle flow rate
r	Estimated charging probability of EVs on the road.
ΔT	Unite time slot
s_n	Trigger point for inventory replenishment at the nth station.
S_n	Initial inventory level of the nth station.

DB_{n,t_n}	Quantity of residual full-energy batteries in the *n*th station, at time t_n.
$T_{tran,n}$	One-way transport duration of the *n*th station.
$S_n(t)$	Real-time inventory level of the *n*th station.
$S'(t)$	Real-time inventory level of the centralized charging center.
P_t	Aggregated charging power at time *t*.
$p_{a,b}$	Probability of moving from inventory level in state *a* to the level in state *b* after time slot ΔT.
$D(P)$	Daily average deviation from the average charging power.
I	Inventory turnover ratio.

Chapter V

v	Average urban driving speed.
S_n^i	Trip start time of the *i*th EV at place *n*.
E_{H}^i	Charging demand of the *i*th EV at place H.
D_{H}^i	Charging duration of the *i*th EV at H.
ξ^i	Customer damage cost (CDC) of the *i*th EV.
λ	Index of planning years.
μ_{c}, δ_{c}	Mean and standard deviation of CDC.
γ_λ	Compensation ratio at year λ.
T_{gc}, D_{gc}	Control start time and lasting period.
e_{c}^i	Energy already charged before T_{gc} of the *i*th EV.
e_{b}^i	Energy discharged of the *i*th EV.
e_{p}^i	Postponed original charging demand of the *i*th EV.
t^*	Reference recharging time.
T_{r}^i, D_{r}^i	Recharging start time and duration of the *i*th EV
P_{d}, κ_{d}	Discharging power and efficiency.
$P_t^{\mathrm{c,EV}}$, $P_t^{\mathrm{d,EV}}$	Total charging/discharging power at time *t*
f^{oper}, f^{cc}, f^{inv}	Operation cost, V2G compensation cost, and infrastructure investment cost.

d^{annual}	Number of days in one year.
Y	Number of years for entire planning horizon.
ρ_t^{da}	Day-ahead electricity price at time t.
ρ^{CO_2}	Fixed carbon tax rate.
ρ^{NL}	Unit line loss rate.
q_λ	Number of total EV users fulfilling prerequisites of V2G at year λ.
$P_{xy,\text{cap}}^l$	Planned capacity of feeders at line xy.
$P_{x,\text{cap}}^s$	Planned capacity of substations at bus x.
$U_{x,t}$	Nodal voltage magnitude at bus x, time t.
G_{xy} , B_{xy}	Real part and imaginary part of the nodal admittance matrix
Ω^l	Set of feeders.
Ω^s	Set of substations.
Ω^x	Set of system nodes.
Ω^t	Set of time intervals in a day.

Chapter I

Introduction

1.1 Background and Incentives of Research

1.1.1 Policies for EV Promotion

Currently, the transport sector relies on 95% liquid fossil fuels and is responsible for 25% of total greenhouse gas emissions related to energy [1]. Popularizing electric vehicles (EV) can be one of the most effective ways to deal with the ever severe air pollution because it is zero-emission. To counter the climate change and air pollution, more countries are enacting laws and providing incentives for promoting EV penetration that brings great challenges to monitoring, control and expansion of the future smart grid. In 2011, President Barack Obama set the goal for the United States to become the first country to achieve one million EVs by the year of 2015 [2]. The Chinese government also initiated the "Ten cities, thousand vehicles" program [3] in 2009, which was designed to encourage public and private use of EVs through the demonstration projects in the selected cities. The target of the government is that the number of EVs in China shall grow to between 500,000 and 1 million by 2015, and gradually increase to 2 million units by 2020 [4]. Norway is the first country where over 1% passenger cars on the roads are EVs. The proposed National Transport Plan [5] in Norway sets the goal that all new cars, buses and light commercial vehicles in 2025 should be zero emission vehicles while heavy-duty vans, 75% of new long-distance buses, and 50% of new trucks must be zero emission vehicles by 2030.

1.1.2 Impact of EV Penetration on Power Systems

An average house with an EV penetration is estimated to have a 56% increase in annual electricity consumption [6] and preliminary studies have illustrated that the increasing integration of EVs with stochastic behavior and uncontrolled charging scheme can disturb the normal operations of the grid [7, 8]. Considering the distribution network, [9] introduces the impact of EV penetration on a residential area. The well-being analysis of generating systems with EV penetration is presented in [10, 11]. Transformer loss of life caused by extensive EV charging is investigated in [12]. Dynamic stability of transmission systems is examined in [13, 14], which illustrates that EV charging has negative damping effects. Therefore, improved methods of EV charging demand forecast, system state estimation (SSE) and power system planning are needed to pave the way for the future smart grid considering the increasing EV penetration with stochastic user behavior. The literature related to my research is listed as follows.

1.1.3 Forecast of EV Charging Demand

As the charging behavior is fairly stochastic, EV travelling route, the start time of charging, state of charge (SOC) and preferred charging duration of users can significantly influence the geographical and temporal energy demand. Many existing papers have proposed methods or assumptions concerning EV charging forecast, however, most of them underestimate the stochasticity of EV user behavior in both traveling and charging. Inflexible charging start time and charging frequency are assumed in [8], [14] and [15] to illustrate uncontrolled charging. In reality, people may resort to multiple charging cycles when necessary and the home charging time could be profoundly influenced by travel history during daytime. Travel scheduling with multiple trips is investigated in [16] but the travel purposes are not differentiated that information from the travel survey is not fully exploited. Global Positioning System (GPS) recording devices are used in [17] to obtain the actual driving routes in the city of Winnipeg. The conditional probability density functions of travel distance and home arrival time are considered in the stochastic model whereas the charging demand in public areas and interrelationships between trips are unclear. Both [18] and [19] use similar methods to forecast EV charging in spatial-temporal spans with actual local travel surveys. The occurrence probability of each kind of travel state during the day is plotted every 15 minutes for analyzing the state change probability between consecutive intervals. However, [20] indicates that travel events can occur at a per-minute level and, therefore, EV states are weakly linked between long steps (like 15 minutes) and they cannot formulate Markov transitions.

Furthermore, most papers have overlooked the unknown factors of EV charging preferences. [16] and [21] assume all EVs being charged every time they stop, which may be impractical as people are free to choose to halt without charging. [21, 22] ignore the variation of residual SOC among different EVs but use the average SOC to calculate total charging demand. Besides, most studies assume full charging as the objective [8]-[19], [21]-[22], but users may not follow given urgencies or personal necessities in reality.

1.1.4 System Monitoring and State Estimation

States for power system operations are classified in Fig. 1.1 [23]. The normal state refers to the situation that all power demands in the system can be fulfilled by the existing generators without violating any operational constraints. A normal state is said to be "secure" if the power system can keep in normal state facing potential critical contingencies. Otherwise, the normal state is classified as "insecure" where the power balance is still met but the system becomes vulnerable under some contingencies. When operating conditions change significantly and violate some of the constraints, the system is said to operate in emergency state while the power supply is still satisfied. In restorative state, corrective control measures should be adopted to avoid system collapse. The system may restore stability with reduced load or reconfigured topology.

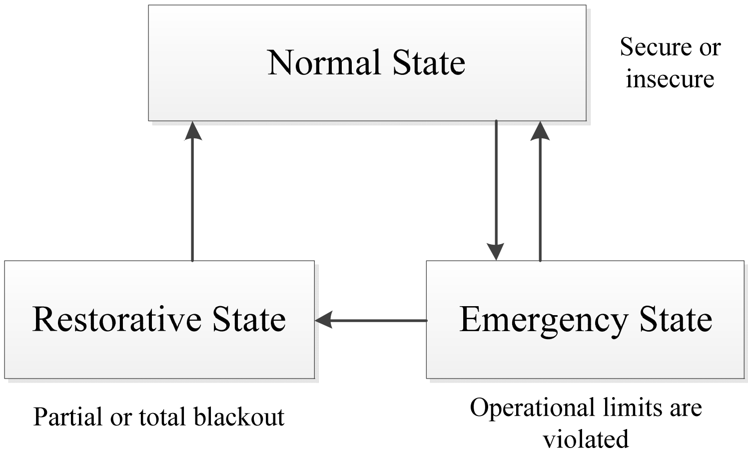

Fig. 1.1: State illustration for power system operation

The main goal of the grid operator is to maintain the power system in the normal secure state considering the variation of operating conditions during daily operation. Initially, power systems were monitored only by supervisory control systems which monitor and control the status of circuit breakers at the substations. Those systems were later upgraded to the Supervisory Control and Data Acquisition (SCADA) Systems with real-time system-wide data acquisition capabilities. However, the information acquired may not always be reliable due to measurement errors or communication failures and the fact that some items cannot be directly measured.

Historically, state estimation was first recognized and addressed in 1970s to filter measurement noise and detect gross errors [23, 24]. Introduction of the state estimation essentially improves the capabilities of the SCADA system and leads to the establishment of the Energy Management Systems (EMS) with online state estimator. The structure of system state estimation (SSE) with online security assessment is shown in Fig. 1.2 which combines the forecast data and measurement data from remote terminal unit (RTU) to estimate the states of a given system. The control scheme is designed based on the estimated states.

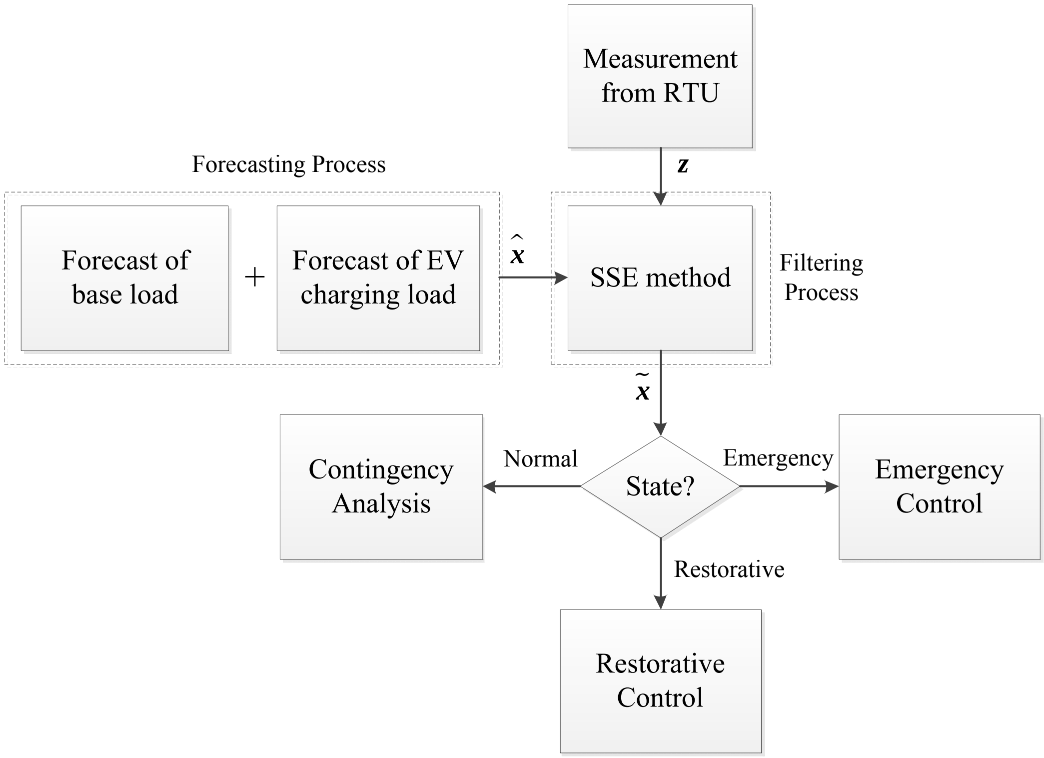

Fig. 1.2: Structure of SSE with online security assessment

Recently, some methods have been proposed on solving the uncertainties brought by phasor measurement unit (PMU) [25, 26] or varying network parameters [27] in transmission systems. However, for now, no one has provided corresponding state estimation methods on systems with stochastic loads, such as EV charging demand, integrated at the distribution networks. Unlike the sophisticated metering infrastructure deployed in transmission networks, the measurement facilities in distribution grids are relatively scarce and cannot ensure high accuracy as well as reliable operations [28]-[30].

SSE with EV penetration is rarely found in the literature. By integrating EV charging load forecast into the forecasting process shown in Fig. 1.2, existing methods are expected to have defects as EV charging preference is unknown. Traditional weighted least square (TWLS) method proposed in [28]-[30] is simple and has acceptable accuracy, but the estimator needs to be reinitialized at every step and cannot predict the state for the next time step. [31] finds that an improved WLS using Newton method rather than Gauss-Newton method adopted by [28]-[30] is more robust but hard to apply in practical programming. Extended Kalman filter (EKF) is a dynamic method [32]-[37] but only uses the first order of the system, making it inefficient when system nonlinearity cannot be ignored [37]. Although unscented Kalman filter (UKF) does well in tackling nonlinear systems [38]-[43], UKF along with EKF highly relies on the effectiveness of the state forecast formula. However, no reliable state forecast is guaranteed considering the aforementioned unknown factors of EV charging, making the estimation of EKF and UKF prone to errors.

1.1.5 Power System Planning

According to the dimensions of power grid, system planning is classified into transmission system planning and distribution system planning. Transmission expansion planning is illustrated in [44]-[47] with objectives including investment and operation cost minimization under security constraints. Special focus is placed on minimizing total congestion cost which corresponds to locational marginal price (LMP). Nodal prices of different buses are made as flat as possible to decrease difference among LMPs and encourage a competitive environment for all participants [44]-[46].

In distribution system planning [48]-[64], LMP is not considered because line congestion rarely takes place in distribution systems. Constructing distributed generations (DGs) which provide wind and solar energy is suggested as an option in [48]-[58] aiming at reducing total infrastructure investment cost and system operation cost. However, the power from DGs is intermittent and cannot guarantee timely support during busy hours. The impact of EV charging on distribution grids is analyzed in [58] from perspectives of an EV aggregator or grid operator, whereas the trade-off between different perspectives is still unknown. The optimal siting and capacity of EV charging stations are investigated in [61]-[64] within metropolitan areas. The transportation network is considered in [61] and the deployment of fast charging stations is investigated for maximum traffic flow capture. Without transportation information, the optimal placement of charging stations in [62]-[64] is designed to effectively cover the area of whole city with least investment cost.

1.1.6 Swapping Station Planning Along Highways

Besides the research of EV charging demand forecast and power system state estimation, the EV charging/swapping stations and the associated infrastructure should also be planned ahead for the sake of system stability and cost reduction. Generally, three kinds of modes exist for EV battery replenishment and their characteristics are summarized in Table 1.1.

Table 1.1: Characteristics of different charging modes

Mode	Advantages	Disadvantages
Ordinary charging	Less investment; Can charge at any time in the public parking lot and home charging post, and easy to use	Time-consuming; Unable to meet emergency charging needs
Fast charging	Time-saving; Stable supply of electricity and easy to use.	High investment in equipment; Fast charging affects battery life; Charging power is too high;
Battery swapping	Easy maintenance of the batteries and extended battery life; Battery swapping time is the shortest; Battery leasing can lower the EV purchasing price.	Connecting point between EV and batteries is easily worn out; High battery purchase cost for stations; Requiring unified specifications of the EV battery market

Although the access to charging stations can be easy, the charging duration required is too long [65] and the peak charging power is hard to be controlled, especially for cars driving on highways during daytime. Battery swapping station is pretty convenient for drivers as they can substitute exhausted batteries for re-charged batteries within only a few minutes. The infrastructure planning of swapping stations is shown in [66]. The comprehensive load forecasting of swapping stations is proposed in [67] considering the stochastic behavior of EV users. Basic operation guidelines of swapping stations are provided in [62], and the life cycle benefit is investigated using Net Present Value (NPV) criterion between rapid-charging stations and battery swapping stations to evaluate their economic feasibility. The recharging of swapped batteries in each swapping station can also be controlled according to spot pricing to minimize charging cost [68]. The day-ahead scheduling process of battery swapping and charging is proposed in [69] which considers Grid-to-Battery (G2B), Battery-to-Grid (B2G) and Battery-to-Battery (B2B) modes. The detailed control strategy and its equivalent model are illustrated in [70] which uses swapped batteries as storage devices. The case study in [69] clearly shows that, under current battery purchasing cost (500-600 $/kWh), the B2G and B2B modes are not economical. However, when the cost of battery itself decreases, the B2G and B2B modes can generate much economic benefit.

Traditionally, each swapping station is independent which provides batteries for substitution and charges swapped batteries within the station [62], [65]-[70]. However, as battery purchasing cost takes the largest part in owning an EV [69], the requirement that battery inventory in a station should be enough to meet probable demand at that station may sometimes lead to wastage as the tendency to charge is fairly stochastic for different EVs on different roads. Therefore, the synergic control of multiple nearby swapping stations can be more beneficial.

1.1.7 Distribution system planning within Residential Areas

For residential EVs, there will usually be a long sojourn time before the departure of next day so that the ordinary charging mode is preferred. To mitigate the impact of EV penetration on power systems, peak shaving is a widely adopted idea and various relevant control approaches have been proposed. The two-stage coordination strategy considered in [71]-[73] optimizes the charging power of the aggregators at the upper level and reschedules individual EVs accordingly at the lower level. Synergistic control of EV charging and other DGs are analyzed in [14], [74]-[76]. Vehicle to grid (V2G) technology can fully utilize the EV battery potentials that discharge during busy hours to support the grid and recharge at valley hours [77]-[79]. However, they seldom consider the willingness of EV users or their temporal availability for obeying the control from grid. The price lever is introduced in [79]-[81] to guide charging behaviors, but different user perspectives with respect to the amount of incentives are not considered. A cooperative game between grid regulators and customers is proposed in [82, 83] in which the decrement of total cost is allocated to each participating player. The game is based on the hypothesis that users are fully responsive, which may not be realistic for the V2G behavior. [84] proposes an innovative distribution system planning by taking customer choices on reliability into account. In our study with EV integration, the grid operators are responsible for setting up control decisions for system reliability and the customer choices on control acceptance should be emphasized.

Besides the control of EV charging, some papers focus on the reinforcement of grid infrastructure and charging station planning for satisfying the increasing load demand in the whole projected horizon. Although the deployment planning of EV charging stations is investigated in [61]-[64] within metropolitan areas, the significant impact of stochastic user behavior on system planning decisions is underestimated. Furthermore, few works have emphasized the planning within the scope of local power companies where EVs are charged at the homes of customers rather than at specialized charging stations.

Considering stochastic V2G behavior at residential areas, probabilistic evaluation of a power system can recognize not only the severity of a state and its impact on system operation, but also the probability of its occurrence. Proper combination of both severity and occurrence probability creates indices that better represent system risk. Distribution system planning scheme is devised based on the probabilistic evaluation of system risk by upgrading system infrastructure to acceptable levels of reliability at the lowest possible cost (including infrastructure investment cost, compensation cost to control acceptance and operation cost after system upgrade). Reliability worth assessment [85] incorporates the investment cost and operation cost analysis, and quantitative reliability assessment into an overall cost minimization procedure. Interruption costs are adopted in [10]-[11] and [86] to provide an indirect measurement of reliability worth whereas the content of interruption cost shall be modified in the situation with V2G application.

1.2 Primary Contributions

The main focus of this thesis is to develop new and practical methodologies for the optimization of power system planning and SSE considering increasing EV penetration and stochastic user behavior. The original contributions of this thesis can be summarized in the following aspects:

1.2.1 EV charging demand forecast

An accurate forecast of EV charging demand is the cornerstone to the research of its impact on power system monitoring and planning. To better interpret the uncertain mobility of EV charging, this thesis divides the user behavior into EV travel behavior and charging behavior. EV trips traveled along the day are categorized according to trip purposes and linked with series trip chains (STCs). The geographical and temporal distribution of EV travel behavior is obtained while the possible range of charging demand at each location is estimated by the distance traveled earlier and the distance to be traveled for the next trip.

The strengths of this thesis concerning the forecast are: First, data of the real-world travel survey (the 2009 National Household Travel Survey [20], for example) can be fully utilized because the inputs of the forecast are in alignment with the items in the travel survey and the forecast in this thesis is conducted at a per-minute level. Secondly, the recorded trips are carefully categorized by different purposes and linked by possible occurrence sequence according to the fact that an EV may have several trips a day and those trips are not independent. Thirdly, to make the forecast more realistic under the situation that no relevant surveys found on investigating user charging preference, the estimated charging behavior at each location is dependent on both the forecast travel behavior and human arbitrary preference.

1.2.2 SSE with stochastic EV user behavior

This thesis provides an innovative idea to consider the impact of unknown user behaviors, which leads to spatial and temporal uncertainty of charging demand forecast, on SSE with EV penetration. Considering the unpredictable forecast error brought by distributed charging demand, an improved filter for SSE is proposed combining quasi-Newton (QN) method and Armijo line search (ALS) to minimize the estimation error in various scenarios without exact state forecast formula. The result of the numerical study shows that the proposed state estimation method can handle the situation with unknown EV charging demand while the algorithm is much faster and more accurate compared to existing SSE methods. To the best of the authors' knowledge, this thesis is the first work that notices the unknown user charging preference and proposes new method to mitigate the influence on SSE.

1.2.3 Swapping station planning on highways

The focus of power system planning scheme is different for the situations on highways and distribution systems within residential areas. For the situation on highways with needs of fast battery energy replenishment, as battery purchasing cost is very high, this thesis schedules and optimizes the recycling of batteries to fulfill the prompt battery needs among several stations with the knowledge of

Logistics. Classical (s, S) model proposed in [87] requires that production stops at the moment that the inventory level is raised to S and production starts again when the inventory level is observed below s. For the planning of multiple stations located alongside different roads, the distributed swapping and centralized charging (DSCC) system proposed in this thesis successfully improves the (s, S) model to maximize the utilization of battery reserves and minimize the impact of aggregated charging load considering stochastic EV penetration on highways with synergic control.

1.2.4 Distribution system planning with stochastic V2G behavior

For the distribution system planning covering the residential areas, EVs are usually charged in the homes of customers and the research focus is different from that on highways.

Considering the practical EV user behavior, this thesis proposes the pioneer work focusing on the influence of customer behaviors on distribution system planning decisions. To be specific, the major contributions of this topic lie in three aspects. First, the stochasticity of EV traveling/charging behavior is fully analyzed with probabilistic techniques. Second, the response of EV users to system control signals is clarified with the concept of customer damage cost (CDC) that the amount of interruption compensation and customers' willingness of accepting control are mutually influenced. The planning scheme is therefore devised based on "degrees of customer acceptance to potential control" rather than the usual "yes or no" logic. Due to the stochasticity of user behavior, some stability margin should be guaranteed and the cost of demand side management (incentives to customers) may be too high. Grid infrastructure reinforcement and the amount of compensation to users are both taken into account in the cost analysis of distribution system planning so that this thesis helps determine the trade-off between spending more money on encouraging control acceptance and investing more in infrastructure for the whole planning horizon.

1.3 Thesis Layout

Chapter II presents the methodology of EV charging demand forecast considering stochastic user behavior. Chapter III takes cognizance of the uncertain user charging preference and provides an innovative SSE with quasi-Newton method for better system monitoring. Power system planning is proposed in Chapter IV and Chapter V. Chapter IV illustrates the optimal deployment of swapping stations along the highways with battery inventory management. In Chapter V, distribution system planning is investigated considering the stochastic V2G behavior within residential areas. Chapter VI concludes the thesis.

Furthermore, the overall organization of this thesis is illustrated in Fig. 1.3.

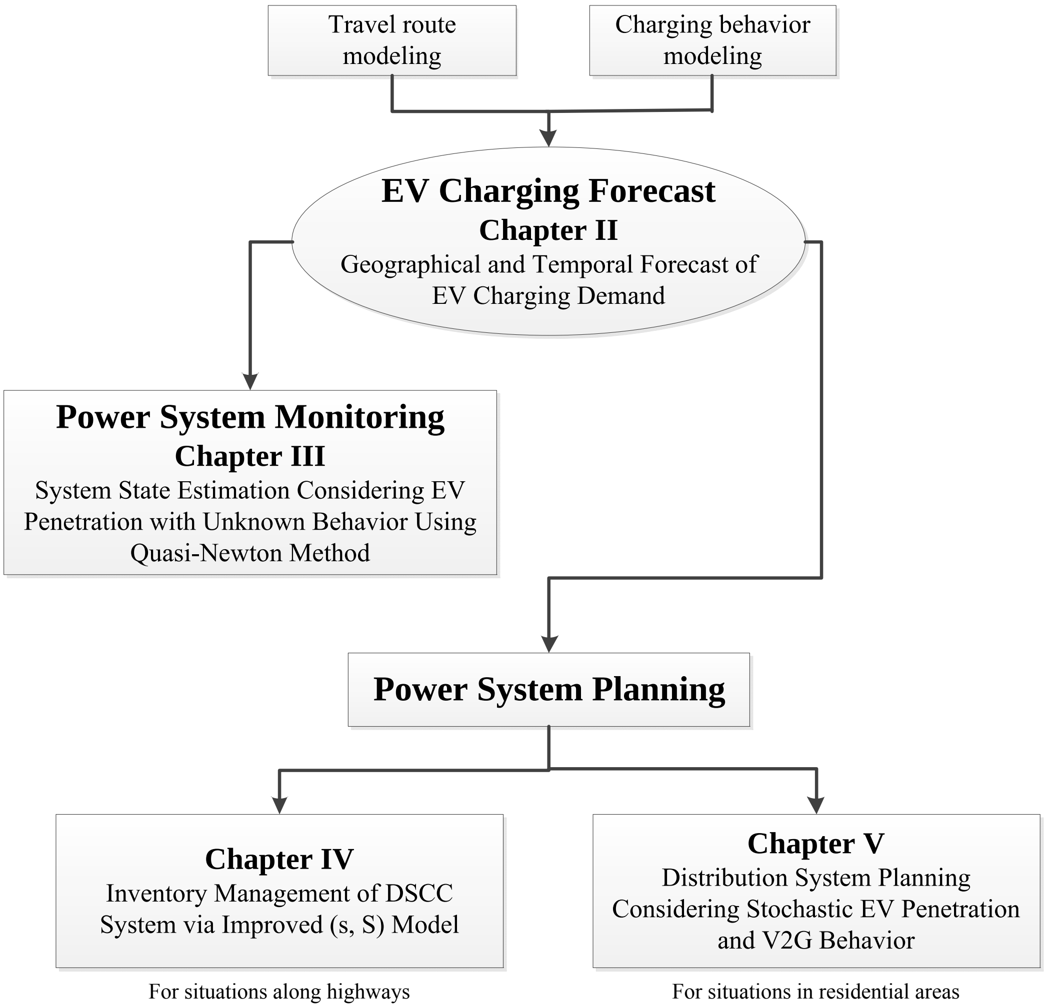

Fig. 1.3: Organization of the thesis

1.4 List of Publications

Journal papers:

1. Y. Nie, C. Y. Chung and N. Z. Xu, “System state estimation considering EV penetration with unknown behavior using quasi-Newton method," *IEEE Trans. Power Sys*t., vol. 31, no. 6, pp. 4605-4615, Nov. 2016. Manuscript ID: TPWRS-00796-2015
2. Y. Nie, C. Y. Chung and X. Wang, “Distribution system planning considering stochastic EV penetration and V2G behavior.” *IEEE Trans. Smart Grid.* (Submitted).
3. Y. Nie and C. Y. Chung, “Geographical & temporal forecast of EV charging and its impact on regional electric grid," *IEEE Trans. Power Syst.*. (Submitted).
4. L. Chen, Y. Nie and Q. Zhong, “Forecast model of electric vehicle charging based on series trip chain.” *Transactions of China Electrotechnical Society*, vol. 30, no. 4, pp. 216-226, Feb. 2015

Conference papers:

1. Y. Nie, C. Y. Chung and L. Chen. “Inventory management of DSCC system via improved (s, S) model.” *IEEE Power & Energy Society General Meeting, Washington DC,* Jul. 2014.
2. X. Wang, K. W. Eric Cheng and Y. Nie, “Integration development for supercapacitor controlled distributed generation system.” *International Conference on Power Electronics Systems and Applications (PESA),* Dec. 2015.
3. T. Wu, W. Mai, C. Y. Chung and Y. Nie, “Economically and environmentally optimal operation of combined cooling heat and power microgrid with plug-in electric vehicles.” *2015 IEEE PowerTech Eindhoven, Netherlands,* Jun. 2015.

4. C. Zhang, B. Dai, C. Y. Chung and Y. Nie. “Model-based volt-var optimization using advanced metering infrastructure in distribution networks.” *2015 IEEE PowerTech Eindhoven, Netherlands,* Jun. 2015.
5. L. Chen, C. Y. Chung and Y. Nie. “Modeling and optimization of electric vehicle charging load in a parking lot.” *The 5th IEEE PES Asia-Pacific Power and Energy Engineering Conference, Hong Kong,* Dec. 2013.

Chapter II

Geographical and Temporal Forecast of EV Charging Demand

2.1 Introduction

In modern power systems, the electricity generation and demand should always be kept in equilibrium to ensure the stability of the grid. Due to the inertia of generators and the fact that electricity cannot be easily stored, the forecast of the power demand becomes extremely important that the grid operators can properly set the control schemes of the generation dispatch in advance or plan the infrastructure upgrade for the development of the upcoming years.

For the future smart grid with increasing EV penetration, the significance of charging demand forecast is promoted as user behavior is fairly stochastic. As summarized in Chapter I, [8] and [14]-[19] neither pay enough attention to the randomness of user travel preference nor compute the state transition of consecutive trips inaccurately. Fixed principles regarding charging behavior are made in [8]-[19] and [21]-[22], but they may not be practical for a group of EV users.

In this thesis, the analysis of EV user behavior is divided into EV travel behavior and EV charging behavior with more realistic consideration. The Monte Carlo simulation (MCS) proposed in [85] is adopted to further reduce the forecast error. The rest of this chapter is organized as follows. In Section 2.2, a general forecast model of EV traveling routes is formulated. In Section 2.3, the charging behavior modeling at different locations is proposed by taking the arbitrary user preference into account. In Section 2.4, the aggregated spatial and temporal charging load forecast is obtained by MCS. In Section 2.5, results of the charging demand forecast are shown in the numerical study and compared with real-world statistics to demonstrate the feasibility of the forecast method. Section 2.6 summarizes this chapter.

2.2 Travel Route Modeling

This section outlines a general method for simulating EV daily routes with multiple travel purposes. Individual trips are linked into complete daily trip chains to find out the interrelationships among consecutive trips.

2.2.1 Modeling of Series Trip Chains

A city is usually composed of several districts with different characteristics, like residential area ($\mathrm{A_H}$), central business district and so on. Trips are classified into different travel purposes, including trips transiting between districts $\{\mathrm{A}_n\} = \{\mathrm{A}_1, \mathrm{A}_2, ..., \mathrm{A}_N, \mathrm{A_H}\}$ (for public places n=1,…,N; for residential areas n=H). Each district is equipped with an aggregator which connects to one bus in the power grid and integrates local charging facilities. An EV may perform several trips a day, and the whole route modeling is described in Fig. 2.1. Possible series trip chains (STC), each composed of different permutations of $\{\mathrm{A}_n\}$ with occurrence probability $\{\mathrm{R}_k\} = \{\mathrm{R}_1, \mathrm{R}_2, ..., \mathrm{R_K}\}$, are derived from actual trip records to link sequential trips in series chains with temporal dependence. R_k is calculated to be the portion of occurrence times of the kth permutation $\{\mathrm{A}_n\}_k$ to the total number of complete routes. $\{T_{n,k}\} = \{T_{1,k}, T_{2,k}, ..., T_{N,k}, T_{\mathrm{H},k}\}$ denotes the trip end time (TET) of each consecutive trip. Although the purpose of each individual trip is unique, arrival time distribution derived from local travel survey may relate to its last TET when considered in the whole trip chain.

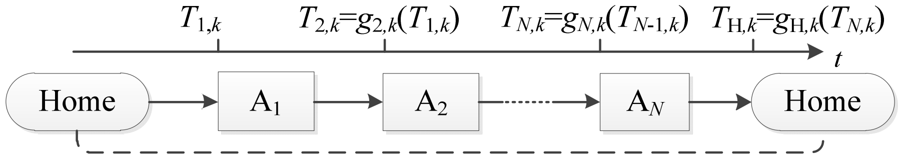

Fig. 2.1: Illustration of STC and TET

2.2.2 Travel Data Fitting

Travel records derived from the local travel survey are fairly stochastic and vary among different travel purposes regarding TET and trip distance. It is necessary to find a flexible distribution form for fitting.

Frequently used normal distribution fitting is only suitable for cases with symmetrical property. Weibull distribution is widely adopted [14, 88] because variation of the shape parameter makes it flexible for diverse situations. The PDF of Weibull distribution is shown in (2.1) and the results of fitting are then assessed by kolmogorov-Smirnov (K-S) test [89].

$$f(x;\beta,\eta,\gamma)=\frac{\beta}{\eta}(\frac{x-\gamma}{\eta})^{\beta-1}e^{-(\frac{x-\gamma}{\eta})^{\beta}},\ x-\gamma\geq 0 \tag{2.1}$$

where β, η and γ are the shape, scale and location parameters respectively, obtaining through maximum likelihood estimation [90]. x represents the travel distance or trip end time.

2.2.3 Transition Relationships of STC

Different from the Markov chain described in [18] and [19], the states in STC$_k$ represent a series of $T_{n,k}$ in each predefined chain rather than the type-of-trip at each fixed time slot. The time unit of forecast is reduced to 1 min to locate the time interval of each trip more accurately.

By linking the fitted distributions to STC$_k$, Pearson product-moment (PPM) correlation coefficient [90] in (2.2) is defined to verify if there is a linear relationship among the TET distributions of consecutive trips.

$$PPM=\frac{\mathrm{Cov}(\boldsymbol{X},\boldsymbol{Y})}{\delta_X\delta_Y} \tag{2.2}$$

where $\boldsymbol{X}$ and $\boldsymbol{Y}$ are the sets of $T_{n,k}$ and $T_{n-1,k}$ records, respectively. The operator Cov is the covariance while δ is the standard deviation.

Data from NHTS [20] denotes that the TETs of trips to/from work have an apparently concentrated distribution while distributions of other purposes are relatively loose. Further investigation of *PPM* between consecutive trips leads to three important observations:

1) There is a strong linear relationship (*PPM*>0.8) between TETs of two trips before W or the two trips after W.
2) The TET of trip going to work and trip back from work in the same STC are independent of each other (*PPM*<0.3).

The first two observations can be explained by the fact that the time to work and the off-duty time are both constrained and independent because of company regulations. The durations of visits to other public places prior to or after a day's work are generally short, so the TETs of these trips show strong linear dependence.

Considered in complete STC$_k$, if records of $T_{n,k}$ have shown strong linear relationships with $T_{n-1,k}$, a function with linear coefficients a_1, a_2 in (2.3) is used to forecast $T_{n,k}$ when its last TET is known.

$$T_{n,k} = g_{n,k}(T_{n-1,k}) = a_1 \cdot T_{n-1,k} + a_2 \tag{2.3}$$

3) Except when the first two observations are applicable, other ensuing trips are closely interrelated but not in linear form (0.3<*PPM*<0.8). The parameters in their distribution functions change accordingly.

This observation can be concluded from other trips which have no unique characteristics. For example, the distribution of TETs for shopping or personal affair trips can last through the whole business hours. Due to the arbitrary nature of the purposes of these trips, the linear relation between two consecutive trips is not that apparent, i.e., the end time of current state is no longer a firm value related to the last state. The shape, scale and location parameters ($\beta_{n,k}, \eta_{n,k}, \gamma_{n,k}$) of the Weibull distribution for current TET can therefore be modified as the function of last TET, as follows:

$$\begin{aligned} f(T_{n,k}; \beta'_{n,k}, \eta'_{n,k}, \gamma'_{n,k} \mid T_{n-1,k}) &= f(T_{n,k}; \beta(T_{n-1,k}), \eta(T_{n-1,k}), \gamma(T_{n-1,k})) \\ &= f(T_{n,k}; \beta_{n,k}, \alpha(T_{n-1,k}) \cdot \eta_{n,k}, T_{n-1,k}) \end{aligned} \tag{2.4}$$

where the shape parameter $\beta_{n,k}$ remains unchanged. However, because the TET distribution of the current trip shall be no earlier than the TET of the last trip, the current location parameter $\gamma^{'}_{n,k}$ should be equal to $T_{n-1,k}$. The current scale parameter $\eta^{'}_{n,k}$ should be curtailed by coefficient $\alpha(T_{n-1,k})$, which is proportional to the residual period in the same day after $T_{n-1,k}$.

2.3 Charging Behavior Modeling

Having obtained the modeling of daily routes, EV charging behavior is estimated by the expected energy consumption of the trips along the travel route. The arbitrary user charging preference is taken into account to make the forecast realistic.

With existing data from travel surveys such as NHTS, $\{T_{n,k}\}$ and $\{l_{n-1,n}\}$ of different STCs can be regarded as predictable values with known distributions. However, whether and for how long an EV will charge at each place n are arbitrary and totally depend upon the drivers' preferences. Without relevant statistics, they should be counted as unknown factors that cannot be predicted from distribution. The range of the possible charging duration is the only information that can be deduced from existing data.

The user behavior is generally different between charging at public places and charging at residential places. For the ith EV which starts in a fully charged state from A_H and stops at the public places along STC$_k$, firstly the energy charged at each stop should not exceed the total SOC deficit; secondly, there should be enough SOC for the next trip after charging. For charging at home, EV users would require their batteries to be fully charged before the next day's trip (H can be regarded as place 0 or N+1). (2.5), (2.6) and (2.7) are therefore constituted to reflect these constraints, respectively.

$$\begin{cases} E_1^i \le \omega \cdot l_{H,1}^i \\ E_2^i \le \omega \cdot (l_{H,1}^i + l_{1,2}^i) - E_1^i \\ \cdots \\ E_N^i \le \omega \cdot \sum_{n=1}^{N} l_{n-1,n}^i - \sum_{n=1}^{N-1} E_n^i \end{cases} \tag{2.5}$$

$$\begin{cases} E_1^i \ge \max\{0, \omega \cdot (l_{H,1}^i + l_{1,2}^i) - B_c\} \\ E_2^i \ge \max\{0, \omega \cdot (l_{H,1}^i + l_{1,2}^i + l_{2,3}^i) - E_1^i - B_c\} \\ \cdots \\ E_N^i \ge \max\{0, \omega \cdot \sum_{n=1}^{H} l_{n-1,n}^i - \sum_{n=1}^{N-1} E_n^i - B_c\} \end{cases} \tag{2.6}$$

$$E_H^i = \omega \cdot \sum_{n=1}^{H} l_{n-1,n}^i - \sum_{n=1}^{N} E_n^i \tag{2.7}$$

$$D_n^i = \frac{E_n^i}{\kappa \cdot P_c} \tag{2.8}$$

where, ω is the energy consumption per km, E_n^i is the energy to be charged at place n ($E_n^i = 0$ represents no need for charging) and B_c is the capacity of EV batteries. Charging duration D_n^i is calculated in (2.8) where P_c and κ are charging power and efficiency, respectively.

As the exact preferences of EV users are fairly arbitrary, the charging demand of the customers at place n varies within the range determined by (2.5) and (2.6). Three possible scenarios are defined in Table 2.1 where customer charging preference at public places changes from “No Interest” to “Highly Prefer”. If any credible survey on charging preference is available in the future, the corresponding distribution function can be easily included in the proposed method.

Table 2.1: Scenarios of charging duration at public stations

Public charging preference	Definition
No Interest	$D_n^i = D_{n,\min}^i$, for $\forall i$
Moderately Prefer	$D_n^i \sim U(D_{n,\min}^i, D_{n,\max}^i)$, for $\forall i$
Highly Prefer	$D_n^i = D_{n,\max}^i$, for $\forall i$

2.4 Charging Demand Forecast Using MCS

Aggregated EV charging demand in each destination is forecast based on the obtained prediction of travel routes and charging preferences. The binary charging choice $u_{n,t}^{i}$ of the *i*th EV is defined in (2.9); its daily charging load profile $P_{n,t}^{i}$ is presented in (2.10).

$$u_{n,t}^{i}(T_n^i \le t \le T_n^i + D_n^i) = 1;\ u_{n,t}^{i} = 0, \text{otherwise} \tag{2.9}$$

$$P_{n,t}^{i} = P_c \cdot u_{n,t}^{i} \tag{2.10}$$

This process is repeated for all *M* EVs and their individual daily load profile is summed up as final daily load profile $P_{n,t}$ at different charging places:.

$$P_{n,t} = \sum_{i=1}^{M} P_c \cdot u_{n,t}^{i} \tag{2.11}$$

Considering the stochastic properties of the probabilistic technique, the total charging loads are not deterministic and the utilization of MCS can better show the characteristics of a group of EV users with uncertain behavior. By stochastically sampling, MCS is proposed to run the above process for *W* times heuristically to mitigate the variance of the forecast. The result $\overline{P_{n,t}}$ of MCS is obtained by (2.12) and it is only valid when (2.13) is achieved.

$$\overline{P_{n,t}} = \frac{1}{W} \sum_{w=1}^{W} \sum_{i=1}^{M} P_c \cdot u_{n,t}^{i} \tag{2.12}$$

$$\tau = \frac{\sigma}{\sqrt{W} \cdot \overline{P_{n,t}}} < \varepsilon \tag{2.13}$$

where σ is the standard deviation of the repeated process; τ is the coefficient of variation while ε is the maximum variance allowed. It can be inferred that the MCS results will be credible after sufficient iteration times.

2.5 Numerical Study

2.5.1 Data of Travel Survey

In this study, the transportation dataset for forecast is derived from week-days' urban records in NHTS (Data file named DAYPUBLL with details on a per minute basis). Specifically, columns WHYFROM and WHYTO explain the trip purposes, namely, Home (H), Work (W), Shopping & Eating (SE), Social & Recreational (SR) and Other Family Errands (O), permutations of which constitute the daily travel routes. The Nissan Leaf model, with battery capacity of 24 kWh and $\omega = 0.24$ kWh/km, is chosen as the typical private EV used in the modeling. Derived from SAE J1772 [91], the individual charging power at H and other public places are 3.3 kW and 19.2 kW, respectively. The total number of EVs in the modeling is set to be M=2000.

2.5.2 Analysis of Possible STCs

Generally, the travel distance of each trip is determined by the geographical information of each destination. In this thesis, with different WHYFROM and WHYTO information, the Weibull distributions of travel distance with different travel purposes are respectively derived from the column TRPMILES.

There is an apparent difference between end times of concentrated work-related distribution and loose non-work related distribution because people who go to work should follow sort of company disciplines while entertainment and shopping malls are open for long business hours. Examples of each are provided to show their independent law of operation. For complete analysis of all possible STCs, the reader is referred to Appendix A for details.

1) Work-related TET

Most of the work-related arrival records are found concentrated within a short period which coincided with the usual stipulation of office hours. In Fig. 2.2, for example, although they first leave H to SE, the arrival records from SE to W peaks over a narrow time span, around 7:00 to 9:00, which means that morning errands like grocery shopping should be done earlier in order not to be late for work. The trip distribution follows $(\beta,\eta,\gamma)=(2.61,210.22,303.18)$. With significance value equals to 5%, the K-S test statistic is 0.07282 which is much smaller than the cut-off value 0.13007. The fitting is therefore accepted.

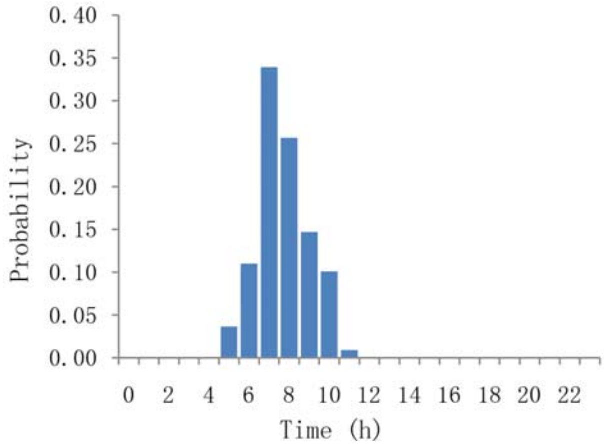

Fig. 2.2: TET distribution of SE-W

2) Non-work related TET

Fig. 2.3 provides the examples of non-work related trips which exhibit relatively scattered distribution. As shopping malls are on business for long hours and there is no strict rule on arriving time, the histogram of H-SE therefore covers a long time span from 7:00 to 20:00 with its scale parameter becoming much larger. The shape parameter is changed and no longer approximates to normal distribution. The fitting is accepted at $(\beta,\eta,\gamma)=(1.85,341.08,413.56)$. With the same significance value, the K-S test statistic is 0.04535 which is smaller than the cut-off value 0.04658.

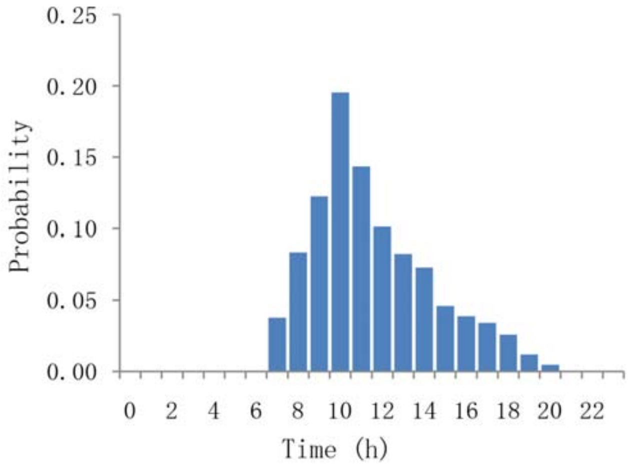

Fig. 2.3: TET distribution of H-SE

The individual TET distributions are linked by STC to formulate the daily travel routes. Forecasts of the typical travel route examples are given to illustrate the observations in Section 2.2.3. The complete PPM investigation of all possible trips is given in the appendix.

1) STC Comprising Work-related Trips

Fig. 2.4 shows the TET distribution of three consecutive trips H-W-SE-H for exemplifying work-related complex chains. It is obvious that TET distribution of the work related trips like H-W and W-SE peaks over a narrow time span compared to that of the three non-work trips in Fig. 2.5, which exhibits relatively scattered distribution. Although the solo SE-H distribution may cover a long time span, which is extremely stochastic, its trip end time overlaps with its last trip W-SE when considered in a complete chain. The PPM coefficient between W-SE and SE-H distribution is 0.81 and it is calculated from (2.3) that $T_{\mathrm{H},k} = 0.83 \cdot T_{\mathrm{SE},k} + 236$. Therefore, the end time of SE-H is predictable in a narrow span because of the regular off-duty time with W-SE trip. The PPM coefficient between the first two work commute trips is 0.25, showing independence.

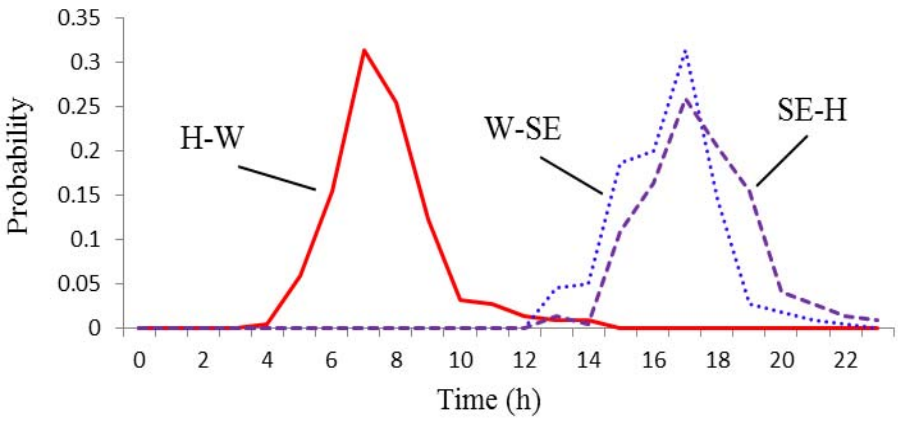

Fig. 2.4: TET distribution in the STC of H-W-SE-H

2) STC without Work-related Trips

The temporal distribution for non-work related H-SE-SR-H is shown in Fig 2.5. Apparently, it is hard to consider the daily consecutive trips separately because their curves overlap with each other at so large a scale that the completion time of the last trip greatly influences the possible time range of the current trip. The PPM coefficients between trips H-SE and SE-SR, SE-SR and SR-H are 0.75 and 0.62, respectively. As a result, the stochastic distribution of each TET is delayed and narrowed down with the sampled former TET according to (2.4).

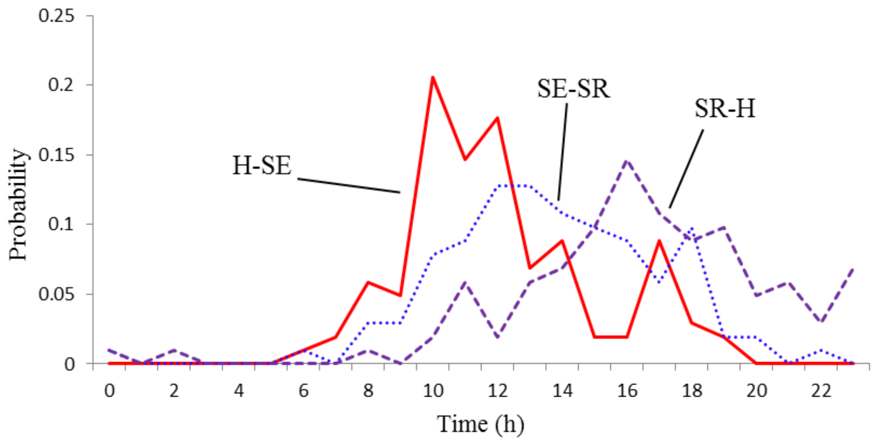

Fig. 2.5: TET distribution in the STC of H-SE-SR-H

2.5.3 Charging Load Forecast

The charging load forecast results at W, SE and H are shown in Figs. 2.6, 2.7, and 2.8, respectively, with different user charging preferences at public stations. The loads in SR and O are omitted for clarity of the figure. It is shown from the figures that the peak charging loads at W and H occur around 8:00 and 19:00, respectively, while the charging demand at SE lasts through the whole business hours. The charging load curve at H is the smoothest because all EVs get charged at their final destination at residential areas while comparatively the least number of EVs park at SE during weekdays that randomness of the charging load at SE is the highest. When considering the scenario which highly prefers charging at public places, the charging demand at W and SE is the highest, making the residual SOC upon arriving home the largest that the aggregated charging load at H becomes the lowest. For the scenario with no interest in charging at public places, EV users will only keep battery energy above the minimum SOC that can support their next trip and the charging demands at W and SE turn to be the lowest.

As a result, the residential charging load will increase significantly and poses larger impact on local grid, as inferred from (2.7).

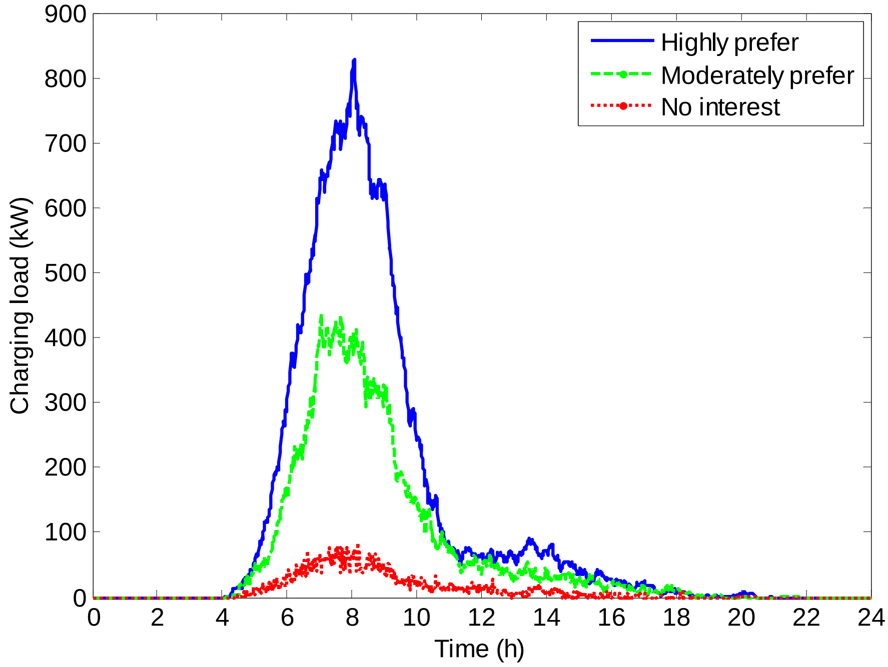

Fig. 2.6: EV charging load at W concerning different charging preferences

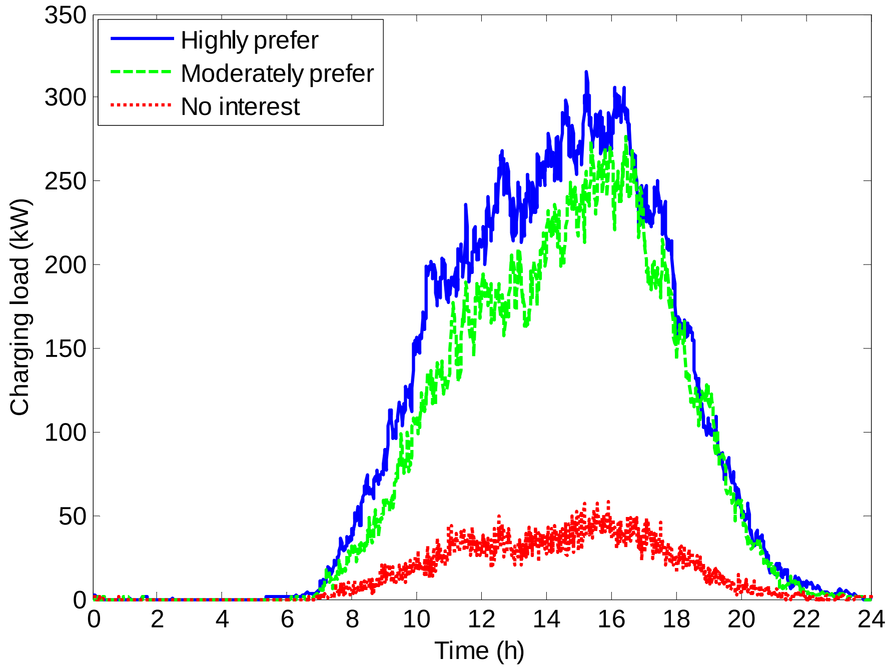

Fig. 2.7: EV charging load at SE concerning different charging preferences

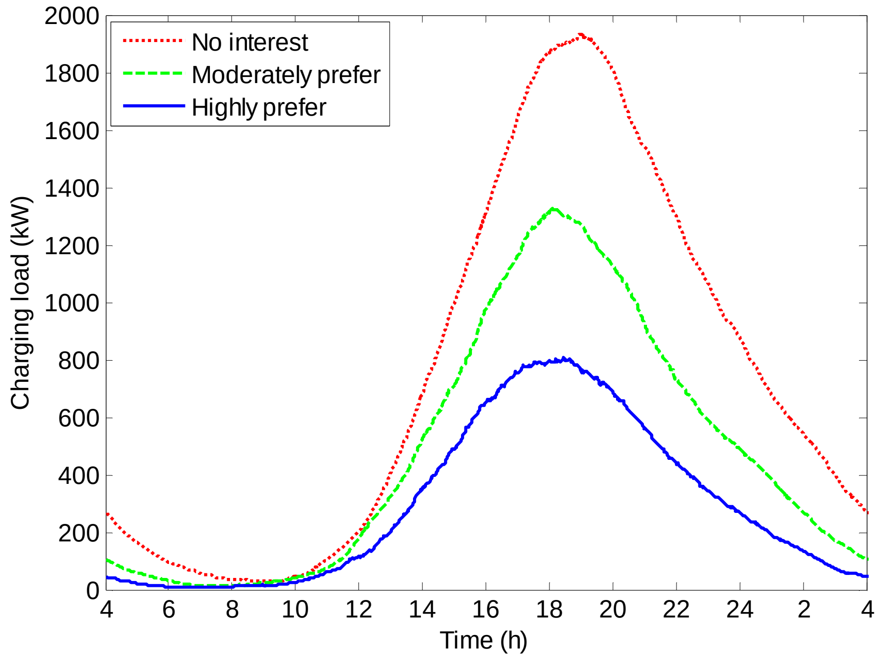

Fig. 2.8: EV charging load at H concerning different charging preferences

2.5.4 Validation

Probabilistic techniques are used in the proposed EV charging load forecast. To validate the feasibility of the proposed forecast method, a deterministic load model is formulated which includes the real travel routes of overall M EVs randomly extracted from NHTS. As no credible user charging preference survey is found for the moment, the scenarios of charging preferences in the deterministic load model are assumed to be the same with the forecast and the real daily charging demand curve is compared with the forecast results shown in Figs. 2.9 and 2.10.

Whether the scenario of public charging preference is “No interest” or “Highly prefer”, the curves of forecast load and real load at H have the same trend and the difference is small. Especially, the results of the forecast load have indicated the peak power and lasting duration with accuracy (maximum forecast error is less than 6%). Considering the fact that the real travel records used in the deterministic model are randomly selected from NHTS, this level of forecast errors is acceptable. Forecasts of the loads at other stations show similar decent performance so that the forecast model is proved feasible. Therefore, it is clear that the inevitable errors in future forecasting will not have significant influence on the analysis of power system monitoring and planning with EV penetration.

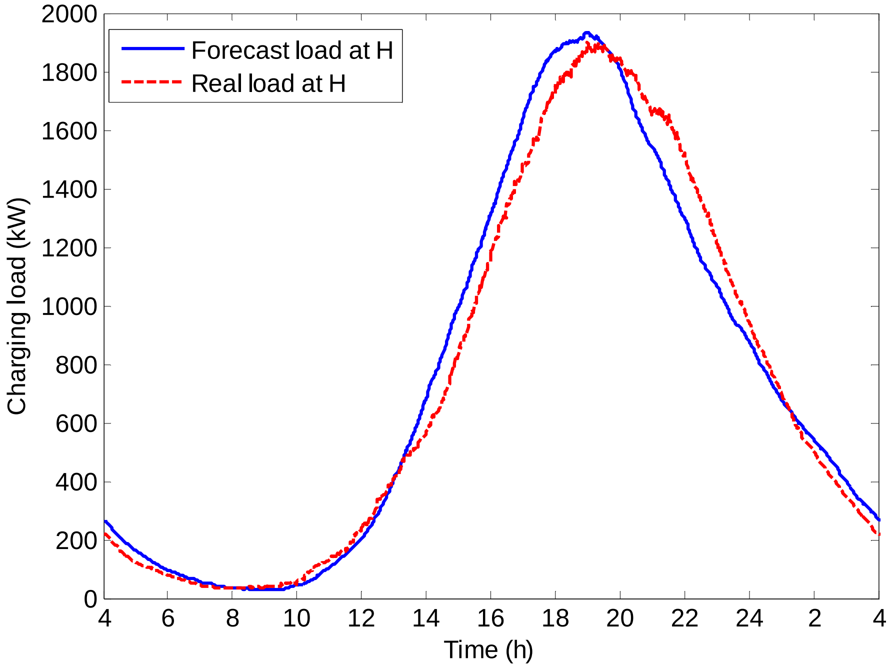

Fig. 2.9: Forecast result validation with scenario of "No interest"

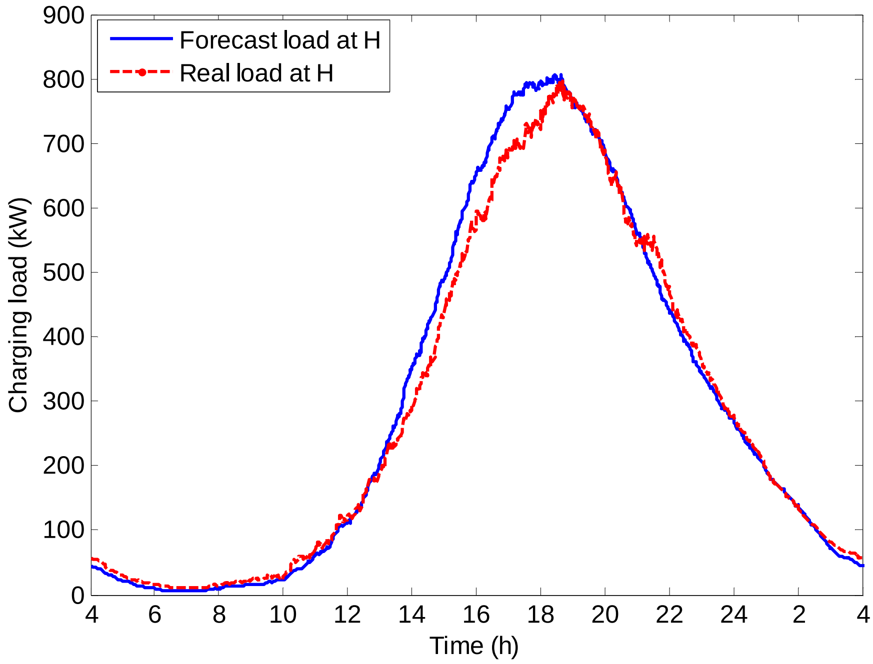

Fig. 2.10: Forecast result validation with scenario of "Highly prefer"

2.6 Summary

In this thesis, a more practical stochastic forecasting model has been proposed with inputs of historical regional travel survey and EV charging preferences. The interrelationship between consecutive trips is linked via STCs to formulate the daily travel route modeling. The charging demand at each location is obtained by taking the arbitrary user charging preference into account. For validation, NHTS data has been used to draw detailed temporal and spatial information of EVs' daily travel route. For validation of the proposed forecast method, a real charging load profile is formulated and compares with results of the stochastic model. The performance is demonstrated to be reliable and can provide useful information for system monitoring and planning of the future smart grid.

Chapter III

System State Estimation Considering EV Penetration with Unknown Behavior Using Quasi-Newton Method

3.1 Introduction

Given a certain level of EV penetration, the results in [6]-[14] show measurable and even significant impacts on not only the distribution system but also the generating system and transmission grids of different scales. Therefore, an improved and universal method of SSE is needed to provide more useful monitoring data due to the growing population of EVs.

The user charging preference is fairly arbitrary as shown in Chapter II and is regarded as unknown behaviors in this chapter. This thesis provides an innovative idea to consider the impact of unknown user behaviors, which leads to spatial and temporal uncertainty of charging demand forecast, on SSE with EV penetration. As existing state estimation methods can hardly handle the unpredictable forecast error brought by distributed charging demand, an improved filter for SSE is proposed combining quasi-Newton (QN) method and Armijo line search (ALS) to minimize the estimation error in various scenarios without exact state forecast formula. The effectiveness of the proposed SSE method is demonstrated in the numerical study and compared with the performance of existing methods.

The rest of this chapter is organized as follows. In Section 3.2, dynamics of forecast load is formulated based on the methodologies proposed in Chapter II. In Section 3.3, the strengths of QN method are illustrated and the forecast loads at different locations are filtered with the proposed method for more accurate estimation. The basic datasets of the case study and the assessment procedures are given in Section 3.4. In Section 3.5, results of the estimation are assessed with different cases and compared with the performance of WLS and EKF methods. Section 3.6 summarizes this chapter.

3.2 Dynamics of Forecast Load

As the exact preferences of EV users are unknown, the charging duration of the customers at public place n is initially assumed to be uniformly distributed in the range of $[D^i_{n,\min}, D^i_{n,\max}]$, which corresponds to the scenario "Moderately Prefer" in Chapter II, for the forecast.

Charging load increment between consecutive time slots at place $n, \Delta\widehat{P}^{\mathrm{EV}}_{n,t}$, can be derived from the above forecast and calculated by deducting the number of EVs stops charging from the number of EVs starts charging at each interval, as described in (3.1)-(3.3):

$$\Delta\widehat{P}^{EV}_{n,t} = \sum_{k}\sum_{i=1}^{M\cdot R_k} P_c\cdot(f^i_{n,k,t} - g^i_{n,k,t}) \tag{3.1}$$

$$f^i_{n,k,t} = \begin{cases} 1, & t = T^i_{n,k},\ \mathrm{A}_n \in \{\mathrm{A}_n\}_k \\ 0, & \text{otherwise} \end{cases} \tag{3.2}$$

$$g^i_{n,k,t} = \begin{cases} 1, & t = T^i_{n,k} + D^i_n + 1,\ \mathrm{A}_n \in \{\mathrm{A}_n\}_k \\ 0, & \text{otherwise} \end{cases} \tag{3.3}$$

where M is the total number of EVs and each EV runs only one complete route during the day. $f^i_{n,k,t}$ and $g^i_{n,k,t}$ are binary variables that reflect the ensuing starting and ending states of charging, respectively, of the ith EV at place n and time t within STC$_k$. The operation interval of this thesis is 1 minute. If the ith EV starts charging at $t = T^i_{n,k}$, the power load is increased at that minute. The charging lasts for D^i_n minutes. At the end of minute $t = T^i_{n,k} + D^i_n$, the charging stops.

For load forecast of the m_b-bus system without considering EV charging, sophisticated methods are described in [33] and [92] which can be directly applied to generate the increment $\Delta\widehat{P}^{\mathrm{base}}_{m,t}$ at bus m, between time t and t-1 in (3.4).

Reactive power $\widehat{Q}_{\mathrm{m},t+1}$ is changed accordingly to keep original power factor constant at each bus. Charging loads of districts $\{\mathrm{A}_n\}=\{\mathrm{A}_1,\mathrm{A}_2,...,\mathrm{A}_N,\mathrm{A}_\mathrm{H}\}$ are added to the corresponding buses $\{n\}$ of the m_b-bus system in (3.5).

$$\widehat{P}_{\mathrm{m},t+1}=\widehat{P}_{m,t}+\Delta\widehat{P}_{m,t}^{base} \tag{3.4}$$

$$\widehat{P}_{n,t+1}=\widehat{P}_{n,t+1}+\Delta\widehat{P}_{n,t}^{EV},\ \{n\}\subseteq\{m\} \tag{3.5}$$

3.3 Problem Formulation

3.3.1 State Filtering with QN Method

The update process of EKF for state estimation is shown in (3.6)-(3.7). It can be inferred from (3.6) that the forecast state error covariance $\boldsymbol{M}$ has much larger influence on the value of Kalman gain than the variation of measurement error $\boldsymbol{R}_z$. As EV charging load is integrated with unknown charging preference, the forecast state error covariance cannot be accurate, making the application of EKF method ineffective.

$$\text{Kalman gain:}\quad \boldsymbol{K}=\boldsymbol{M}\cdot\boldsymbol{H}^T\cdot(\boldsymbol{H}\cdot\boldsymbol{M}\cdot\boldsymbol{H}^T+\boldsymbol{R}_z)^{-1} \tag{3.6}$$

$$\text{Updated state estimate:}\quad \tilde{\boldsymbol{x}}=\hat{\boldsymbol{x}}+\boldsymbol{K}\cdot(\boldsymbol{z}-h(\hat{\boldsymbol{x}})) \tag{3.7}$$

Compared to TWLS method which starts from phase angle $\theta_m=0$ and voltage $V_m=1$ of each bus, SSE methods use forecast states obtained from forecast system load with power flow analysis, $\hat{\boldsymbol{x}}_{t+1}=[\hat{\theta}_{1,t+1},...,\hat{\theta}_{m_b,t+1},\widehat{V}_{1,t+1},...,\widehat{V}_{m_b,t+1}]$, as the initial guess before state filtering. When the measurement $\boldsymbol{z}$ from the RTUs at different places becomes available after a delay, WLS is formulated based on a nonlinear minimization of the objective $J(\boldsymbol{x})$:

$$J(\boldsymbol{x})=\frac{1}{2}[\boldsymbol{z}-\boldsymbol{h}(\boldsymbol{x})]^T\boldsymbol{R}_z^{-1}[\boldsymbol{z}-\boldsymbol{h}(\boldsymbol{x})]=\frac{1}{2}\boldsymbol{r}^T\boldsymbol{R}_z^{-1}\boldsymbol{r} \tag{3.8}$$

$$\boldsymbol{z}=\boldsymbol{h}(\boldsymbol{x})+\boldsymbol{e} \tag{3.9}$$

where $\boldsymbol{h}(\boldsymbol{x})$ is the power flow equations corresponding to the types of $\boldsymbol{z}$ and $\boldsymbol{r}$ is the estimation residual. Measurements gathered from RTUs usually come with stochastic errors $\boldsymbol{e}$, where $\boldsymbol{e}_j\sim N(0,\sigma_j)$. $\boldsymbol{R}_z=diag\{\sigma_1^2,...,\sigma_j^2\}$ is the measurement error covariance and its reciprocal is regarded as weights in (3.8).

$\boldsymbol{H}$ is the Jacobian matrix of $\boldsymbol{h}(\boldsymbol{x})$ and the first-order optimal condition of $J(\boldsymbol{x})$ is given as follows:

$$\boldsymbol{J}'(\boldsymbol{x}) = -\sum_j \frac{r_j}{\sigma_j^2} \frac{\partial h_j(\boldsymbol{x})}{\partial \boldsymbol{x}} = -\boldsymbol{H}^T \boldsymbol{R}_z^{-1} \boldsymbol{r} = 0 \tag{3.10}$$

The Taylor expansion approximates the gradient function by ignoring higher orders:

$$\boldsymbol{J}'(\boldsymbol{x})|_{(\boldsymbol{x}+\Delta \boldsymbol{x})} = \boldsymbol{J}'(\boldsymbol{x})|_{(\boldsymbol{x})} + \boldsymbol{J}''(\boldsymbol{x})|_{(\boldsymbol{x})} \cdot \Delta \boldsymbol{x} = 0 \tag{3.11}$$

where,

$$\begin{aligned} \boldsymbol{J}''(\boldsymbol{x}) &= \sum_j \frac{1}{\sigma_j^2} \frac{\partial h_j(\boldsymbol{x})}{\partial \boldsymbol{x}} \left(\frac{\partial h_j(\boldsymbol{x})}{\partial \boldsymbol{x}}\right)^T - \sum_j \frac{r_j}{\sigma_j^2} \frac{\partial^2 h_j(\boldsymbol{x})}{\partial \boldsymbol{x}^2} \\ &= \boldsymbol{H}^T \boldsymbol{R}_z^{-1} \boldsymbol{H} - \sum_j \frac{r_j}{\sigma_j^2} \frac{\partial^2 h_j(\boldsymbol{x})}{\partial \boldsymbol{x}^2} \end{aligned} \tag{3.12}$$

WLS adopts Gauss-Newton method which only uses gain matrix $\boldsymbol{G} = \boldsymbol{H}^T \boldsymbol{R}_z^{-1} \boldsymbol{H}$ to replace the Hessian matrix $\boldsymbol{J}''(\boldsymbol{x})$ in (3.12) for simplicity and acceptable accuracy. However, when power system nonlinearity coincides with topology errors or sudden large load changes, WLS shows inferior performance [31].

If we use Newton method with accurate Hessian matrix, problems still exist. Firstly, Newton method is not globally convergent [93] and the Hessian matrix may not always be positive definite when forecast states with unknown factors is far away from the local minimizer. Secondly, Hessian matrix is hard to calculate, especially for large power systems.

This thesis proposes an effective filter based on QN method which approximates the inverse of Hessian matrix $(\boldsymbol{J}''(\boldsymbol{x}))^{-1}$ by a symmetric positive definite matrix $\boldsymbol{B}$ and updates at each iteration. The Broyden–Fletcher–Goldfarb–Shanno (BFGS) formula [93] is currently the most widely used QN method because it does better for low accuracy line searches and is globally convergent when conditions (3.14)-(3.15) hold. Its algorithm with ALS [94] is given below:

The initial point $\hat{\boldsymbol{x}}_t^{(1)}$ at time t, convergence criterion ε >0, 0< λ <1, 0< c_1 < c_2 <1, iteration sequence q=1 and unit matrix $\boldsymbol{B}^{(1)}$ are given.

While $\left|\boldsymbol{J}'(\boldsymbol{x}^{(q)})\right| \geq \varepsilon$

(i) (Newton's Step) Determine a search direction $\boldsymbol{s}^{(q)}$ at the qth iteration:

$$\boldsymbol{s}^{(q)} = -\boldsymbol{B}^{(q)} \cdot \boldsymbol{J}'(\boldsymbol{x}^{(q)}) \tag{3.13}$$

(ii) (ALS's Step) Find the smallest nonnegative integer u such that $\alpha^{(q)} = \lambda^u$ satisfies:

$$J(\boldsymbol{x}^{(q)} + \alpha^{(q)}\boldsymbol{s}^{(q)}) \leq J(\boldsymbol{x}^{(q)}) + c_1\alpha^{(q)}(\boldsymbol{s}^{(q)})^T \boldsymbol{J}'(\boldsymbol{x}^{(q)}) \tag{3.14}$$

$$\left|\boldsymbol{J}'(\boldsymbol{x}^{(q)} + \alpha^{(q)}\boldsymbol{s}^{(q)})^T \cdot \boldsymbol{s}^{(q)}\right| \leq -c_2(\boldsymbol{s}^{(q)})^T \boldsymbol{J}'(\boldsymbol{x}^{(q)}) \tag{3.15}$$

(iii) Set $\boldsymbol{x}^{(q+1)} = \boldsymbol{x}^{(q)} + \alpha^{(q)}\boldsymbol{s}^{(q)}$ (3.16)

(iv) (BFGS method update) Suppose $\boldsymbol{d}^{(q)} = \boldsymbol{x}^{(q+1)} - \boldsymbol{x}^{(q)}$ and $\boldsymbol{y}^{(q)} = \boldsymbol{J}'(\boldsymbol{x}^{(q+1)}) - \boldsymbol{J}'(\boldsymbol{x}^{(q)})$, $\boldsymbol{B}$ matrix is updated:

$$\begin{aligned}\boldsymbol{B}^{(q+1)} &= \boldsymbol{B}^{(q)} + \left(1 + \frac{(\boldsymbol{y}^{(q)})^T \boldsymbol{B}^{(q)} \boldsymbol{y}^{(q)}}{(\boldsymbol{d}^{(q)})^T \boldsymbol{y}^{(q)}}\right) \frac{\boldsymbol{d}^{(q)}(\boldsymbol{d}^{(q)})^T}{(\boldsymbol{d}^{q})^T \boldsymbol{y}^{(q)}} \\ &\quad - \frac{\boldsymbol{d}^{(q)}(\boldsymbol{y}^{(q)})^T \boldsymbol{B}^{(q)} + \boldsymbol{B}^{(q)}\boldsymbol{y}^{(q)}(\boldsymbol{d}^{(q)})^T}{(\boldsymbol{d}^{q})^T \boldsymbol{y}^{(q)}}\end{aligned} \tag{3.17}$$

$$q = q + 1 \tag{3.18}$$

End

With the help of QN method, matrix $\boldsymbol{B}$ replaces $(\boldsymbol{J}''(\boldsymbol{x}))^{-1}$ to formulate a new Newton's step in (3.13) which avoids formidable matrix inverse of large systems and a possible singular $\boldsymbol{J}''(\boldsymbol{x})$ in case forecast is far from the optimum. Matrix B is proved to be always positive definite with BFGS update [93] to ensure a descending search direction in (3.13). Criteria (3.14) and (3.15) are called strong Wolfe conditions [94] guaranteeing that the step length α decreases $J(\boldsymbol{x})$ and $\boldsymbol{J}'(\boldsymbol{x})$ sufficiently to accelerate convergence.

The estimated $\tilde{P}_{m,t}$ and $\tilde{Q}_{m,t}$ are calculated by the estimated states $\tilde{\boldsymbol{x}}_t$, which is the minimizer of $J(\boldsymbol{x})$. $\tilde{P}_{m,t}$ and $\tilde{Q}_{m,t}$ are then regarded as the forecast $\hat{P}_{m,t}$ and $\hat{Q}_{m,t}$ when entering the forecast of the next time slot in (3.4) and (3.5) to rule out errors in the previous time slot in SSE.

3.3.2 Summary of the Whole Estimation Process

The complete closed-loop procedure is summarized in Fig. 3.1. The first block "EV Charging Forecast" is done once a day with historical travel data. At the beginning of each minute, the input of the loop includes forecast load increment and immediate measurements gathered from RTUs. Together with the methodology provided above, accurately estimated system states are the expected output. $\widehat{P}_{m,t}$ and $\widehat{Q}_{m,t}$ are then updated to adapt to the forecast errors of charging demand at that minute.

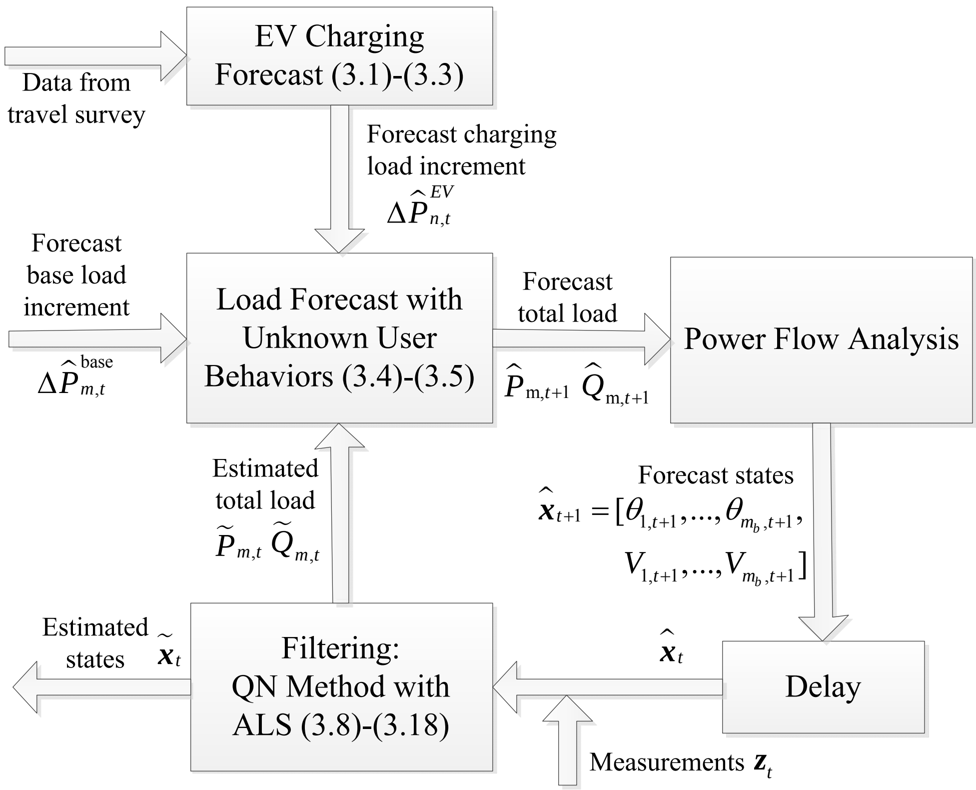

Fig. 3.1: Structure of the proposed SSE method

3.4 Numerical Study

3.4.1 Data of Travel Survey

In this study, the transportation dataset for forecast is also derived from weekdays' urban records in NHTS. Other data related to the travel forecast is the same with Chapter II.

For the actual travel data, records around Sept. 9 in NHTS are used directly in this thesis. Unlike the uniform distribution assumed in the forecast, the real charging duration of the *i*th EV at public charging station *n* is determined as a given portion of the maximum possible range:

$$D_n^{i,real} = 0.8 \times (\max(D_n^i) - \min(D_n^i)) \tag{3.19}$$

where the details are subject to adjustment if credible user charging records are available in the future.

3.4.2 Test Systems and Measurements

The IEEE 14-bus test system [39], composed of both distribution and transmission networks, is used for the case study. The part of distribution network is shown in [95], including buses 6, 9, 10, 11, 12, 13 and 14 of the test system. The charging stations are connected to the distribution network (W-6, H-9, SE-10, SR-13 and O-14). Recorded load data of New York City (NYC) on Sept. 9, 2014 from New York Independent System Operator (NYISO) [96] is depicted as the red solid line in Fig. 3.2 and used as real data to formulate $\Delta P_{m,t}^{base,real}$.

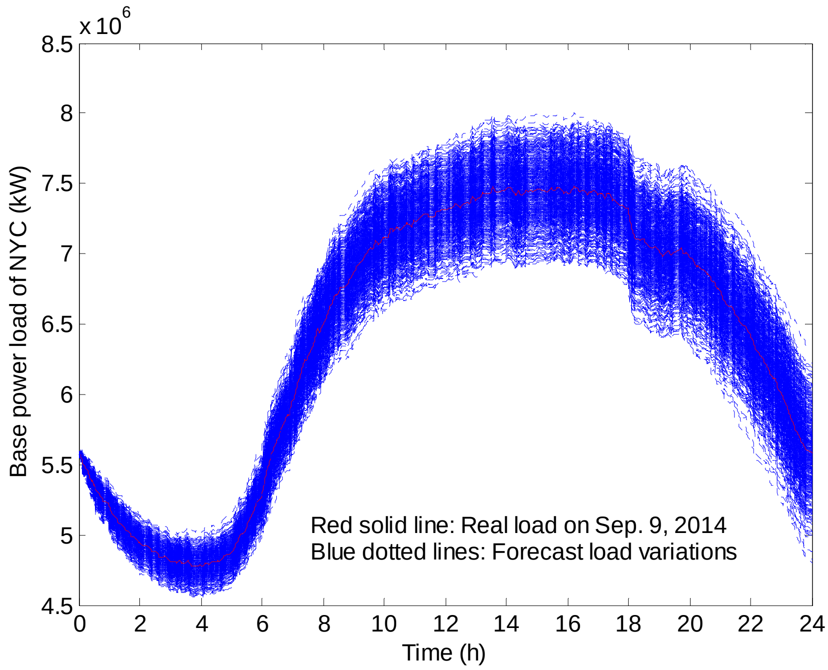

Fig. 3.2: Real and forecast base load of NYC

The forecast base load increment is fully predictable and is simply assumed to follow normal distribution with both mean and magnitude of variance equal to $\Delta P_{m,t}^{base,real}$ as shown in (3.20).

$$\Delta \widehat{P}_{m,t}^{base} \sim N(\Delta P_{m,t}^{base,real}, |\Delta P_{m,t}^{base,real}|) \tag{3.20}$$

For validation, the load at t=0 min is increased by the amount of randomly generated forecast increment (according to (3.20)) minute by minute until reaching t=1440 min to constitute the daily forecast load. The process is repeated for 1000 times and the daily forecast load variations are depicted as the dotted lines in Fig. 3.2. It is found that the dotted area in Fig. 3.2 matches the 99% confidence interval of the normal distribution derived from the real data.

In order to make it compatible with EV charging load, the original load data from NYISO with time intervals of 5 min each are interpolated to a per-minute base. The practically used real states and real measurements in the per-minute unit are generated as below:

1) Determine the operation starting time of SSE. Normalize the actual load from NYISO at the operation starting time to the initial active and reactive load at each bus of the 14-bus system. The per unit value of active and reactive power dynamics are obtained accordingly.
2) Determine the number of EVs that charge from the power grid. From (3.1)-(3.3), the real charging load dynamics are obtained with travel records and real charging durations. The charging power is also changed to per unit value.
3) The real total load dynamics is calculated by (3.4)-(3.5). Find the real system states $\boldsymbol{x}_t^{\text{real}} = [\theta_{1,t}^{\text{real}},...,\theta_{m_b,t}^{\text{real}},V_{1,t}^{\text{real}},...,V_{m_b,t}^{\text{real}}]$ of each time slot from the solution of power flow analysis.
4) Calculate the accurate measurement data $\boldsymbol{z}_t^{real} = \boldsymbol{h}(\boldsymbol{x}_t^{real})$ from the real states at each time slot. Add Gaussian measurement errors with zero mean and standard deviations σ_v =0.004, σ_{inj} =0.01 and σ_f =0.008 [21] to all the accurate voltage, power injection and power flow measurements, respectively, to constitute the real measurements.

For the IEEE 30-bus test system [40], its part of distribution network is also shown in [95]. The one-day data in NYISO is normalized as well with active and reactive load at all buses. EV charging stations are located at the buses of distribution network (W-12, H-21, SE-15, SR-17 and O-30). Remaining procedures are the same as the case of 14-bus system.

The base case containing 100 thousand EVs is investigated with full observability and the measurement errors listed above. Full observability to the IEEE 14-bus system includes measurements of voltage at bus 1 and 2, active/reactive power injection at 28 buses and active/reactive power flow at 40 lines. The IEEE 30-bus system includes the same two bus voltage measurements, 60 power injection and 82 power flow measurements. There are no bus voltage measurements installed at buses of the distribution networks.

3.4.3 Performance Indicators

The estimated states are compared with the real states for performance assessment. The performance indicators of this thesis include the daily average of the relative absolute phase and voltage errors in (3.21) and (3.22) as well as the summation of all state errors at each minute in (3.23).

$$\xi^{\theta} = \frac{1}{1440(m_b - 1)} \sum_{t=1}^{1440} \sum_{m=2}^{m_b} \left| \frac{\tilde{\theta}_{m,t} - \theta_{m,t}^{\mathrm{real}}}{\theta_{m,t}^{\mathrm{real}}} \right| \tag{3.21}$$

$$\xi^{V} = \frac{1}{1440 \cdot m_b} \sum_{t=1}^{1440} \sum_{m=1}^{m_b} \left| \frac{\tilde{V}_{m,t} - V_{m,t}^{\mathrm{real}}}{V_{m,t}^{\mathrm{real}}} \right| \tag{3.22}$$

$$\psi_t = \frac{1}{m_b - 1} \sum_{m=2}^{m_b} \left| \frac{\tilde{\theta}_{m,t} - \theta_{m,t}^{real}}{\theta_{m,t}^{real}} \right| + \frac{1}{m_b} \sum_{m=1}^{m_b} \left| \frac{\tilde{V}_{m,t} - V_{m,t}^{real}}{V_{m,t}^{real}} \right| \tag{3.23}$$

The performance of different estimators, namely TWLS, SSE with Gauss-Newton method (SSE-WLS), SSE with QN method (SSE-QN) and EKF, is assessed by cases with different levels of EV penetration, measurement error and observability. When one variable changes in each case, other variables are kept the same as in the base case.

3.5 Test Results

3.5.1 Real and Forecast Charging Load

As the EV charging load forecast is introduced with unknown user behaviors, the distribution of charging starting time and travel distance can be forecast with accuracy while how long an EV will be charged at each place can only be defined within a broad range. The stochastic distribution of EV charging load in the base case is shown in Fig. 3.3, where loads in SR and O are omitted for clarity of the figure. Compared to the real charging load, although the user charging behavior is unknown, the forecast load at each place successfully indicates its range and peak hours. The difference between real and forecast load at place W and H is much larger during peak hours (31.63% and 29.13% of real load, respectively) and it is expected to increase with the number of EVs. However, the difference could be smaller in practical situations as the preferred charging duration may have a wide-range distribution rather than a given portion in (3.19), provided an EV charging survey is available in the future.

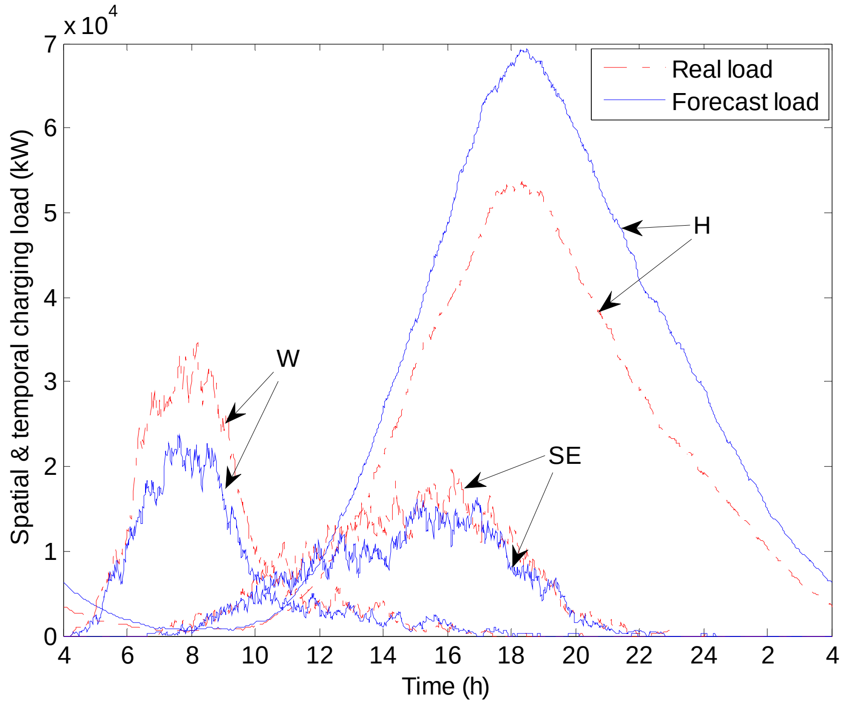

Fig. 3.3: Charging load comparison with 100 thousand EVs

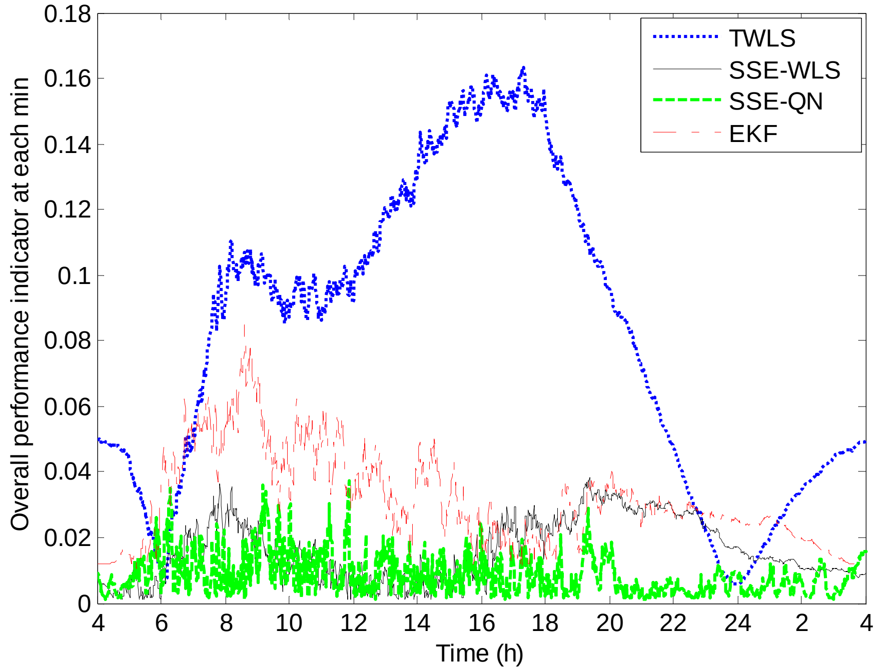

Fig. 3.4: Daily performance ψ_t in the base case

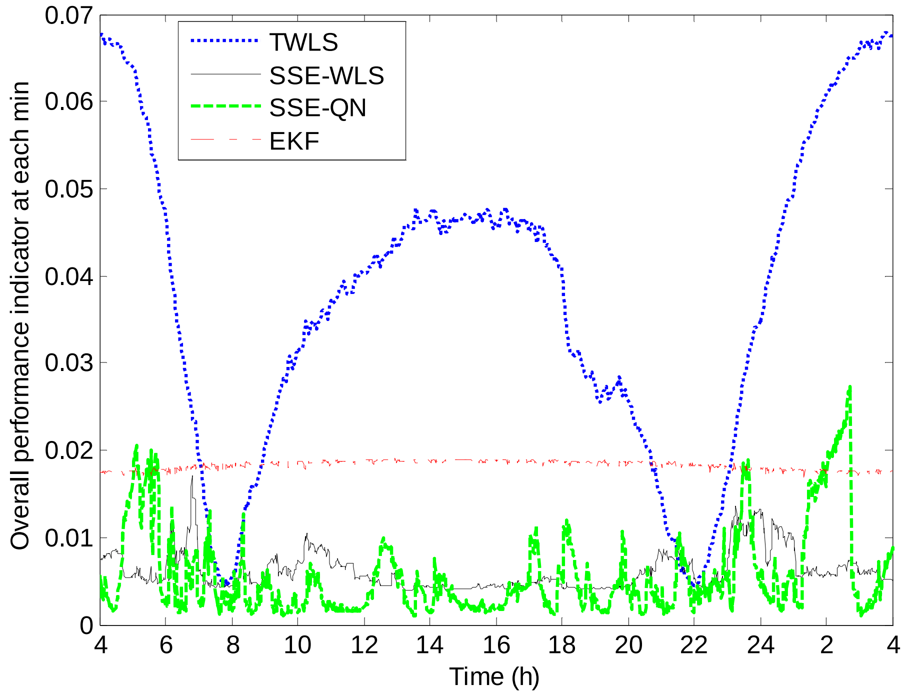

Fig. 3.5: Daily performance ψ_t in the case without EV

3.5.2 Daily Variation of Estimation Error

To examine the integrated effect of the forecast errors at different buses in Fig. 3.3 and the forecast errors of base load in (3.20), daily variations of ψ_t with time are shown in Fig. 3.4 and Fig. 3.5 for the base case and the case without

EVs, respectively. As the weights in (3.8) are assigned to get the overall best estimation of all states [23], ψ_t .can clearly tell the source of system-wise estimation error at each minute.

Because TWLS method starts from $\theta_m = 0$ and $V_m = 1$ of each bus, which is independent of forecast results, it is expected that the more the real measurements deviate from their rated values, the comparatively lager estimation error will be generated. In the base case, the first two peak errors occur around 8:00 and 17:00 when the peaks of charging load at W and H coincide with heavy base load. The third one is during the small hours (24:00 to 6:00) when base load reaches the lowest, which is far below its rated value. The estimation error around 17:00 is largely reduced by 71.01% in the case without EV integration.

From the EKF formula (3.6)-(3.7), forecast state error covariance plays a crucial role in state filtering. In the base case, the unknown charging behavior makes the forecast state error covariance unreliable. The estimation error of EKF peaks at around 8:00 a.m. when the forecast load error at W is the highest. It is because fewer EVs being charged at W than at H that results in more randomness in the forecast state error covariance. In the case without EV, the estimation error stays around 0.018 and relatively unchanged with time because the forecast error of base power load is predictable.

In the base case, with the updating procedure of the forecast $\widehat{P}_{m,t}$ and $\widehat{Q}_{m,t}$, and the use of forecast states as the initial guess, overall the SSE-WLS has better performance than TWLS. But it still lacks accuracy during periods in Fig. 3.3 when difference between real and forecast loads is large because of the Gauss-Newton method used in filtering stage. The estimation accuracy of SSE-QN is comparatively unaffected by the variation of forecast error and has the overall best performance along the day. In the case without EVs, approximation of the Hessian matrix in SSE-QN cannot outperform the Gauss-Newton method used in SSE-WLS, because the base load is predictable and the forecast states are not far from the minimizer of (3.8).

3.5.3 Cases with Increased EV Penetration

As EV penetration increases, its impact on power grid is expected to be higher and the requirement for a more accurate and fast-response SSE estimator becomes more serious. Figs. 3.6 and 3.7 respectively show the trends of ξ^{θ} and ξ^{V} in IEEE 14-bus system when EV penetration increases from 0 to 150 thousands. The estimation error of the SSE-QN method is always the lowest except that its ξ^{θ} is slightly higher than that of SSE-WLS method when there is no EV penetration. The errors of the other three estimators manifest an uptrend with the increase of EV population except that the ξ^{V} of EKF remains almost the same. Figs. 3.8 and 3.9 show the respective trends in IEEE 30-bus system. Comparatively, the slopes for the 30-bus system are lower. Because the scale of the 30-bus system is much larger so that the EV charging load takes smaller parts of the total load and imposes less impact on the original network. When EV population is no larger than 50 thousand, the forecast error of charging demand is too small compared to the 30-bus base power load that the estimator of SSE-WLS is better than SSE-QN regarding ξ^{θ} .

A computer with Intel i5 CPU and 4G RAM was used for the case study. The daily average computation time required (all shown in milliseconds in Tables 3.1 to 3.3) for state estimation of minute intervals is shown in Table 3.1. It generally requires more time to complete the estimation when EV population increases or the system scale increases. In our study, SSE-QN needs the least number of iterations in both systems at all levels of EV penetration to complete the daily estimation, indicating fastest convergence. However, the process of searching $\alpha^{(q)}$ in the ALS's step makes its computation time close to SSE-WLS. EKF is a non-iterative estimator; however, the need to prepare the forecast state error covariance at each interval makes it slower than SSE-QN.

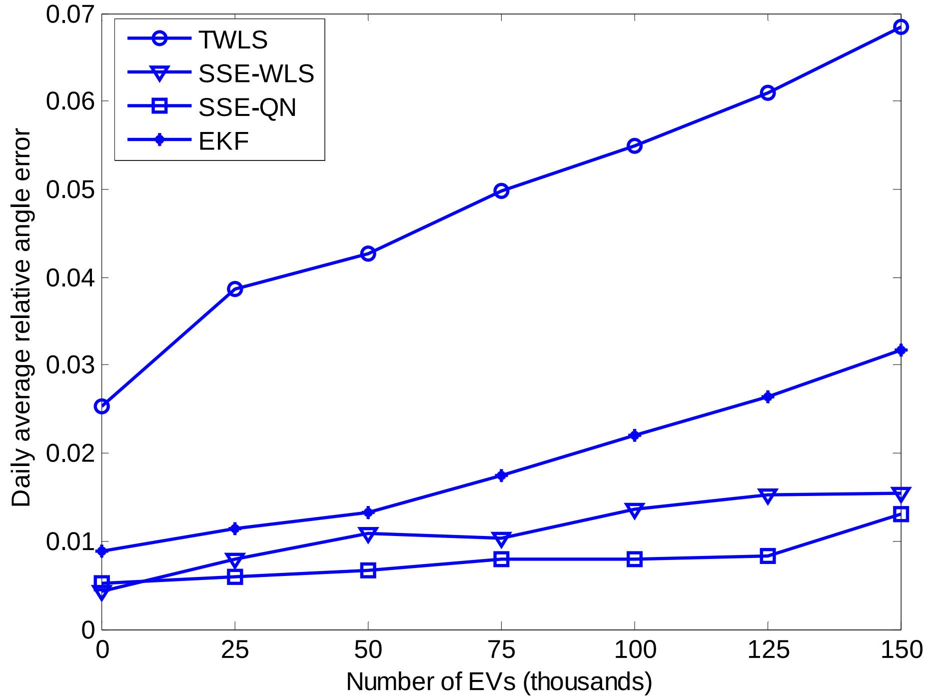

Fig. 3.6: Estimators comparison regarding ξ^{θ} in IEEE 14-bus system

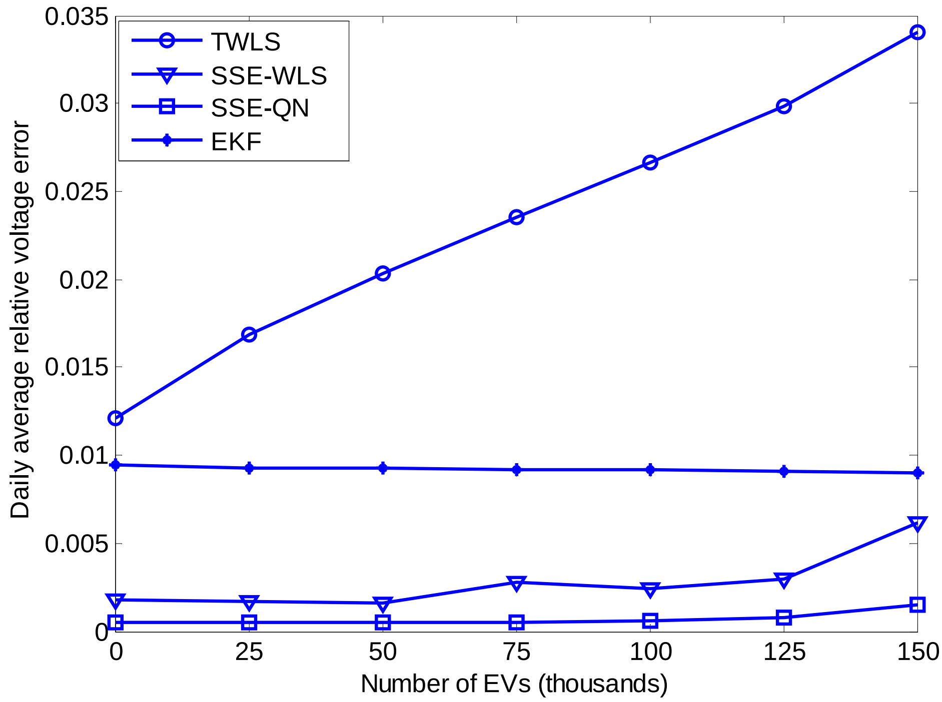

Fig. 3.7: Estimators comparison regarding ξ^{V} in IEEE 14-bus system

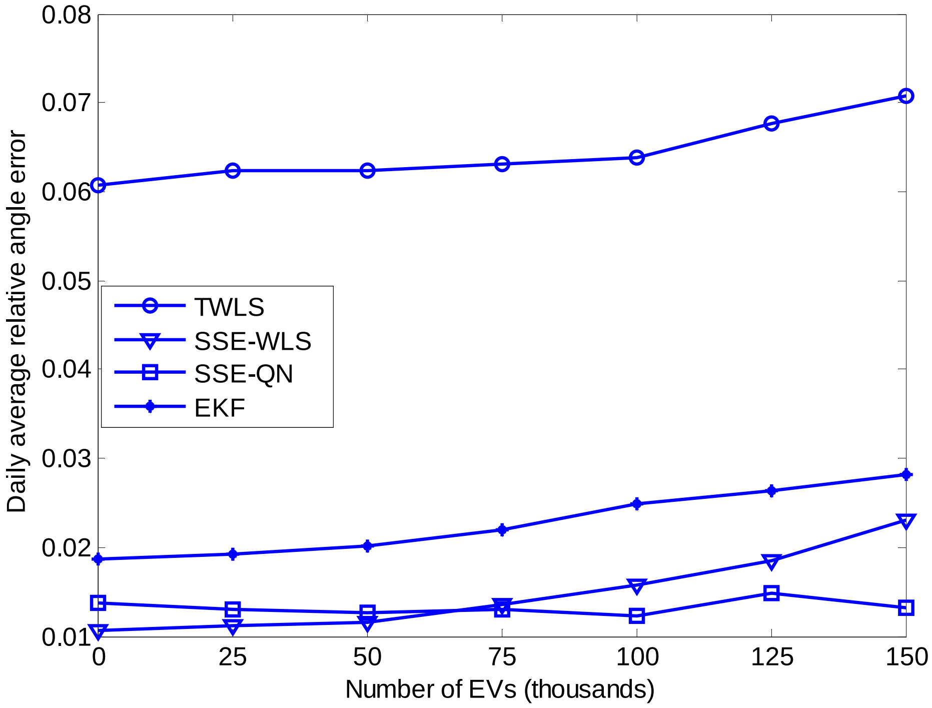

Fig. 3.8: Estimators comparison regarding ξ^{θ} in IEEE 30-bus system

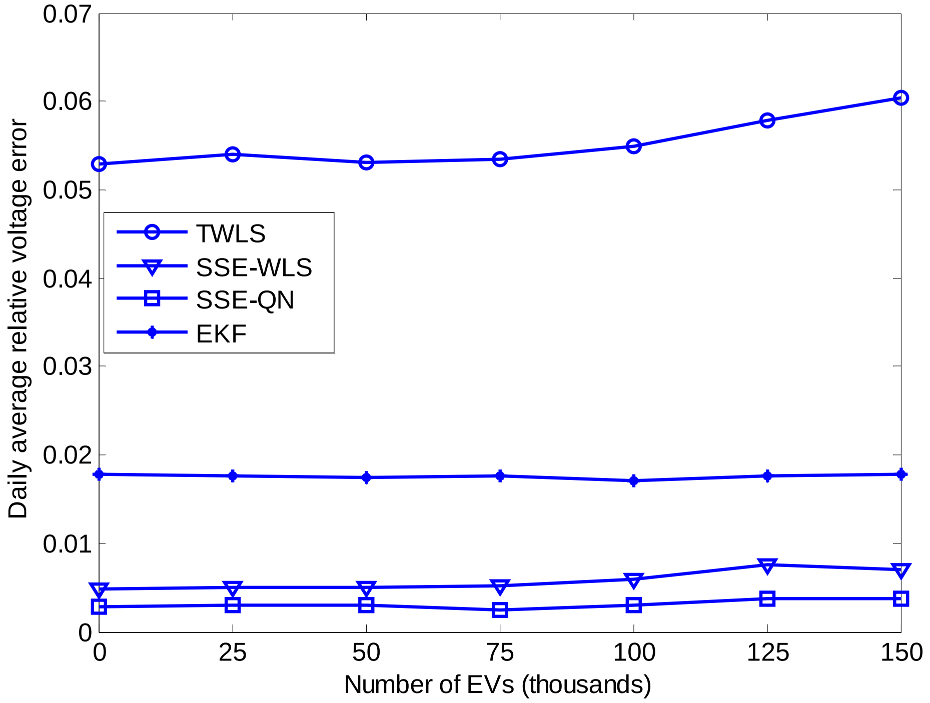

Fig. 3.9: Estimators comparison regarding ξ^{V} in IEEE 30-bus system

Table 3.1: Daily average computation time (ms) of Section 3.5.3

EVs	TWLS		SSE-WLS		SSE-QN		EKF	
	14 bus	30 bus	14 bus	30 bus	14 bus	30 bus	14 bus	30 bus
0	145	476	16	124	17	132	560	1182
50	151	485	18	138	17	140	583	1191
100	152	560	22	159	20	155	561	1244
150	160	583	29	161	24	158	568	1256

3.5.4 Cases with Increased Measurement Errors

Affected by aging or random faults of the meters, the distribution of measurement error may differ from the standard deviation in Section 3.4.2 without any notice. This section then investigates the adaptability of these estimators to the measurement error variations in the distribution network, as given by Figs. 3.10, 3.11 and Table 3.2, where the variance of all measurement errors is varied among 0.5, 1,…, 2.5 times of $\{\sigma_v, \sigma_{inj}, \sigma_f\}$ in the base case.

The estimation error of EKF remains almost the same regarding both ξ^θ and ξ^V when measurement error increases. This is because the weight of forecast state error covariance is much higher than measurement error in the gain matrix of EKF. For the performance of SSE-WLS and SSE-QN, the slopes in the variation of ξ^θ are generally larger than that of ξ^V. The estimation error ξ^θ of SSE-WLS increases a lot with the augmentation of measurement error level and exceeds that of EKF at level 2.5×. The variation for SSE-QN is much smaller, indicating the best adaptability of SSE-QN to the change of measurement errors. Different from the case of EV penetration increase which influences the real measurements of several selected buses, all measurements in this section change in the same proportion. The estimation errors and average computation time of TWLS therefore do not change much. The computation time of the rest estimators increases with measurement error level.

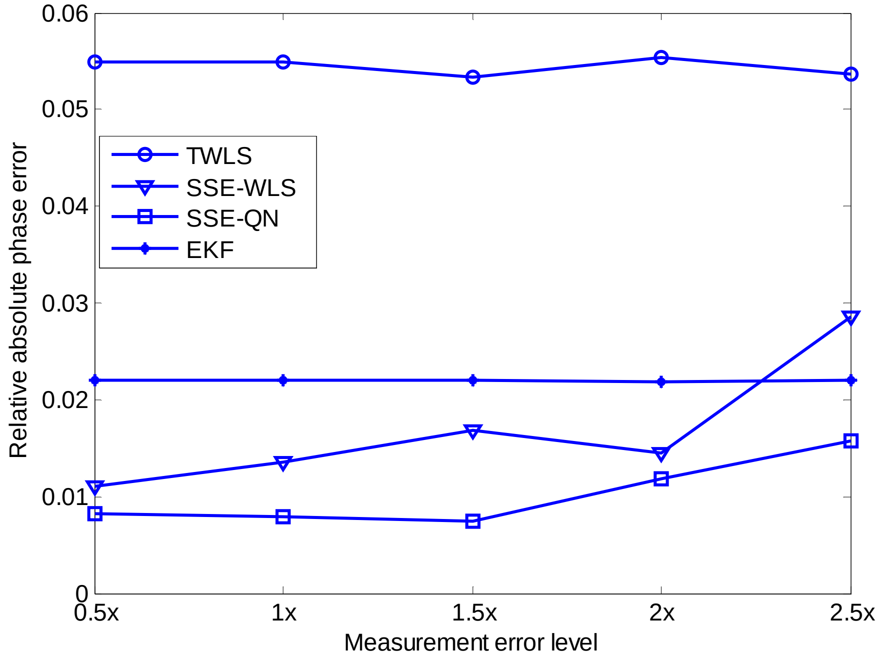

Fig. 3.10: Performance regarding ξ^{θ} with increased measurement errors

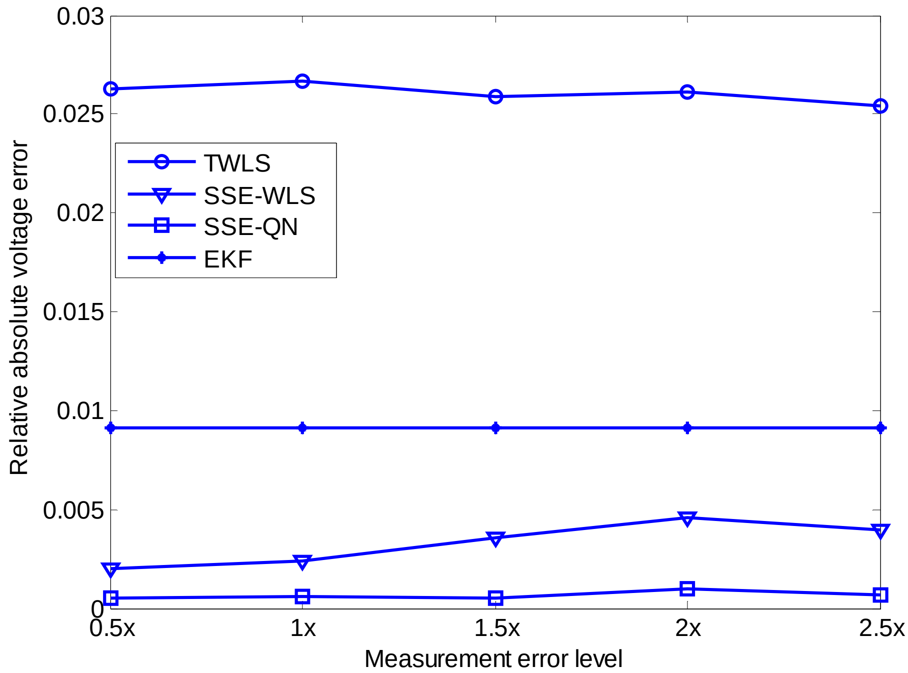

Fig. 3.11: Performance regarding ξ^{V} with increased measurement errors

Table 3.2: Daily average computation time (ms) of Section 3.5.4

Error level	TWLS	SSE-WLS	SSE-QN	EKF
0.5×	155	22	20	553
1×	152	22	20	561
1.5×	148	24	22	560
2×	154	25	23	565
2.5×	150	27	24	569

3.5.5 Cases without Full Observability

Constrained by the construction cost and possible commutation failure, the system state estimation may perform under weak observability of the distribution network. This section tests cases where measurements at buses with charging stations are unavailable, to emphasize the estimator performance under stochastic EV penetration. The results are given in Table 3.3. Case E1 operates with unavailable active/reactive power load measurements of W-6, H-9 in IEEE 14-bus. All active/reactive load measurements of buses with EV penetration are unavailable in Case E2.

It is shown in Table 3.3 that the estimation error of EKF still changes little with different degrees of observability. It is affected more by the reliability of the forecast procedure. For TWLS and SSE-WLS, both the estimation errors and average computation time increase drastically when measurements at W and H become unavailable, indicating their inferior performance compared to that of SSE-QN. In case E2, where all load measurements at W, H, SE, SR and O are unavailable, the matrix $\boldsymbol{G} = \boldsymbol{H}^T \boldsymbol{R}_z^{-1} \boldsymbol{H}$ becomes singular and TWLS fails to find the minimizer of $J(\boldsymbol{x})$ at the first minute while SSE-WLS fails after several intervals when the forecast error is larger. The results show that SSE-QN is able to solve the problem of insufficient observability with faster and more accurate estimation because the matrix $\boldsymbol{B}$ in QN method is kept positive definite to simulate $(\boldsymbol{J}''(\boldsymbol{x}))^{-1}$ so that singular $\boldsymbol{J}''(\boldsymbol{x})$ is avoided.

Table 3.3: Performance with different degrees of observability

Case	Base Case		Case E1		Case E2	
	$\xi^{\theta}+\xi^{V}$	Time (ms)	$\xi^{\theta}+\xi^{V}$	Time (ms)	$\xi^{\theta}+\xi^{V}$	Time (ms)
TWLS	0.08164	152	0.12231	594	N/A	N/A
SSE-WLS	0.01599	22	0.03456	37	N/A	N/A
SSE-QN	0.00858	20	0.01474	21	0.01654	23
EKF	0.03119	561	0.03165	563	0.03151	565

3.5.6 Bad Data Detection

As the effectiveness of bad data detection for Kalman filters and WLS has already been proved by [38], [39] and [92] in cases without EVs, this thesis identifies the gross errors during SSE-QN method through a set of normalized residuals (NRs) defined in (3.24).

$$NR_{j,t} = \frac{\left| z_{j,t} - h_j(\tilde{\boldsymbol{x}}_t) \right|}{\sqrt{\boldsymbol{\Omega}_{jj,t}}} \tag{3.24}$$

As the forecast states in this thesis are obtained with unknown EV charging behaviors, the bad data detection is possible only with the reliable estimated states $\tilde{\boldsymbol{x}}_t$, differing from the "pre-estimation" method provided in [92]. The reader is referred to [23] for details.

In the base case and the case without EVs mentioned previously, the faulty measurements (bad data) are set up by adding gross errors to the corresponding real measurements at 17:00, including 0.1 p.u. to the voltage magnitude at bus 2 as well as 0.2 p.u. to the active power injection at bus 6 and the active power flow of line 9-14 in the distribution network. When the process of SSE-QN method comes to t=1020 min, the bad data occurs and the detection results are shown in Table 3.4.

Table3.4: Performance of bad data detection

Measurement	$NR_{j,1020}$	
	Base Case	Case without EVs
Voltage magnitude of bus 2 (bad data)	19.84	22.90
Voltage magnitude of bus 1 (non-bad data)	5.31	3.76
Active power injection of bus 6 (bad data)	62.79	25.65
Active power injection of bus 8 (non-bad data)	5.65	3.72
Active power flow of line 9-14 (bad data)	18.59	17.02
Active power flow of line 13-14 (non-bad data)	4.76	2.74

It is denoted from Table 3.4 that the NRs are much higher corresponding to the faulty measurements. The lowest NR value of the bad data is 18.59/5.65=3.29 and 17.02/3.76=4.53 times more than the highest NR value of the non-bad data for the base case and the case without EVs, respectively. The detection threshold is selected based on the desired level of detection sensitivity [23]. When the threshold is chosen to be too high (18, for example), some bad data in the power flow measurements cannot be detected. While the threshold is chosen to be too low (4, for example), some measurements of the load buses with EV penetration may be falsely detected as bad data.

Simulations have shown that the bad data detection is effective with SSE-QN method when detection threshold is chosen to be 10. After elimination of bad data, state estimation and detection is repeated using the modified measurement set until no NRs surpassing the threshold. According to the results in Section 3.5.5, the reduction of measurements caused by bad data elimination may impair the estimation accuracy when using TWLS and SSE-WLS methods while the influence is largely reduced with SSE-QN method.

3.6 Summary

This thesis takes cognizance of EV charging uncertainties in the realm of SSE which finds that the average SSE error brought by EV penetration is quite remarkable on the whole system level. A faster, more accurate and more reliable state estimation with QN method is proposed to alleviate such influence. The feasibility of the proposed forecast method that considers unknown factors is first demonstrated by the superiority of SSE-WLS to TWLS. The test results have shown that the proposed SSE-QN constantly outperforms TWLS, SSE-WLS and EKF especially when EV penetration becomes larger or the measurement error level increases. Besides, SSE-QN also performs well when observability is insufficient or bad data exists. It shows great reliability in the circumstance of potential measurement malfunction. Applications of this SSE-QN estimator are needed to formulate a faster and more effective information collection and control scheme facing the growing penetration of EVs in the future smart grid.

Chapter IV

Inventory Management of DSCC System via Improved (s, S) Model

4.1 Introduction

The increasing penetration of EVs leads to the augmentation of stochastic EV charging demand, as presented by the results of EV charging forecast and system monitoring. The adequacy of battery charging facilities can be one of the major obstacles to the popularization of EVs.

Generally, battery charging and battery swapping are two feasible methods for refilling depleted batteries. Different from the situation of charging at home, the waiting time of the battery replenishment along the highways should be as short as possible because people may have urgent tasks at hands or easily get bored in the charging stations. Therefore, this thesis proposes the distributed swapping & centralized charging (DSCC) system along the highways to satisfy the demand of quick battery replenishment. As the daily traffic conditions of different roads are distinct, the proposed DSCC system maximizes battery inventory turnover rate and minimize daily total power variations of the planned stations with the help of an improved (*s*, *S*) inventory management model.

The rest of this chapter is organized as follows. Section 4.2 describes the daily EV arrival rate of certain highway stations in relation to the nearby traffic conditions. The operation of swapping stations and centralized charging stations is put forward in Section 4.3 which regulates battery charging and dispatching according to the improved (s, S) inventory management. Section 4.4 investigates possible control schemes to minimize the needed batteries for suppliers or the impact on the power grid. Simulation results are provided in Section 4.5 to verify the feasibility of the proposed system. Section 4.6 summarizes this chapter.

4.2 Highway Model Formulation

Deployment of swapping stations along a unidirectional single-lane highway is shown in Fig. 4.1 considering the condition of roads including the topology of traffic network and length of each branch. The initial state-of-charge of the ith EV SOC_{ini}^{i} is assumed when coming by the swapping station and the distance between two consecutive stations is l. The path shown in Fig. 4.2 demonstrates the situation with multiple crossroads which is still composed of several basic unidirectional highways.

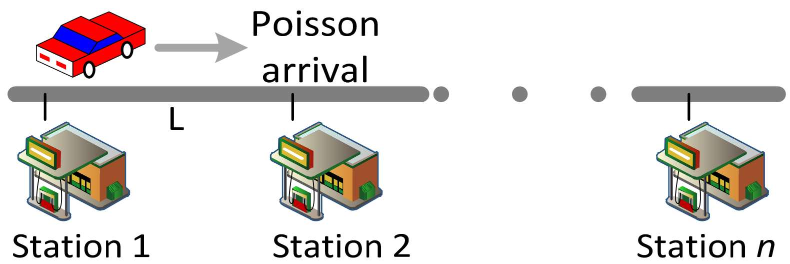

Fig. 4.1: Swapping stations along a unidirectional single-lane highway

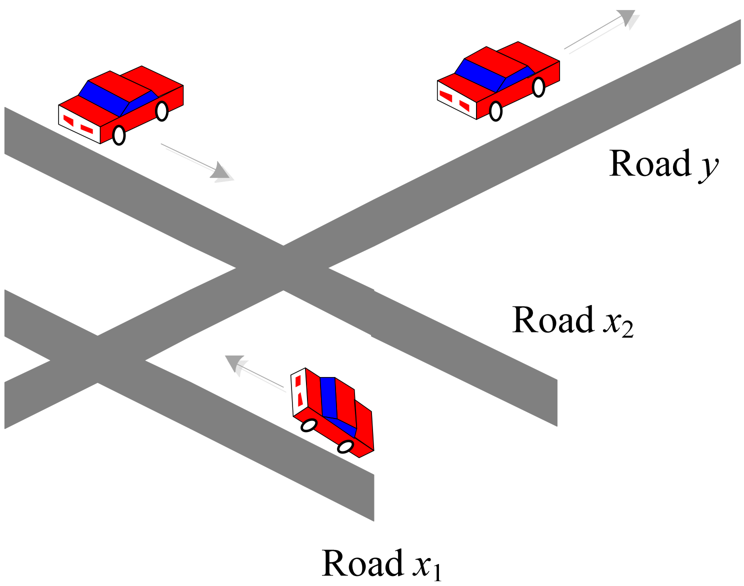

Fig. 4.2: Topology of multiple crossroads

EV user's decision of whether or not charging at a specific station for renewing batteries usually depends upon the energy adequacy for the next trip. When coming by the first station, SOC_{ini}^{i} of the ith EV follows the uniform distribution shown in (4.1). As there is distance l before arriving at the next station, swapping shall be performed if (4.2) is fulfilled.

$$SOC_{\mathrm{ini}}^{i} \sim U(SOC_{\min}, SOC_{\max}) \tag{4.1}$$

$$SOC_{\mathrm{ini}}^{i} \cdot B_{\mathrm{c}} - \omega \cdot l < th\% \cdot B_{\mathrm{c}} \tag{4.2}$$

where B_{c} is the capacity of the battery, ω is the energy consumption per km. $th\%$ is the alarming threshold that users must charge their batteries in case of potential damages. It should be noted that (4.2) is one of the feasible assumptions within the constraints (2.5) and (2.6).

A day's 24 hours are divided into consecutive time slots ΔT. The EV average flow rate ζ in the time slot ΔT is assumed to follow Poisson process [97] on a unidirectional single-lane highway. Therefore, the probability of observing h EVs coming by the swapping station in a time slot ΔT is demonstrated in (4.3). The number of EVs arriving at a swapping station λ follows the binomial distribution $B(h, \mathrm{r})$ and is calculated in (4.4). Derived from (4.1) and (4.2), r is the charging probability of an independent EV when coming by the station and is illustrated in (4.5).

$$f(h, \zeta \cdot \Delta T) = P(\mathrm{totalEV}(\Delta T) = h) = e^{-\zeta \cdot \Delta T} \frac{(\zeta \cdot \Delta T)^{h}}{h!} \tag{4.3}$$

$$\lambda = h \cdot r \tag{4.4}$$

$$r = \frac{\omega \cdot l - (SOC_{\min} - th\%) \cdot B_{\mathrm{c}}}{(SOC_{\max} - SOC_{\min}) \cdot B_{\mathrm{c}}} \tag{4.5}$$

The number of EVs arriving at the station on the yth road in Fig. 4.2 is demonstrated in (4.6), which is the summation of influx from multiple roads.

$$\lambda_{\mathrm{y}} = \sum_{x} h_{y,x} r_{y,x} \tag{4.6}$$

where $h_{y,x}$ and $r_{y,x}$ are the travel flow and estimated charging probability of EVs, respectively, which drive from the xth road but turn to the yth road eventually.

4.3 Battery Inventory Management

Inventory of usable recharged batteries is the key element in the operation of swapping stations. The operating principle of the DSCC system is investigated and the logistics plan of demand and order is drawn up based on the daily EV energy needs and battery charging speed.

4.3.1 Operation of Swapping Stations

Inventory management protects the regular and sufficient inventory level against the random disturbance of redundant storage or running out of goods. In this thesis, the battery inventory management is different from traditional logistical cases because batteries are not simply sold but are recycled between suppliers and users.

Fig. 4.3 describes the roadmap of the DSCC model in which $T_{\mathrm{tran},n}$ represents the one-way transport duration of the *n*th station. For an individual swapping station, EVs come into the swapping station at time slot ΔT and all depleted batteries are swapped for recharged batteries, which process can be completed within minutes. Derived from the (*s*, *S*) model, s_n is assumed to be the trigger point for inventory replenishment while S_n is assumed to be the initial inventory level of the *n*th station.

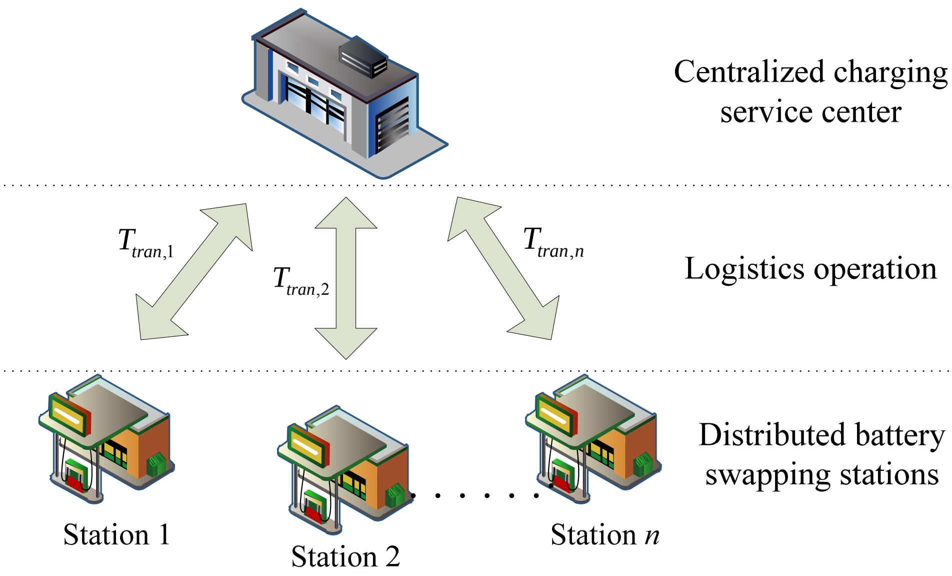

Fig. 4.3: Centralized battery charging & dispatching mode

Goods can be promptly replenished in traditional inventory management whereas batteries need long time to be recharged for recycling. The anticipation stock is considered in the improved (*s*, *S*) model because the expected battery demands during the transportation time $T_{\text{tran},n}$ vary greatly with Poisson process. In order to prevent stockout, the trigger point s_{n,t_n} of the *n*th station at time t_n for starting inventory replenishment shall be set as (4.7) taking anticipation stock into account.

$$s_{n,t_n} = F^{-1}(p', \lambda_{t_n+\Delta T} \cdot \frac{T_{\text{tran},n}}{\Delta T}) \tag{4.7}$$

where F^{-1} is the inverse function of Poisson cumulative distribution. $\lambda_{t_n+\Delta T}$ is the estimation of the arrival rate during the next time slot. Guarantee level p' ensures that the probability of possible battery stockout during battery transportation interval shall be less than $(1-p')$.

Over-storage increases the cost, so the number of recharged batteries delivered back from the centralized charging center is carefully determined in (4.8):

$$C_{n,t_n} = S_n - DB_{n,t_n} + s_{n,t_n} \tag{4.8}$$

where DB_{n,t_n} is the quantity of residual full-energy batteries in the *n*th station, at time t_n.

4.3.2 Operation of Centralized Charging Center

One centralized charging center is assigned to charge the depleted batteries transported from several nearby swapping stations. *S'* is assumed to be the initial inventory of the charging center.

The work-in-process (WIP) represents the batteries being charged. As the charging load cannot be too high to impact the stability of the local power system, some of the depleted batteries may not be charged immediately or the charging power can be lowered in peak times. Different operation strategies will influence the end time of WIP and further the inventory preparation of *S'*.

Constant power is assumed during the charging process, the charging duration D_c^i is therefore calculated as (4.9).

$$D_{\mathrm{c}}^{i}=\frac{(1-SOC_{\mathrm{ini}}^{i})\cdot B_{\mathrm{c}}}{\kappa_{\mathrm{c}}\cdot P_{\mathrm{c}}} \tag{4.9}$$

where P_c is the charging power with efficiency κ_c.

Recharged batteries can be delivered back to swapping stations for later use. The recharged batteries leave the charging center at time t_n while the deplete batteries arrive at the charging center at time $T_{\mathrm{c},n}$ shown in (4.10). u_{c}^{i} illustrates the charging state of the battery of the *i*th EV at a specific time span which is denoted as in (4.11). The real-time charging load of the centralized charging center P_t is obtained in (4.12) by superposition of all the power demand of *M* individual batteries.

$$T_{\mathrm{c},n}=t_n+T_{\mathrm{tran},n} \tag{4.10}$$

$$\begin{cases} u_{\mathrm{c}}^{i}(T_{\mathrm{c},n}\le t\le T_{\mathrm{c},n}+D_{\mathrm{c}}^{i})=1 \\ u_{\mathrm{c}}^{i}=0,\ \text{otherwise} \end{cases} \tag{4.11}$$

$$P_t=\sum_{i=1}^{M}P_{\mathrm{c}}\cdot u_{\mathrm{c}}^{i} \tag{4.12}$$

4.3.3 Logistics planning

To fulfill the requirements of inventory management, a healthy and sustainable recycling between swapping stations and charging center shall be established.

Traditional (s, S) behavior is modeled as Markov process in [98] where the states are located within the interval (*s*, *S*]. This thesis proposes an improved Markov process to describe the discrete-time stochastic inventory variation of a swapping station. The transition matrix can be represented by (4.13).

$$\begin{bmatrix}
p_{1,1} & p_{1,2} & \cdots & p_{1,s} & \cdots & p_{1,S-\delta} & p_{1,S} & p_{1,S+\delta} \\
p_{2,1} & p_{2,2} & & \cdots & & & \cdots & \\
\cdots & & & & & & & \\
p_{s,1} & \cdots & & p_{s,s} & & & \cdots & \\
\cdots & & & & & & & \\
p_{S-\delta,1} & & & & & & & \\
p_{S,1} & \cdots & & \cdots & & & p_{S,S} & \\
p_{S+\delta,1} & & & & & & & \cdots
\end{bmatrix} \tag{4.13}$$

where δ represents the possible overload or underload which is small compared to *S*. $p_{a,b}$ denotes the probability of moving from inventory level in state *a* to the level in state *b* after time slot ΔT.

The values of each $p_{a,b}$ shown in (4.14)-(4.16) represent the occurrence probability of each transition.

$$p_{a,b} > 0 \text{ when } a < s < b \in [S-\delta, S+\delta], \sum_{b=S-\delta}^{S+\delta} p_{a,b} = 1 \tag{4.14}$$

$$p_{a,b} > 0 \text{ when } a > b, \ p_{a,b} = f(a-b, \lambda_t \cdot \Delta T) \tag{4.15}$$

$$p_{a,b} = 0 \text{ when } s < a < b \tag{4.16}$$

where (4.14) denotes the arrival process of recharged batteries in the swapping station when trigger point *s* is ignited while (4.15) is the process of battery swapping which corresponds to the arrival of EVs and also follows Poisson distribution. As illustrated in (4.16), when the level of battery inventory is higher than the trigger point *s*, no inventory change occurs.

4.4 Control Scheme

For planning of this DSCC system, several essential aspects should be considered, including the cost of running the system, communication of distributed stations [99], charging load impact on local power systems and the battery inventory turnover. Inventory preparation and recycling of batteries draw special attention because battery purchasing cost takes up a large part of the budget in the planning of DSCC system [62, 69].

A novel scheme is devised to achieve the best integrated performance of minimum possible impact on the established power system and maximum possible inventory turnover ratio. The optimization is formulated as follows:

Objective:

$$\text{Min } Obj = \alpha_1 \cdot D(P) + \alpha_2 \cdot \frac{1}{I} \tag{4.17}$$

$$D(P) = \frac{1}{T}\sqrt{\sum_{t=1}^{T}(P_t - \mu_T)^2} \tag{4.18}$$

$$I = \frac{\sum_{t=1}^{T} \lambda_t \cdot \Delta T}{\sum_{n=1}^{N} S_n + S'} \tag{4.19}$$

Constraint:

$$S_n(t) > 0, \; S'(t) > 0, \; \forall t \tag{4.20}$$

$$0 < P_{\mathrm{c}} < P_{\mathrm{cmax}} \tag{4.21}$$

where α_1, α_2 are weight coefficients. *D(P)* denotes the daily average deviation from the average charging power μ_T. Inventory turnover ratio *I*, which is calculated as the goods sold divided by the average inventory, reflects the efficiency of inventory management. *N* is the total number of swapping stations and the real-time inventory levels are represented by $S_n(t)$, $S'(t)$.

For the consideration of this DSCC operation, charging in the centralized charging center cannot be postponed until midnight since the recharged and depleted batteries are frequently exchanged according to the energy needs of EVs. Therefore, charging power adjustment during busy hours (11:00-21:00) is adopted to mitigate the variance of daily power demand. Constraint (4.21) shows the maximum charging power P_{cmax}. Genetic algorithm is used to search the optimal centralized charging schedule and allocation of the initial inventory to each station. Stockout shall be avoided at all times.

4.5 Numerical study

In this study, the Nissan Leaf, with a lithium-ion battery of 24 kWh is chosen as the typical EV driving on a cloverleaf junction. The traffic can be simply regarded as two independent neighboring roads shown in Fig. 4.1. Because the loading and unloading of batteries take several minutes, the time slot ΔT is selected to be 15 minutes to counteract the uneven periods of each swap. The flowrate ζ_1, which denotes the road for outing and ζ_2, which represents the road commuting back home are shown in Fig. 4.4(a) and Fig. 4.4(b), respectively.

Guarantee level p' is assumed to be 0.95 and the simulation process is repeated until meeting the criterion that the probability of stockout is under 5%. The threshold *th*% is set to be 30% as the battery SOC shall be kept no less than 30% for safety reasons [9] in normal conditions. Other simulation parameters are shown in Table 4.1.

Table 4.1: Simulation parameters

ω	0.15	$SOC_{\min}$	0.5
B_c	24 kWh	$SOC_{\max}$	0.65
l_1	50 km	$T_{\text{tran},1}$	30 min
l_2	40 km	$T_{\text{tran},2}$	30 min

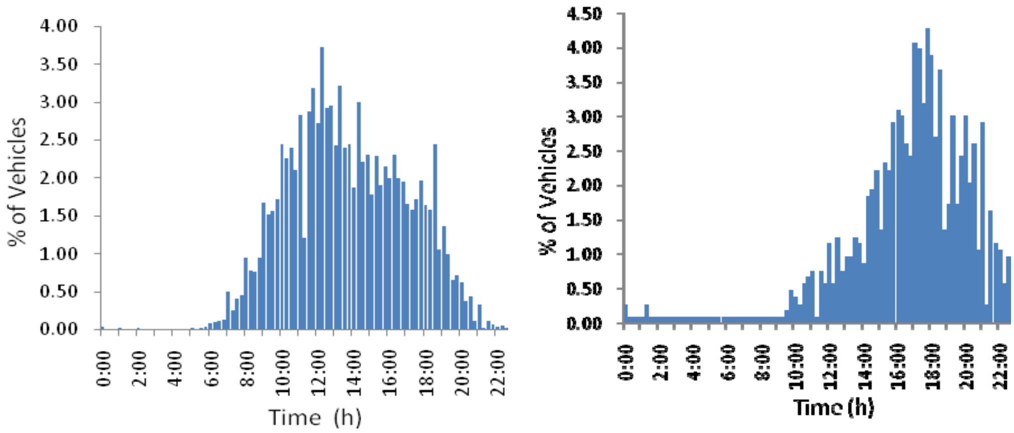

(a) (b)

Fig. 4.4: Daily flowrate of specific roads. (a) Road for daily outing. (b) Road to home

A typical value of P_c is 8kW according to [91]. In this base case, the resulting parameters indicated from the DSCC system is that $I = 2.34$, $D(P) = 0.820$. The weight coefficients α_1, α_2 of the grid impact and inventory turnover respectively are tuned with people's point of emphasis. By adjusting power output P_c of the charging posts to fulfill the objective in (4.17), the improved results are shown in Table 4.2 while the daily variations of inventory and total charging power in the charging center are depicted in Fig. 4.5 and Fig. 4.6, respectively.

Table 4.2: Simulation results

Emphasis	Inventory		P_c	D(P)	I	Obj
ITE	S_1	85	6.55 kW	0.701	2.70	0.470
	S_2	90				
	S'	501				
PIE	S_1	86	5.25 kW	0.688	2.41	0.610
	S_2	116				
	S'	535				

A higher value of inventory turnover ratio generally indicates better performance of battery management while smaller daily power deviation reflects less impact on local power system. It is demonstrated that the performance is largely improved with controlled charging power in DSCC system concerning both inventory efficiency and grid impact.

As it is shown in Table 4.2, weight coefficients of $\alpha_1 = 0.3$, $\alpha_2 = 0.7$ indicate the inventory turnover emphasized scenario (ITE) which generates a comparatively greater turnover ratio of 2.70. In this scenario, the initial inventory level of each station is controlled strictly and the charging power should be higher than the power impact emphasized scenario (PIE) with $\alpha_1 = 0.7$,$\alpha_2 = 0.3$. As depicted in Fig. 4.5, the inventory preparation in ITE is lower to save battery purchase cost and the battery recycling is much faster because of its higher charging power than PIE.

According to Fig. 4.6, no charging occurs during small hours (0:00~9:00) while the peak time is concentrated and lasts through the busy commuting hours. For comparison, the charging power demand curve of ITE is more temporally concentrated than that of PIE and the maximum power in ITE is slightly higher. Therefore, the value of *D(P)* is higher in the scenario of ITE which implies a larger impact on local power grid operation.

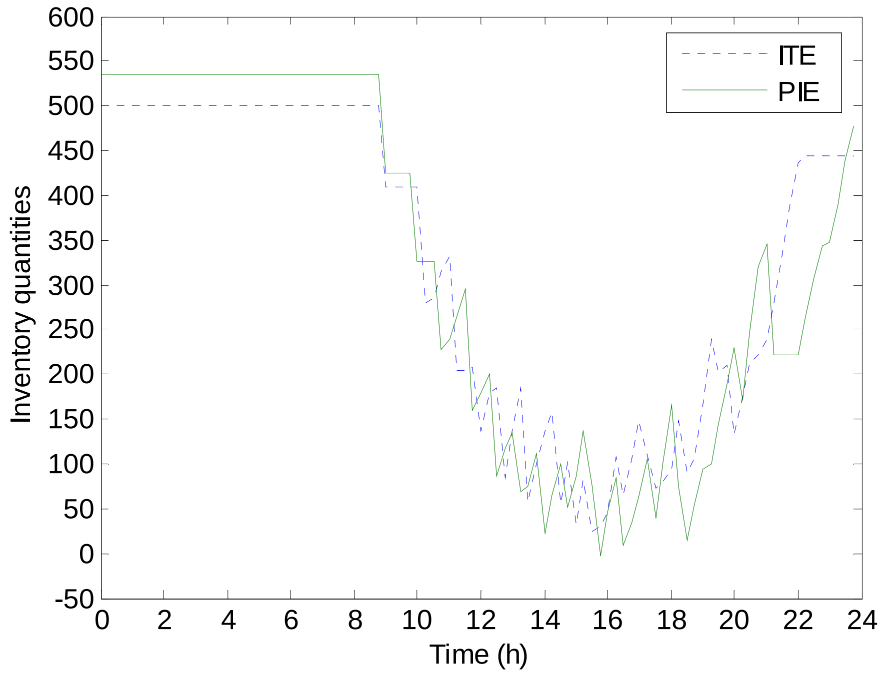

Fig. 4.5: Comparison of inventory variation in charging center

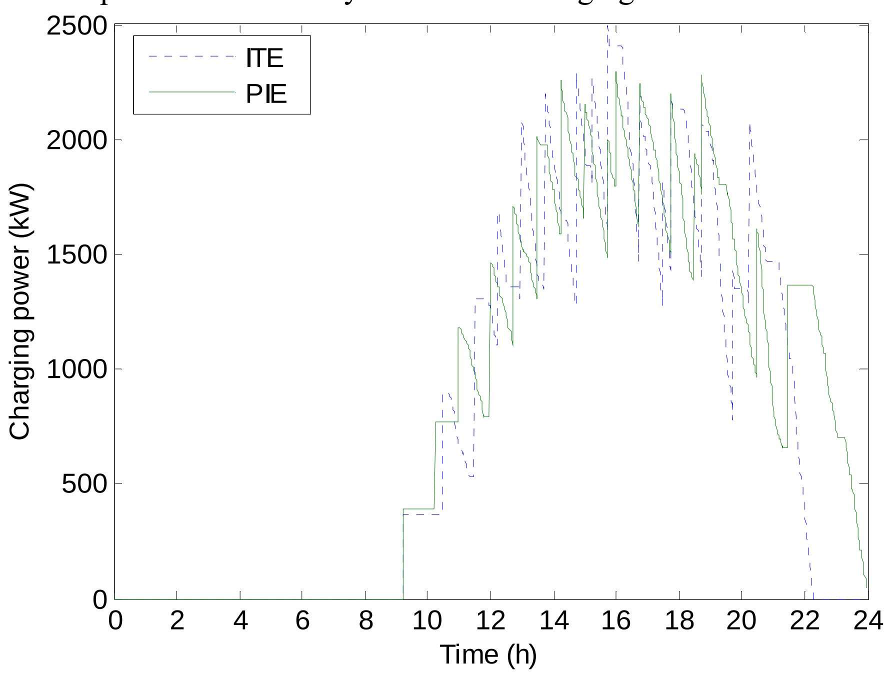

Fig. 4.6: Comparison of daily charging power demand

Although the optimization of maximizing inventory turnover and minimizing impact on power system seems to be contradictory with each other, the goal of this thesis is to obtain the best overall performance considering both sides. Under practical situations, the planners of swapping and charging services have to place more emphasis on promoting inventory turnover ratio to gain more profit while power system planners should focus more on tackling the potential power demand increase before constructing new battery charging/swapping stations. Both sides collaborate to obtain the best planning schemes.

4.6 Summary

This thesis proposes a comprehensive planning of DSCC system which runs with high recycling efficiency, less initial investment and lower grid impact. The EV batteries are treated as special goods, inventory of which is managed to reduce the possibility of stockout or over-storage to the minimum. The numerical results have shown that although the daily arrival rates of different swapping stations are fairly different, the DSCC system can properly control the charging power and distribute the planned battery inventory intelligently among different stations to achieve the optimal inventory turnover and least impact on the existing grid.

Chapter V

Distribution System Planning Considering Stochastic EV Penetration and V2G Behavior

5.1 Introduction

For EVs plugging in home garages, there is much longer spare time for charging batteries to full compared to the short sojourn time at public charging stations. Therefore, V2G technology can fully utilize EV battery potentials that discharge during busy hours to support the grid and recharge to full at valley hours. However, the stochasticity of EV user behaviors poses challenges to the regulators of distribution systems. How regulators decide upon a control strategy for V2G and how EV users respond to the strategy will significantly influence the variation of load profiles in the planning horizon. The distribution system planning scheme in this thesis is devised based on the probabilistic evaluation of system risk by upgrading system infrastructure to acceptable levels of reliability at the lowest possible cost (including infrastructure investment cost, compensation cost to control acceptance and operation cost after system upgrade). The trade-off between encouraging more control acceptance and investing more in infrastructure is determined by taking the variation in EV penetration, charging preference, and customer damage cost (CDC) into account.

The rest of this chapter is organized as follows. In Section 5.2, a general model for forecasting residential EV charging demand is formulated. In Section 5.3, modeling of the V2G profile is proposed considering EV user behavior and the corresponding system control signal. A comprehensive planning cost analysis is given in Section 5.4 that takes customer compensation cost into account. The planning optimization procedure is provided in Section 5.5 and its effectiveness is assessed by a numerical study in Section 5.6. Section 5.7 summarizes this chapter.

5.2 Modeling of EV Charging Demand

This section outlines a general probabilistic technique for forecasting daily EV charging demand. As EV user behavior is stochastic, gathering the forecast information is crucial to regulators.

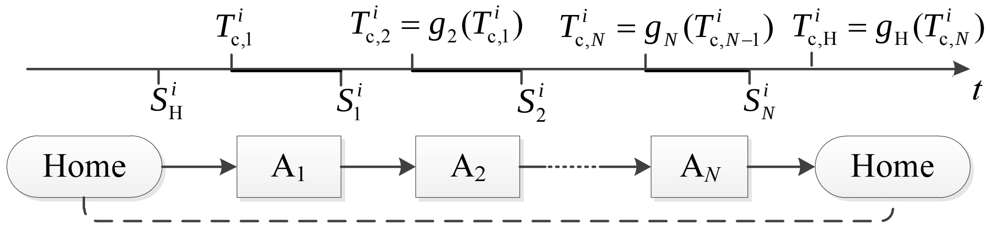

Fig. 5.1: Illustration of travel route modeling

5.2.1 Travel Route Modeling

Daily trips that start and end at residential areas (H) are classified into different travel purposes, including trips transiting between districts $\{A_n\} = \{A_1, A_2, ..., A_N, A_H\}$. Each district is equipped with an aggregator that connects to one bus in the distribution network and integrates local charging/discharging facilities. An EV may perform several trips a day, and the series trip chain is described in Fig. 5.1. By using the data from local travel surveys, the output of travel route modeling includes the forecast for each trip end time in the trip chain $\{T^i_{c,n}\} = \{T^i_{c,1}, T^i_{c,2}, ..., T^i_{c,N}, T^i_{c,H}\}$ and each travel distance $\{l_{n,n+1}\}$. For details of the travel route modeling, the reader is referred to Chapter 1. If the average urban driving speed is v, the trip start time at place n can be estimated as:

$$S^i_n = T^i_{c,n+1} - \frac{l^i_{n,n+1}}{v} \tag{5.1}$$

5.2.2 Charging Behavior Modeling

For the *i*th EV, which starts in a fully charged state from $\mathrm{A_H}$ and travels along the series trip chain, constraints exist for the amount of energy charged at public places. First, the energy charged at each stop should not exceed the total state of charge (SOC) deficit; second, there should be enough SOC for the next trip after charging. For a day's final destination at H, EV users would fully charge their batteries before the start of the next day's trip. Equations (5.2), (5.3) and (5.4) are constituted to reflect these respective constraints (H can be regarded as place 0 or $N+1$):

$$\begin{cases} E_1^i \le \omega \cdot l_{\mathrm{H},1}^i \\ E_2^i \le \omega \cdot (l_{\mathrm{H},1}^i + l_{1,2}^i) - E_1^i \\ \cdots \\ E_N^i \le \omega \cdot \sum_{n=1}^{N} l_{n\text{-}1,n}^i - \sum_{n=1}^{N-1} E_n^i \end{cases} \tag{5.2}$$

$$\begin{cases} E_1^i \ge \max\{0, \omega \cdot (l_{\mathrm{H},1}^i + l_{1,2}^i) - B_\mathrm{c}\} \\ E_2^i \ge \max\{0, \omega \cdot (l_{\mathrm{H},1}^i + l_{1,2}^i + l_{2,3}^i) - E_1^i - B_\mathrm{c}\} \\ \cdots \\ E_N^i \ge \max\{0, \omega \cdot \sum_{n=1}^{H} l_{n\text{-}1,n}^i - \sum_{n=1}^{N-1} E_n^i - B_\mathrm{c}\} \end{cases} \tag{5.3}$$

$$E_\mathrm{H}^i = \omega \cdot \sum_{n=1}^{\mathrm{H}} l_{n\text{-}1,n}^i - \sum_{n=1}^{N} E_n^i \tag{5.4}$$

where ω is the energy consumption per km, E_n^i is the energy to be charged at place *n*, and B_c is the capacity of EV batteries. As the charging preference at public places is stochastic, as reflected in (5.2) and (5.3), three possible scenarios are defined in Table 5.1.

Table 5.1: Scenarios of charging demand at public stations

Public charging preference	Definition
No	$E_n^i = E_{n,\min}^i$, for $\forall i$
Moderate	$E_n^i \sim U(E_{n,\min}^i, E_{n,\max}^i)$, for $\forall i$
High	$E_n^i = E_{n,\max}^i$, for $\forall i$

In this chapter, only the residential charging demand E_H^i is considered in the distribution system (the charging place parameter *n* is therefore omitted in the following analysis) but it will be greatly influenced by the stochastic charging behavior at public places as shown in (5.4). The charging duration D_{H}^i at home is calculated in (5.5) :

$$D_{\mathrm{H}}^i = \frac{E_{\mathrm{H}}^i}{\kappa_{\mathrm{c}} \cdot P_{\mathrm{c}}} \tag{5.5}$$

where P_{c} and κ_{c} are charging power and efficiency, respectively.

5.3 Modeling of V2G Profile

This section describes the prerequisites for performing V2G, namely, the fulfillment of individual CDC, temporal feasibility for discharging, and enough time for recharging after V2G.

5.3.1 Amount of Compensation to Customers

For EV customers, accepting V2G control may raise privacy concerns, influence convenience, and affect EV battery life. In fact, the flexible pricing proposed in [79]-[81] may not naturally make all customers charge during the low-tariff period because their attitude towards the revenue gained by accepting control is fairly arbitrary. A comprehensive customer survey is conducted in [85] to quantify user behavior by investigating customer’s willingness to pay to avoid a power interruption and the willingness to accept compensation for having had one. The amount of CDC obtained from the survey directly portrays the unit interruption compensation ($/kWh) claimed by individual customers.

In this thesis, CDC can be regarded as the extra amount of compensation claimed by EV customers for obeying V2G control in addition to the revenue gained from flexible pricing. The average CDC for residential EV customers is represented by μ_c. Combining the survey results in [85] and the modeling in [84], CDC of the *i*th customer is represented as ξ^i which follows the normal distribution shown in (5.6):

$$\xi^i \sim N(\mu_c, \delta_c) \tag{5.6}$$

Before undertaking system planning for future years, the grid operator should have carefully investigated the habits of local EV customers. The parameters μ_c and δ_c are assumed to be known to the grid operator and the best compensation ratio γ_λ at the λth year is determined based on the information. Therefore, only those users fulfilling (5.7) potentially consider accepting V2G control.

$$\xi^i \le \gamma_\lambda \cdot \mu_c \tag{5.7}$$

5.3.2 Energy Amount for Discharging

Fig. 5.2 shows the timeline of V2G control for the ith EV. T_{gc} and D_{gc} are the grid control start time and the lasting period, respectively. The original charging arrangement T_{c}^i and D_{c}^i vary among different users but V2G is temporally feasible only if the trip end time T_{c}^i is satisfied according to:

$$T_{\mathrm{c}}^i \le T_{\mathrm{gc}} + D_{\mathrm{gc}} \tag{5.8}$$

For those EVs under control, e_{p}^i, the part of original charging arrangement falling within the period [T_{gc}, T_{gc}+D_{gc}] should be postponed. The residual battery energy at time T_{gc} is calculated using (5.9) and the energy discharged back during [T_{gc}, T_{gc}+D_{gc}] is determined in (5.10):

$$e_{\mathrm{residual}} = B_{\mathrm{c}} - E_{\mathrm{H}}^i + e_{\mathrm{c}}^i \tag{5.9}$$

$$e_{\mathrm{b}}^i = \min(e_{\mathrm{residual}}, \frac{P_{\mathrm{d}}}{\kappa_{\mathrm{d}}} \cdot (T_{\mathrm{gc}} + D_{\mathrm{gc}} - \max(T_{\mathrm{c}}^i, T_{\mathrm{gc}}))) \tag{5.10}$$

where e_{c}^i is the energy already charged at H before T_{gc} ($e_{\mathrm{c}}^i = 0$ if $T_{\mathrm{c}}^i > T_{\mathrm{gc}}$). P_{d} and κ_{d} are discharging power and efficiency, respectively.

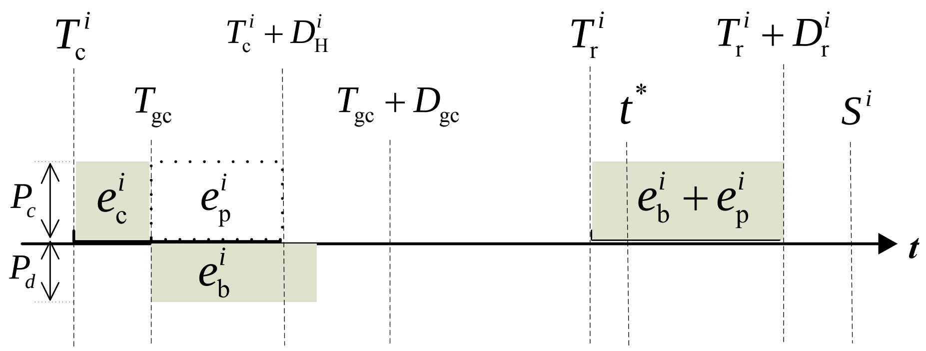

Fig. 5.2: Timeline and energy flow of V2G control

5.3.3 Recharging Demand after V2G

One of the premises for V2G control is that the normal activity of EVs ought not to be affected. Therefore, EVs should be recharged to fulfill the original charging demand after the V2G control period. The time needed for recharging is calculated using :

$$D_{\mathrm{r}}^{i}=\frac{e_{\mathrm{b}}^{i}+e_{\mathrm{p}}^{i}}{\kappa_{\mathrm{c}}\cdot P_{\mathrm{c}}} \tag{5.11}$$

Experiments suggest that recharging immediately after the termination of control will create another power demand peak ensuing time $T_{gc}+D_{gc}$. Unlike other existing works, this thesis puts forward the concept of reference recharging time t^*. Considering the urgency of and fairness to each EV customer, the recharging start time for the ith EV based on t^* is given by:

$$T_{\mathrm{r}}^{i}=t^{*}+h_{1}\cdot(S^{i}-t^{*}-D_{\mathrm{r}}^{i})-h_{2}\cdot(t^{*}-T_{\mathrm{c}}^{i}) \tag{5.12}$$

where h_1 associates with urgency, in that EVs with less spare time before the start of next trip are assigned earlier charging, and h_2 associates with fairness, i.e., the regulators assign relatively earlier recharging start times to EVs plugging in earlier.

The following constraint (5.13) guarantees that recharging will complete before the start of next trip:

$$T_{\mathrm{r}}^{i}+D_{\mathrm{r}}^{i}\leq S^{i} \tag{5.13}$$

5.3.4 Aggregated Charging and Discharging Profile

The aggregated charging/discharging power $P_t^{\mathrm{c,EV}}$ and $P_t^{\mathrm{d,EV}}$ are obtained via the process presented in Fig. 5.3 by superposition of the individual charging/discharging power of all EVs performed at each time of the day. Fig. 5.3 shows that the aggregated load profile is greatly influenced by EV behavior and system control scheme defined by (5.7), (5.8) and (5.13).

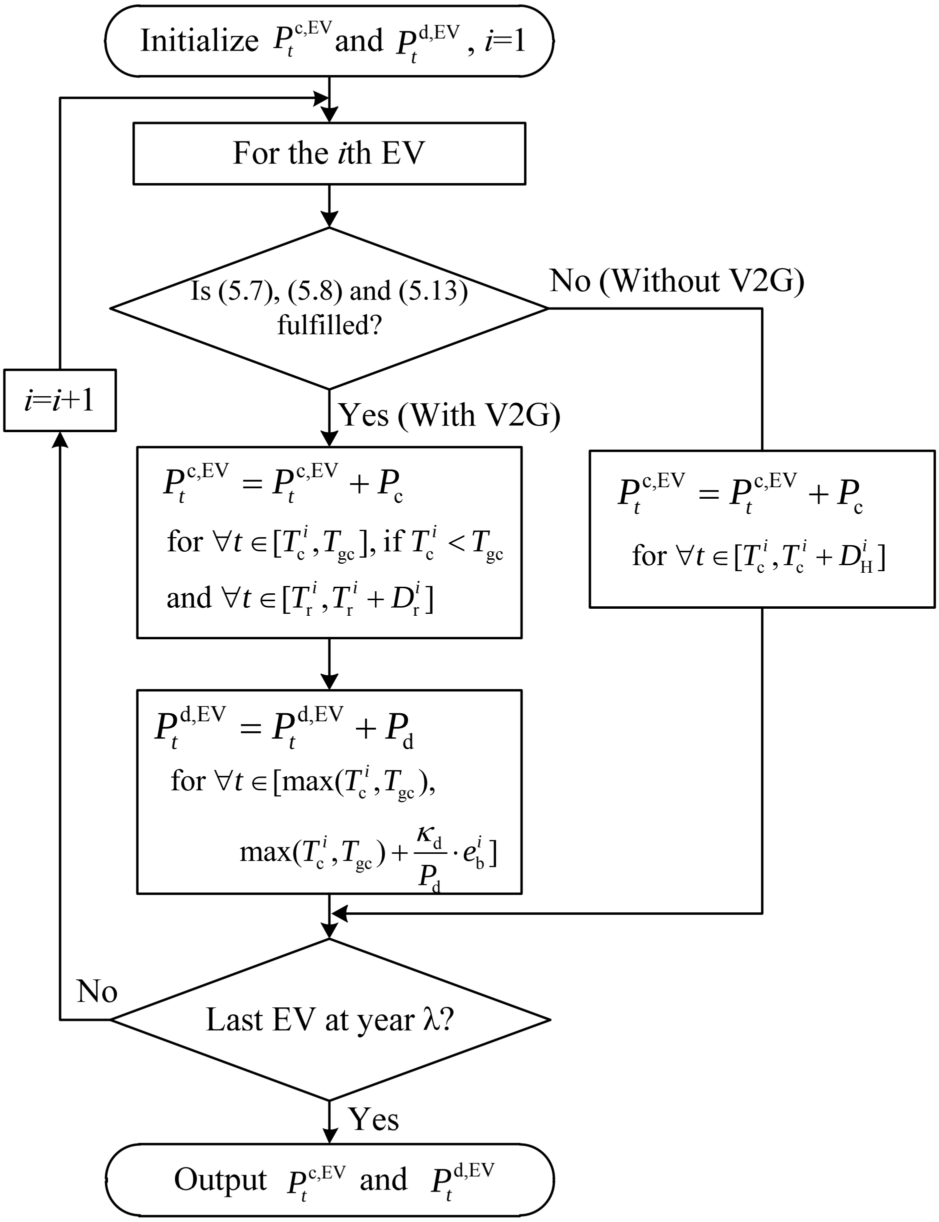

Fig. 5.3: Flowchart for power aggregation

5.4 Cost Analysis for Distribution System Planning

Due to the stochasticity of user behavior, some stability margin should be guaranteed and the incentives claimed by customers may be too high. Therefore, the cost analysis in this thesis simultaneously ponders the mutually influenced parts, including operation cost, V2G compensation cost and infrastructure investment cost, and obtains the trade-offs among them. According to the variation of base load demand and number of EVs integrated each year, the local regulator can control the overall V2G profile by adjusting the compensation ratio γ_λ to satisfy system stability requirements and total cost reduction.

The total cost of the Y-year distribution system planning is given as follows:

Objective: $$\min\ f = f^{oper} + f^{cc} + f^{inv} \tag{5.14}$$

$$f^{oper} = d^{\text{annual}} \sum_{\lambda=1}^{Y} \Big(\sum_{t\in\Omega^t} (\rho_t^{\text{da}} + \rho^{\text{CO}_2}) P_{t,\lambda}^{s} + \rho^{\text{NL}} \sum_{t\in\Omega^t} P_{t,\lambda}^{loss} \Big) \tag{5.15}$$

$$f^{cc} = d^{\text{annual}} \sum_{\lambda=1}^{Y} \Big(\gamma_\lambda \mu_{\text{c}} \cdot \sum_{i}^{q_\lambda} e_{\text{b}}^{i} \Big) \tag{5.16}$$

$$f^{inv} = Y \cdot [\pi^{LL} (\rho^{EL} + \rho^{CL} \sum_{xy\in\Omega^l} P_{xy,\text{cap}}^{l}) + \pi^{LS} (\rho^{ES} + \rho^{CS} \sum_{x\in\Omega^s} P_{x,\text{cap}}^{s})] \tag{5.17}$$

where

$$P_{xy,\text{cap}}^{l} = P_{xy,\max}\ , \qquad \forall xy \in \Omega^l \tag{5.18}$$

$$P_{x,\text{cap}}^{s} = P_{x,\max}\ , \qquad \forall x \in \Omega^s \tag{5.19}$$

$$\pi^{LL} = \frac{\varepsilon(1+\varepsilon)^{LL}}{(1+\varepsilon)^{LL} - 1}\ ,\ \pi^{LS} = \frac{\varepsilon(1+\varepsilon)^{LS}}{(1+\varepsilon)^{LS} - 1} \tag{5.20}$$

subject to:

$$P_{x,t}^{s} - (P_{x,t}^{\text{c,EV}} - P_{x,t}^{\text{d,EV}} + P_{x,t}^{\text{base}}) = U_{x,t} \sum_{y\in\Omega^n} U_{y,t} (G_{xy} \cos\theta_{xy,t} + B_{xy} \sin\theta_{xy,t}) \quad \forall x \in \Omega^x, \forall t \in \Omega^t \tag{5.21}$$

$$Q_{x,t}^{s} - Q_{x,t}^{\text{base}} = U_{x,t} \sum_{y\in\Omega^n} U_{y,t} (G_{xy} \sin\theta_{xy,t} - B_{xy} \cos\theta_{xy,t}) \quad \forall x \in \Omega^x, \forall t \in \Omega^t \tag{5.22}$$

$$U_{\min} \le U_{x,t} \le U_{\max} \tag{5.23}$$

The objective function (5.14) aims to minimize the overall operation, customer compensation, and investment costs across the planning horizon. The operation cost in (5.15) is composed of the electricity purchase cost from the wholesale market and the network line loss cost. d^{annual} is the number of days in one year. ρ_t^{da}, ρ^{CO_2}, and ρ^{NL} represent the day-ahead electricity price at time t, the fixed carbon tax rate, and unit line loss rate, respectively. $P_{t,\lambda}^{s}$ and $P_{t,\lambda}^{loss}$ denote the total power demand at the substation and the total system line loss power, respectively. The total cost of customer compensation is calculated in (5.16) where q_λ represents the number of total EV users fulfilling all the prerequisites (5.7), (5.8) and (5.13) at year λ with compensation ratio γ_λ.

In (5.17), the equivalent total infrastructure investment cost for the planning horizon is presented. The adequate capacities of feeders $P^{l}_{xy,\mathrm{cap}}$ and substation $P^{s}_{x,\mathrm{cap}}$ are appropriately planned by satisfying the maximum power flow at line *xy* (5.18) and maximum power demand of the substation located at node *x* (5.19) over the *Y*-year planning horizon. ρ^{EL}, ρ^{ES} and ρ^{CL}, ρ^{CS} are the engineering, procurement and construction (EPC) fixed cost and capital cost, respectively for constructing feeders and substations. π^{LL} and π^{LS} calculated from (5.20) transform the construction cost of feeders and substations into annuities which are related to the interest rate ε and their respective lifespans LL and LS.

The AC power flow equality constraints are depicted in (5.21) and (5.22). $P^{\mathrm{c,EV}}_{x,t}$, $P^{\mathrm{d,EV}}_{x,t}$, and $P^{\mathrm{base}}_{x,t}$ are the charging, discharging, and base power load, respectively, at node *x* time *t*. The nodal voltage constraint is given in (5.23).

5.5 Planning Optimization Procedure

For a given system with annual load growth rate *a* and EV penetration growth rate *b*, the total cost of distribution system planning depends on the power load profile each year, the compensation paid to customers for improving the load profile, and the infrastructure investment required to satisfy the maximum load demand over the planning horizon. As the EV charging demand and V2G profile are really stochastic, the MCS [85] is adopted for error reduction and reliability evaluation. To be consistent with the methodologies proposed in Chapter 1, the same EV travel behavior forecast (Section 5.2.1) is carried out whereas the general charging behaviors before arriving home (5.2) and (5.3) are assumed to be known to the local grid operator. The optimization procedure for the *Y*-year system planning is summarized as follows:

Step 1) Input distribution system topology, EV travel statistics, charging behavior at public stations (5.2)-(5.3), and CDC distribution (5.7).

Step 2) Generate the chromosomes with control variables T_{gc}, D_{gc}, i^*, and γ_λ for each planning year.

Step 3) Obtain T_{c}^{i}, D_{c}^{i}, S^{i} and ξ^{i} for all EVs penetrating the system at year λ by using the probabilistic technique proposed in Sections 5.2 and 5.3.1.

Step 4) Obtain the V2G profile for year λ with (5.6)-(5.13) corresponding to the control variables.

Step 5) Repeat Steps 2-4 for all Y years over the planning horizon. It should be noted that the base load and the number of EVs penetrating the system increase with each successive year.

Step 6) Calculate the total planning cost from (5.14)-(5.23).

Step 7) Repeat Steps 3-6 with the MCS method and obtain the expected total planning cost corresponding to the chromosomes.

Step 8) Perform selection, crossover and mutation to generate chromosomes of the next generation.

Step 9) Repeat Steps 2-8 until maximum generation is reached or no improvement found for several generations to obtain the optimal planning scheme with the least cost.

Step 10) Perform a stability evaluation for the obtained planning scheme with indices including the minimum nodal voltage Vmin and expected energy not supplied (EENS) [52, 78, and 85] for the planning horizon.

5.6 Numerical Study

5.6.1 Test System and Basic Data

To assess the effectiveness of the proposed planning optimization algorithm, the 32-bus radial distribution system shown in Fig. 5.4 [100] is chosen because, as stated by *M. E. Baran*, “The system is not well-compensated and lossy”. For a planning horizon of 5 years (Y=5), the obsolete feeders and the substation at Bus-0 shall be completely replaced to satisfy load growth and increasing EV penetration. This distribution system is designed to supply power to residential customers. The residential EVs cover the nodes of 5 to 17 and 25 to 32, and are distributed among the nodes based on the proportions of base power load at those nodes. For the analysis of EENS for all nodes with EV penetration, the failure rate of the feeder at line 4-5 is assumed to be 0.065 faults/year [52] and the repair time is 1 hour.

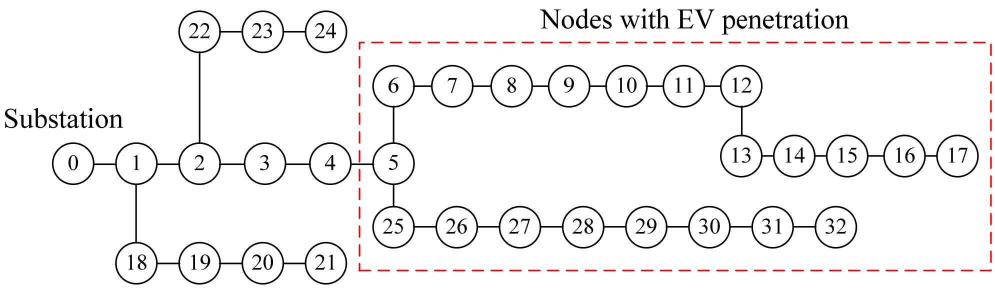

Fig. 5.4: 32-bus distribution test system

Daily variation of the residential base load is collected from the Residential Energy Consumption Survey [101] and the variation of day-ahead electricity price is obtained from PJM data [102]. The EV travel behavior is derived from the NHTS [20]. The data for infrastructure investment costs ρ^{EL}, ρ^{ES}, ρ^{CL} and ρ^{CS} are derived from [53]. As the EPC fixed costs ρ^{EL} and ρ^{ES} are much higher than the capital costs ρ^{CL} and ρ^{CS}, the capacity of feeders and substations should be sufficient for the entire 5-year development and therefore reconstruction is avoided. The standard deviation of CDC is in fixed relation to the mean value (δ_c=0.5μ_c). Other parameters are listed in Table 5.2.

Table 5.2: System planning parameters

Symbol	Value	Symbol	Value
a	0.05	b	0.1
LL	15 years [48]	LS	15 years [48]
ρ^{CO_2}	\$0.0092/kWh [48]	ρ^{NL}	\$0.036/kWh [48]
$U_{\min}$	0.95 [48]	$U_{\max}$	1.05 [48]
P_c	3.3 kW [7]	P_d	3.3 kW [7]
ω	0.24 kWh/km [7]	B_c	24 kWh [7]

In the base case, the initial number of EVs penetrating the grid in the first year is 1000. Charging at public places is moderately preferred and the mean value of CDC μ_c=0.02. The efficiency of the planning optimization is assessed based on cases with different initial EV penetration, user charging preference, and CDC distribution. For each case, only one variable changes with the others kept the same as in the base case.

5.6.2 Planning with Different Initial EV Penetration

When the initial number of penetrating EVs increases, both the charging demand and the potential energy for V2G grow accordingly. The planning comparison is shown in Table 5.3 with the initial EV penetration changing from 0 to 500 to 1000. The annual growth rates of the base load and EV penetration are given in Table 5.2 and remain the same for all cases.

Table 5.3 demonstrates that the system operation cost increases with the augmentation of EV penetration because the total daily power demand increases with the number of penetrating EVs regardless of V2G scheduling. Both the infrastructure investment cost and the minimum nodal voltage with V2G control are significantly improved by the proposed planning optimization compared to the case without EVs because the annual peak load demand is largely reduced.

Table 5.3: Planning with different initial EVs

Initial EVs	f^{oper} ($\$\times10^6$)	f^{cc} ($\$\times10^5$)	f^{inv} ($\$\times10^6$)	f ($\$\times10^6$)	V_{min} (p.u.)
0	5.073	0	1.037	6.110	0.9428
500	5.186	1.096	1.021	6.316	0.9614
1000	5.381	1.531	1.026	6.559	0.9555

The comparison of system-wide daily power demand profiles in the fifth year is shown in Fig. 5.5 as an example to demonstrate the effectiveness of the proposed optimal planning. Considering the growth of base load and EV penetration during the planning horizon, the blue dotted line denotes the trend of base load power derived from [28]. Corresponding to the result in Table 5.3, its peak load is so high that more investment in feeders and substations is required. For the two cases with EV penetration, their V2G control intervals are both constrained from 18:00 to 22:00, which greatly improves the peak load profiles with acceptable compensation paid to users. The load profiles from 17:00 to 22:00 follow a zig-zag trend because the compensation ratio γ_λ is kept the same during the whole control period. For example, raising γ_λ at 20:00 will be unfair to those starting V2G earlier and will discourage them from accepting V2G at an earlier hour. Furthermore, the recharging arrangement proposed in Section III.C works efficiently and makes the recharging demand of all controlled EVs well-distributed within the low-tariff period (from 24:00 to 7:00).

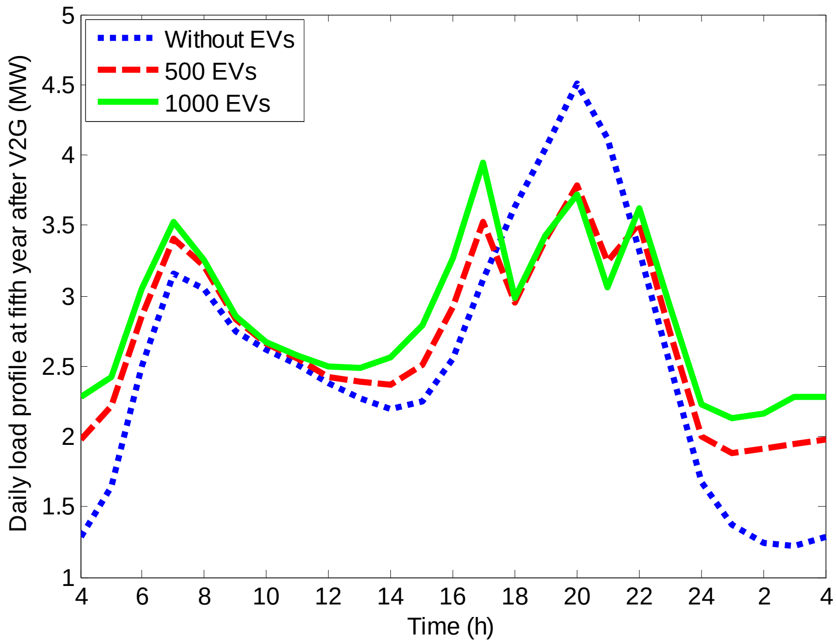

Fig. 5.5 Load comparison with respect to initial EV penetration

5.6.3 Planning with Different Charging Preference

The charging preference in public places can be stochastic, as shown in (5.2) and (5.3). The relationship between public charging preference and residential charging demand is demonstrated in (5.4). A planning comparison of the three charging preference scenarios specified in Table 5.1 is shown in Table 5.4.

Although the residential charging demands of the three cases are fairly different, the planning optimization proposed efficiently raises the minimum voltage to meet the system stability requirement (5.23). The case of no interest in public charging means that EV users will only keep the battery energy above the minimum SOC that can support their next trip. As a result, the residential charging demand will increase significantly, as inferred from (5.4), making the operation cost and infrastructure investment of this case higher compared to the other two cases.

Table 5.4: Planning with different charging preference

Public charging preference	f^{oper} ($\$\times10^6$)	f^{cc} ($\$\times10^5$)	f^{inv} ($\$\times10^6$)	f ($\$\times10^6$)	V_{min} (p.u.)
No	5.667	1.820	1.028	6.876	0.9515
Moderate	5.381	1.531	1.026	6.559	0.9555
High	5.168	1.500	1.018	6.337	0.9590

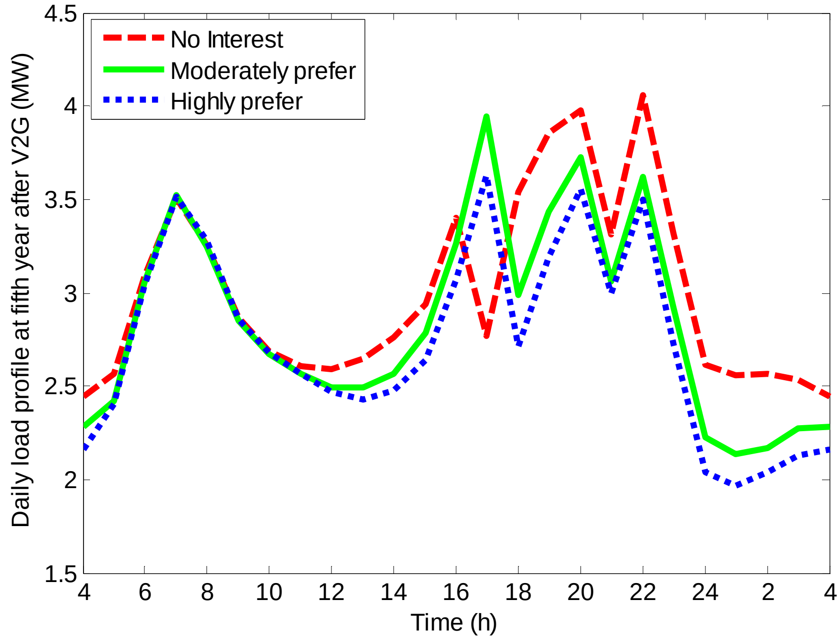

Fig. 5.6 Load comparison with respect to charging preference

For the daily load comparison of the fifth year shown in Fig. 5.6, the proposed planning optimization successfully lowers the peak load to an acceptable level and makes the recharging demand well-distributed in the low-tariff periods regardless of the charging preference. For the case with no interest in public charging, the residential charging demand is so high that the V2G control starts earlier, i.e., 17:00 instead of 18:00. As a result, the power load at 17:00 is significantly reduced compared to the peak loads of the other two cases at that time. With respect to the cases with moderate and high preference for public charging, variation trends in the load profile with V2G control are largely the same.

5.6.4 Planning with Different CDC Distributions

In this section, the optimal planning scheme varies with different CDC distributions. The planning comparison in Table 5.5 is made among the cases of full cooperation between grid operator and EV customers (μ_c=0), μ_c=0.01 to 0.03, and the case of no cooperation whatsoever (μ_c=∞, equivalent to the case without V2G).

Table 5.5: Planning with different CDC distributions

μ_c	f^{oper} (\$×10^6)	f^{cc} (\$×10^5)	f^{inv} (\$×10^6)	f (\$×10^6)	V_{min} (p.u.)	EENS (kWh)
0	5.130	0	1.025	6.155	0.9562	55.817
0.01	5.233	1.795	1.025	6.438	0.9559	55.673
0.02	5.381	1.531	1.026	6.559	0.9555	55.619
0.03	5.467	1.217	1.027	6.616	0.9551	55.643
∞	5.673	0	1.054	6.727	0.9230	55.819

Based on Table 5.5, the operation cost decreases with the reduction of μ_c due to the fact that when less CDC is claimed by EV customers, a relatively larger compensation ratio γ_λ can be applied to attract more control acceptance. The electricity purchase cost and network line loss cost will simultaneously decrease owing to the control that more power can be discharged back in busy hours and recharged at valley periods. The fact that many more customers will be attracted to accept V2G control when μ_c is lower also makes the total compensation cost f^{cc} increases from \$1.217×10^5 to \$1.795×10^5 when μ_c decreases from 0.03 to 0.01.

For the case with no cooperation, no EV users will obey the control signals but charge upon arrival at home instead. The operation cost and investment cost are both the highest among all cases because of the coincidence of base peak load and EV charging peak load. Moreover, the minimum nodal voltage will drop to as low as 0.9230, which contravenes constraint (5.23). EENS also increases considerably compared to the cases with μ_c=0.01 to 0.03. Thus, a complete lack of cooperation between grid operator and EV customers will not only increase the total planning cost but also make system unstable.

The total planning cost is the lowest for the case with full cooperation. Note that this scenario conforms to the hypothesis proposed in [82, 83], in that users are fully responsive and the cost decrement will be allocated to users. Here, the planning cost reduction is considered without variation of electricity purchase cost (as CDC is claimed in addition to the revenue from flexible pricing). Changing from the case with $\mu_c=\infty$ to that with $\mu_c=0$, the planning cost reduction is \$2.126$\times10^4$ with a total of 2.007$\times10^7$ kWh discharged over the entire planning horizon. It is calculated that only \$0.0016/kWh can be allocated to users accepting V2G control. This amount of compensation is so small compared to the residential electricity price that only the revenue from flexible pricing cannot guarantee the "full responsiveness" of all users. Furthermore, excess discharging will create another recharging peak during the original valley hours so that the EENS is higher than for the cases with μ_c=0.01 to 0.03.

5.7 Summary

This thesis puts forward an innovative idea that takes cognizance of stochastic user behavior in the realm of distribution system planning. The variation of user behavior involves different levels of EV penetration, charging preference, and CDC distributions. On the one hand, the increase of stochastic charging demand will put extra pressure on system operation and boost infrastructure investment. On the other hand, if properly controlled, the discharging potential of EV batteries can support the distribution grid during busy hours to mitigate the pressure, with customer compensation cost increased accordingly.

With comprehensive analysis of EV user behavior, a planning optimization algorithm is proposed by obtaining the trade-off among system operation cost, customer compensation cost, and investment cost. Numerical study is conducted with real-world statistics on improving an obsolete 32-bus distribution system considering 5-year development. The results show that the proposed algorithm effectively resolves the optimal planning for cases with different user behaviors. Integrating the analysis of user behavior into the planning of the future smart grid is of great importance to fully exploit potential available energy.

Chapter VI

Conclusions and Future Work

6.1 Summary

The contemporary environmental deterioration impels most of countries across the world to implement energy saving and emission reduction policies for greener economy. The popularization of EVs is receiving ever more policy support while new issues have since been raised as the EV user behavior is fairly stochastic. With real-world travel survey and power system statistics, investigating the stochasticity of EV user behavior and making corresponding improvements in the monitoring and planning of future smart grid become the central themes of this thesis.

In Chapter II, a more practical EV forecasting model has been proposed with inputs of historical regional travel survey. By comparing to a real charging load profile, performance of the proposed forecast method is demonstrated to be accurate and reliable. The numerical study also shows that distinct user charging preferences at different locations significantly influence the forecast results of EV charging demand.

A faster, more accurate and more reliable state estimation with QN method is proposed in Chapter III to alleviate the SSE error brought by stochastic EV penetration. By comparing to the performance with existing TWLS, SSE-WLS, EKF and UKF methods, the innovative SSE-QN method shows better accuracy with increasing EV penetration and greater reliability in the circumstance of potential measurement malfunction.

Chapter IV proposes a comprehensive scheme of DSCC system which runs with high recycling efficiency, less initial investment and lower possible grid impact. The numerical study shows that the proposed DSCC system does well in the planning of stations along the highways and the possibility of battery stock-out or over-storage is reduced to the minimum.

For system planning within residential areas, Chapter V puts forward an innovative idea that takes cognizance of the influence of EV user behavior on distribution system planning decisions. Numerical study is conducted with real-world economic statistics and successfully determines the optimal planning schemes with least cost for cases with different user behaviors.

6.2 Future Work

This thesis has laid a substantial foundation for practical EV charging load forecast, power system monitoring and planning considering EV penetration. To extend application of the methods proposed in this thesis, following research directions may be worthy of further studying in the future:

6.2.1 Operation Strategies for Supercapacitor/Battery Hybrid Vehicle

In general, battery has much higher specific energy with low specific power so that the driving comfort of current EVs is inferior to that of ICE vehicles, especially when going uphill. Hybridizing battery EVs with onboard supercapacitors can be one of the promising solutions as supercapacitors can provide high bursts of power even when EV battery capabilities have decreased, maintaining the accelerative performance. Supercapacitors can also protect batteries from high peak currents and benefit from regenerative braking.

This thesis is focused on the forecast of EV travel behavior and EV energy consumption along the daily travel route. In the future research, the city transportation network and real-time traffic conditions are considered to formulate the detailed drive speed forecast of EVs including information of acceleration and braking.

The power electronics architecture of the battery/supercapacitor hybrid system is shown in Fig. 6.1 [103]. It can be seen that the supercapacitor can provide voltage regulation for the reliability of the circuit and burst power to the operation of EV. Having obtained the detailed drive speed forecast within the city layout, the optimal efficiency of operation of the EV battery/supercapacitor hybrid system can be achieved with control variables: regenerative braking profiles, use of air conditioning, capacities of batteries and supercapacitor.

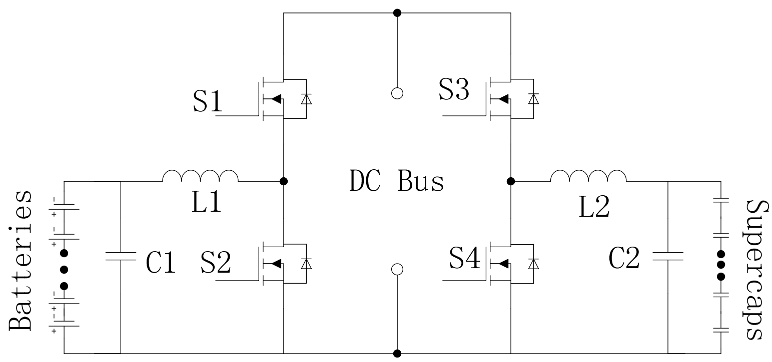

Fig. 6.1: Architecture of the battery/supercapacitor hybrid system

6.2.2 Optimal Measurement Placement Considering Mobility of EVs

As real measurement is relatively scarce in distribution grids, meter placement optimization for the purpose of improving estimation quality should be investigated for the future smart grid considering the geographical distribution of stochastic EV charging load and measurement errors. This research of measurement placement should address the minimization of estimation errors and improvement of grid observability with respect to the assessment process proposed in Chapter III.

6.2.3 Metropolitan Charging Station Planning with Big Data

This thesis manipulates existing data with traditional data processing applications. The concept of “Big data” arises in the realm of power system planning because of the increasing need to tackle massive data for improving forecast accuracy. The big data used for metropolitan charging station planning may include information from Google Map (for transportation network topology and traffic flow), weather forecast (associated with the energy consumption of air conditioning) and more detailed records of EV travel and charging behavior.

Appendices

A. Detailed Analytical Results of All Possible STCs

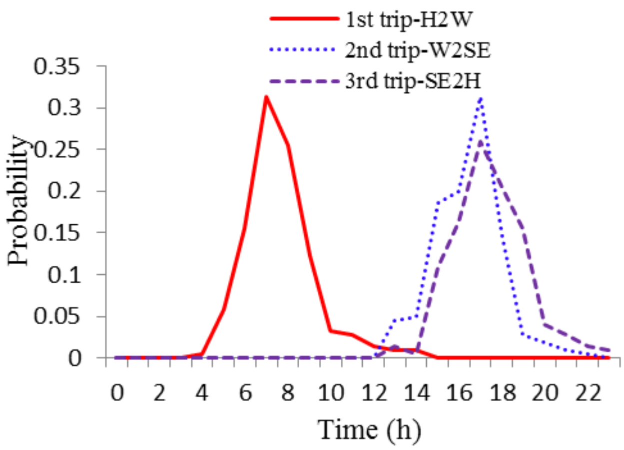

Fig. A.1: TET distribution of H-W-SE-H

Table A.1: Calculated PPM of H-W-SE-H

trip12	trip23	trip13
0.25	0.81	0.29

TET with liner relationship:

X(T3)=0.83*X(T2)+236

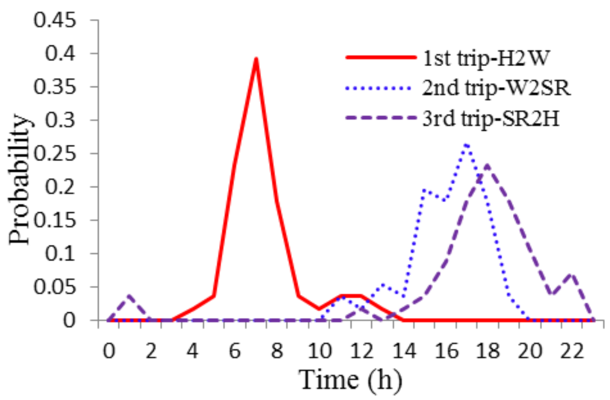

Fig. A.2: TET distribution of H-W-SR-H

Table A.2: Calculated PPM of H-W-SR-H

trip12	trip23	trip13
-0.09	0.08	-0.50

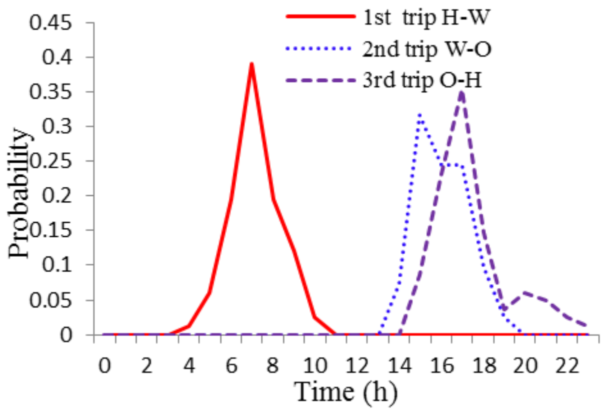

Fig. A.3: TET distribution of H-W-O-H

Table A.3: Calculated PPM of H-W-O-H

trip12	trip23	trip13
-0.06	0.81	-0.01

TET with liner relationship:

X(T3)=0.81*X(T2)+271

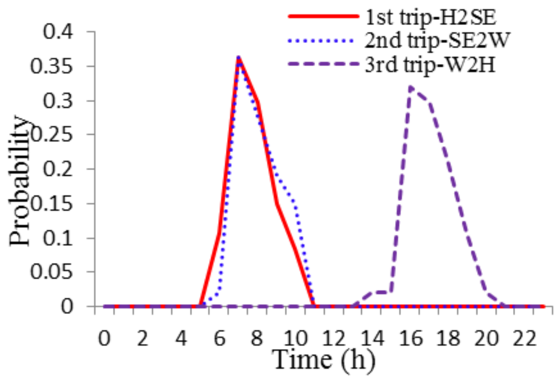

Fig. A.4: TET distribution of H-SE-W-H

Table A.4: Calculated PPM of H-SE-W-H

trip12	trip23	trip13
0.88	0.14	0.18

TET with liner relationship:

X(T2)=0.89*X(T1)+81

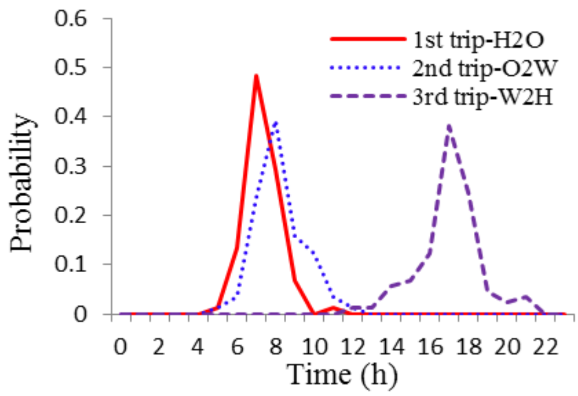

Fig. A.5: TET distribution of H-O-W-H

Table A.5: Calculated PPM of H-O-W-H

trip12	trip23	trip13
0.80	0.01	-0.01

TET with liner relationship:

X(T2)=0.96*X(T1)+69

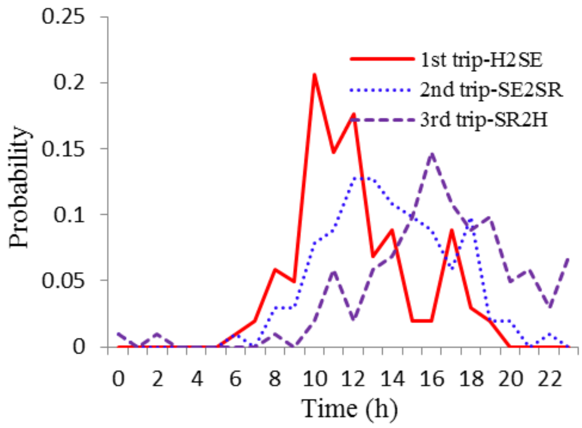

Fig. A.6: TET distribution of H-SE-SR-H

Table A.6: Calculated PPM of H-SE-SR-H

trip12	trip23	trip13
0.75	0.62	0.47

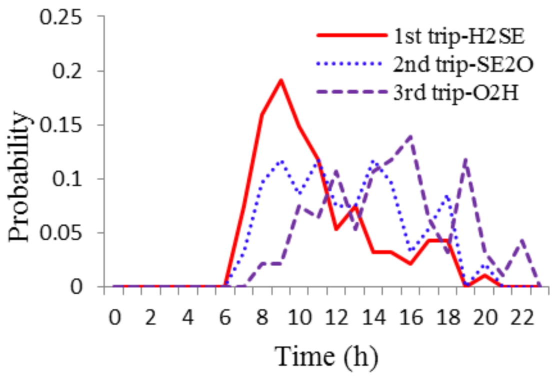

Fig. A.7: TET distribution of H-SE-O-H

Table A.7: Calculated PPM of H-SE-O-H

trip12	trip23	trip13
0.76	0.67	0.61

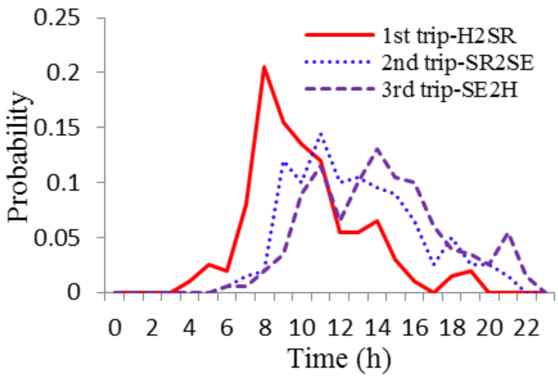

Fig. A.8: TET distribution of H-SR-SE-H

Table A.8: Calculated PPM of H-SR-SE-H

trip12	trip23	trip13
0.71	0.91	0.67

TET with liner relationship:

X(T3)=0.96*X(T2)+110

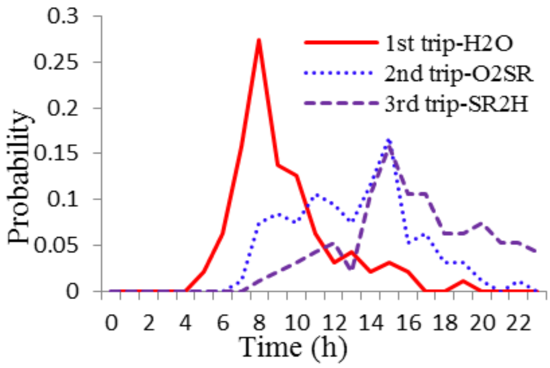

Table A.9: Calculated PPM of H-O-SR-H

trip12	trip23	trip13
0.31	0.72	0.17

Fig. A.9: TET distribution of H-O-SR-H

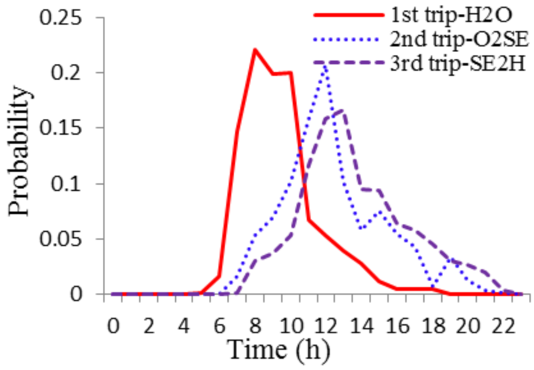

Table A.10: Calculated PPM of H-O-SE-H

trip12	trip23	trip13
0.37	0.70	0.40

Fig. A.10: TET distribution of H-O-SE-H

B. Data of IEEE 14-Bus Test Power System

Note: If not specified, all data in per unit are calculated on the basis of power rating of 100MVA.

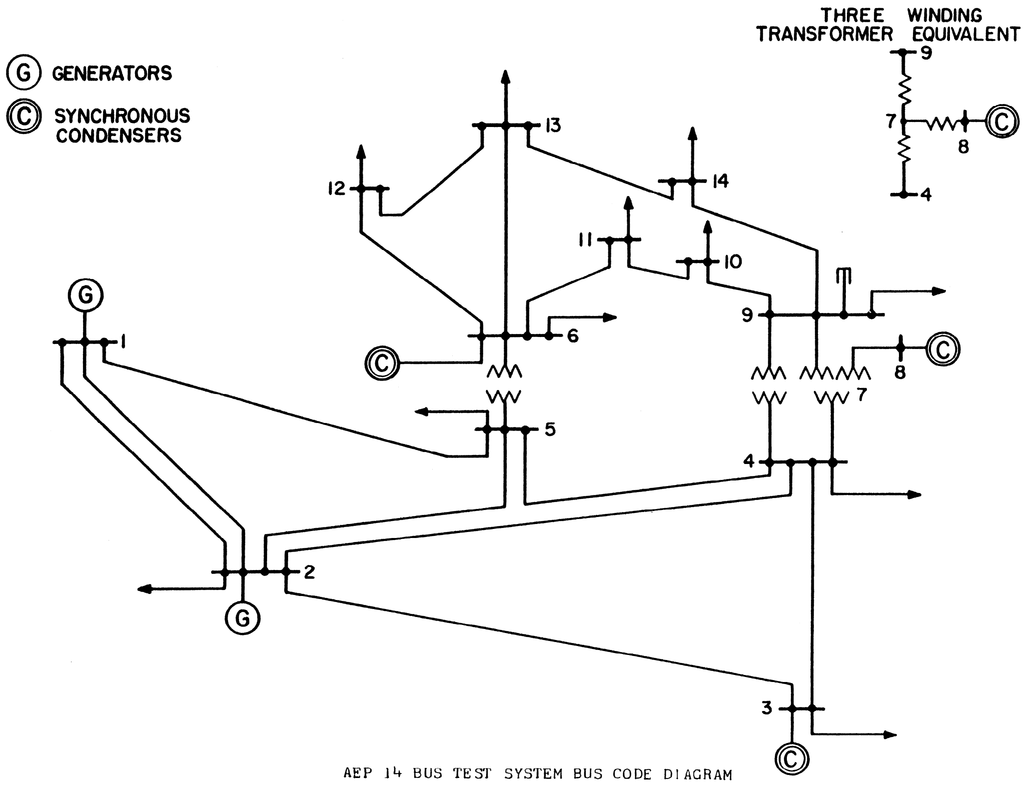

Fig. B.1: Single-line diagram of IEEE 14-bus test system

Table B.1: Bus configuration of IEEE 14-bus system

Bus#	Voltage	Angle	P_G	Q_G	P_L	Q_L	Type
1	1.060	0	2.324	-0.169	0	0	Slack
2	1.045	0	0.400	0.424	0.217	0.127	PV
3	1.010	0	0	0.234	0.942	0.190	PV
4	1.019	0	0	0	0.478	-0.039	PQ
5	1.020	0	0	0	0.076	0.016	PQ
6	1.070	0	0	0.122	0.112	0.075	PV

7	1.062	0	0	0	0	0	PQ
8	1.090	0	0	0.174	0	0	PV
9	1.056	0	0	0	0.295	0.166	PQ
10	1.051	0	0	0	0.090	0.058	PQ
11	1.057	0	0	0	0.035	0.018	PQ
12	1.055	0	0	0	0.061	0.016	PQ
13	1.050	0	0	0	0.135	0.058	PQ
14	1.036	0	0	0	0.149	0.050	PQ

Table B.2: Line configuration of IEEE 14-bus system

From Bus#	To Bus#	R	X	B/2	Tap ratio
1	2	0.01938	0.05917	0.0264	1
1	5	0.05403	0.22304	0.0246	1
2	3	0.04699	0.19797	0.0219	1
2	4	0.05811	0.17632	0.0170	1
2	5	0.05695	0.17388	0.0173	1
3	4	0.06701	0.17103	0.0064	1
4	5	0.01335	0.04211	0	1
4	7	0	0.20912	0	0.978
4	9	0	0.55618	0	0.969
5	6	0	0.25202	0	0.932
6	11	0.09498	0.19890	0	1
6	12	0.12291	0.25581	0	1
6	13	0.06615	0.13027	0	1
7	8	0	0.17615	0	1
7	9	0	0.11001	0	1
9	10	0.03181	0.08450	0	1

9	14	0.12711	0.27038	0	1
10	11	0.08205	0.19207	0	1
12	13	0.22092	0.19988	0	1
13	14	0.17093	0.34802	0	1

C. Data of IEEE 30-Bus Test Power System

Note: If not specified, all data in per unit are calculated on the basis of power rating of 100MVA.

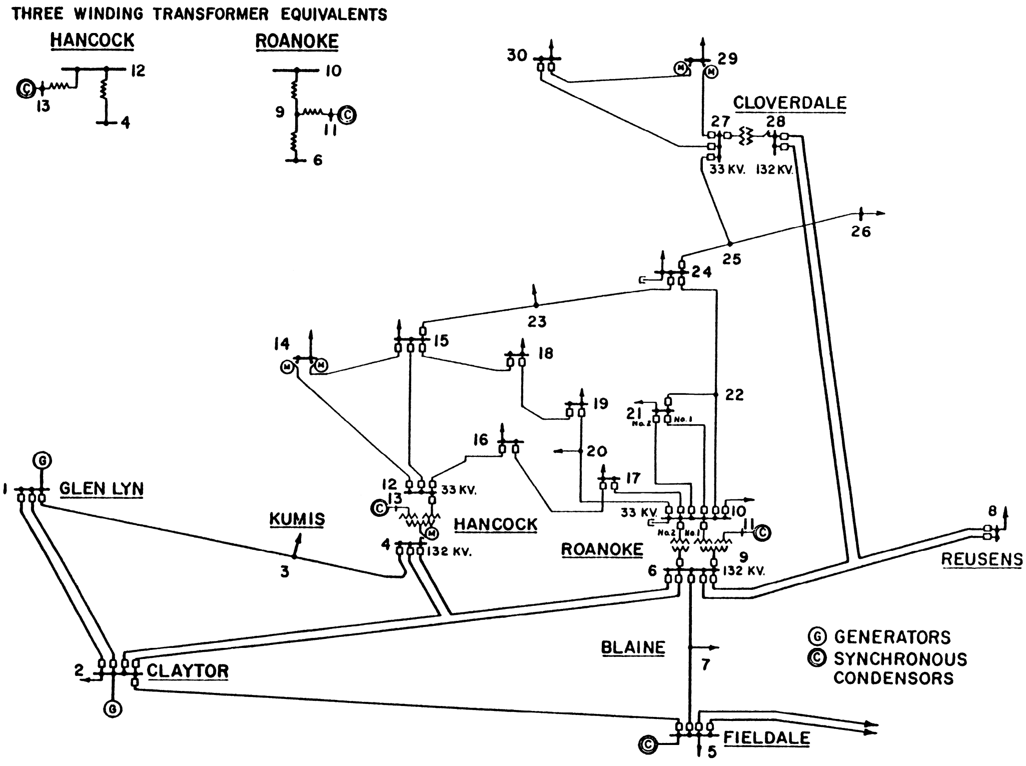

Fig. C.1: Single-line diagram of IEEE 30-bus test system

Table C.1: Bus configuration of IEEE 30-bus system

Bus#	Voltage	Angle	P_G	Q_G	P_L	Q_L	Type
1	1.060	0	2.602	-0.161	0	0	Slack
2	1.043	0	0.400	0.500	0.217	0.127	PV
3	1.021	0	0	0	0.024	0.012	PQ
4	1.012	0	0	0	0.076	0.016	PQ
5	1.010	0	0	0.370	0.942	0.190	PV
6	1.010	0	0	0	0	0	PQ
7	1.002	0	0	0	0.228	0.109	PQ

8	1.010	0	0	0.373	0.300	0.300	PV
9	1.051	0	0	0	0	0	PQ
10	1.045	0	0	0	0.058	0.020	PQ
11	1.082	0	0	0.162	0	0	PV
12	1.057	0	0	0	0.112	0.075	PQ
13	1.071	0	0	0.106	0	0	PV
14	1.042	0	0	0	0.062	0.016	PQ
15	1.038	0	0	0	0.082	0.025	PQ
16	1.045	0	0	0	0.035	0.018	PQ
17	1.040	0	0	0	0.090	0.058	PQ
18	1.028	0	0	0	0.032	0.009	PQ
19	1.026	0	0	0	0.095	0.034	PQ
20	1.030	0	0	0	0.022	0.007	PQ
21	1.033	0	0	0	0.175	0.112	PQ
22	1.033	0	0	0	0	0	PQ
23	1.027	0	0	0	0.032	0.016	PQ
24	1.021	0	0	0	0.087	0.067	PQ
25	1.017	0	0	0	0	0	PQ
26	1	0	0	0	0.035	0.023	PQ
27	1.023	0	0	0	0	0	PQ
28	1.007	0	0	0	0	0	PQ
29	1.003	0	0	0	0.024	0.009	PQ
30	0.992	0	0	0	0.106	0.019	PQ

Table C.2: Line configuration of IEEE 30-bus system

From Bus#	To Bus#	R	X	B/2	Tap ratio
1	2	0.0192	0.0575	0.0264	1

1	3	0.0452	0.1652	0.0204	1
2	4	0.0570	0.1737	0.0184	1
3	4	0.0132	0.0379	0.0042	1
2	5	0.0472	0.1983	0.0209	1
2	6	0.0581	0.1763	0.0187	1
4	6	0.0119	0.0414	0.0045	1
5	7	0.0460	0.1160	0.0102	1
6	7	0.0267	0.0820	0.0085	1
6	8	0.0120	0.0420	0.0045	1
6	9	0	0.2080	0	0.978
6	10	0	0.5560	0	0.969
9	11	0	0.2080	0	1
9	10	0	0.1100	0	1
4	12	0	0.2560	0	0.932
12	13	0	0.1400	0	1
12	14	0.1231	0.2559	0	1
12	15	0.0662	0.1304	0	1
12	16	0.0945	0.1987	0	1
14	15	0.2210	0.1997	0	1
16	17	0.0524	0.1923	0	1
15	18	0.1073	0.2185	0	1
18	19	0.0639	0.1292	0	1
19	20	0.0340	0.0680	0	1
10	20	0.0936	0.2090	0	1
10	17	0.0324	0.0845	0	1
10	21	0.0348	0.0749	0	1
10	22	0.0727	0.1499	0	1
21	22	0.0116	0.0236	0	1

15	23	0.1000	0.2020	0	1
22	24	0.1150	0.1790	0	1
23	24	0.1320	0.2700	0	1
24	25	0.1885	0.3292	0	1
25	26	0.2544	0.3800	0	1
25	27	0.1093	0.2087	0	1
28	27	0	0.3960	0	0.968
27	29	0.2198	0.4153	0	1
27	30	0.3202	0.6027	0	1
29	30	0.2399	0.4533	0	1
8	28	0.0636	0.2000	0.0214	1

D. Data of 32-Bus Radial Distribution System

Note: If not specified, all data in per unit are calculated on the basis of power rating of 1MVA.

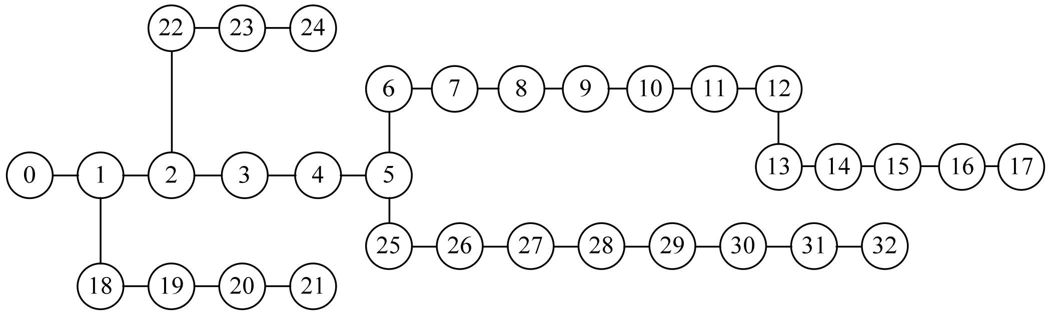

Fig. D.1: Single-line diagram of 32-bus radial distribution system

Table D.1: Bus configuration of 32-bus radial distribution system

Bus#	Voltage	Angle	P_G	Q_G	P_L	Q_L	Type
0	1.050	0	5.084	2.547	0	0	Slack
1	1	0	0	0	0.100	0.060	PQ
2	1	0	0	0	0.090	0.040	PQ
3	1	0	0	0	0.120	0.080	PQ
4	1	0	0	0	0.060	0.030	PQ
5	1	0	0	0	0.060	0.020	PQ
6	1	0	0	0	0.200	0.100	PQ
7	1	0	0	0	0.420	0.200	PQ
8	1	0	0	0	0.060	0.020	PQ
9	1	0	0	0	0.060	0.020	PQ
10	1	0	0	0	0.040	0.030	PQ
11	1	0	0	0	0.060	0.035	PQ
12	1	0	0	0	0.060	0.035	PQ
13	1	0	0	0	0.120	0.080	PQ

14	1	0	0	0	0.060	0.010	PQ
15	1	0	0	0	0.060	0.020	PQ
16	1	0	0	0	0.060	0.020	PQ
17	1	0	0	0	0.090	0.040	PQ
18	1	0	0	0	0.090	0.040	PQ
19	1	0	0	0	0.090	0.040	PQ
20	1	0	0	0	0.090	0.040	PQ
21	1	0	0	0	0.090	0.040	PQ
22	1	0	0	0	0.090	0.040	PQ
23	1	0	0	0	0.200	0.100	PQ
24	1	0	0	0	0.420	0.200	PQ
25	1	0	0	0	0.060	0.025	PQ
26	1	0	0	0	0.060	0.025	PQ
27	1	0	0	0	0.060	0.020	PQ
28	1	0	0	0	0.120	0.070	PQ
29	1	0	0	0	0.200	0.600	PQ
30	1	0	0	0	0.150	0.070	PQ
31	1	0	0	0	0.210	0.100	PQ
32	1	0	0	0	0.060	0.040	PQ

Table D.2: Line configuration of 32-bus radial distribution system

From Bus#	To Bus#	R	X	B/2	Tap ratio
0	1	0.000574	0.000293	0	1
1	2	0.003070	0.001564	0	1
2	3	0.002279	0.001161	0	1
3	4	0.002373	0.001209	0	1
4	5	0.005100	0.004402	0	1

5	6	0.001166	0.003853	0	1
6	7	0.004430	0.001464	0	1
7	8	0.006413	0.004608	0	1
8	9	0.006501	0.004608	0	1
9	10	0.001224	0.000405	0	1
10	11	0.002331	0.000771	0	1
11	12	0.009141	0.007192	0	1
12	13	0.003372	0.004439	0	1
13	14	0.003680	0.003275	0	1
14	15	0.004647	0.003394	0	1
15	16	0.008026	0.010716	0	1
16	17	0.004558	0.003574	0	1
1	18	0.001021	0.000974	0	1
18	19	0.009366	0.008440	0	1
19	20	0.002550	0.002979	0	1
20	21	0.004414	0.005836	0	1
2	22	0.002809	0.001920	0	1
22	23	0.005592	0.004415	0	1
23	24	0.005579	0.004366	0	1
5	25	0.001264	0.000644	0	1
25	26	0.001770	0.000901	0	1
26	27	0.006594	0.005814	0	1
27	28	0.005007	0.004362	0	1
28	29	0.003160	0.001610	0	1
29	30	0.006067	0.005996	0	1
30	31	0.001933	0.002253	0	1

Reference

[1] "The 2008 Living Planet Report", World Wide Fund for Nature (WWF), [Online]. Available: http://www.wwf.se/source.php/1199652/Living%20Planet%20Report%202008.pdf

[2] B. Obama and J. Biden, "New Energy for America" [Online]. Available: http://energy.gov/sites/prod/files/edg/media/Obama_New_Energy_0804.pdf

[3] "The China New Energy Vehicles Program", the World Bank, [Online]. Available: http://siteresources.worldbank.org/EXTNEWSCHINESE/Resources/3196537-1202098669693/EV_Report_en.pdf

[4] "Chinese New Energy Automotive Industry Development Report", the State Council, [Online]. Available: http://www.gov.cn/zwgk/2012-07/09/content_2179032.htm

[5] "National Transport Plan 2014–2023", Norwegian Ministry of Transport and Communications, [Online]. Available: https://www.regjeringen.no/contentassets/3fff99ead75f4f5e8bd751161006bffa/pdfs/stm201220130026000en_pdfs.pdf

[6] Q. Wu, *Grid Integration of Electric Vehicles in Open Electricity Markets*, Wiley, Jun. 2013.

[7] Y. Nie, C. Y. Chung and N. Z. Xu, “System state estimation considering EV penetration with unknown behavior using quasi-Newton method," *IEEE Trans. Power Syst.*, vol. 31, no. 6, pp. 4605-4615, Nov. 2016.

[8] K. Qian, C. Zhou, and M. Allan, “ Modeling of load demand due to EV battery charging in distribution systems," *IEEE Trans. Power Syst.*, vol. 26, no.

2, pp. 802-810, May 2011.

[9] K. Clement-Nyns, E. Haesen, and J. Driesen, " The impact of charging plug-in hybrid electric vehicles on a residential distribution grid," *IEEE Trans. Power Syst.*, vol. 25, no. 1, pp. 371-380, Feb. 2010.

[10] N. Z. Xu and C. Y. Chung, "Well-being analysis of generating systems considering electric vehicle charging," *IEEE Trans. Power Syst.*, vol. 29, no. 5, pp. 2311-2320, Sep. 2014.

[11] N. Z. Xu and C. Y. Chung, "Uncertainties of EV charging and effects on well-being analysis of generating systems," *IEEE Trans. Power Syst.*, vol. 30, no. 5, pp. 2547-2557, Sep. 2015.

[12] R. Vicini, O. Micheloud, H. Kumar and A. Kwasinski, "Transformer and home energy management systems to lessen electrical vehicle impact on the grid," *IET Gen., Transm., Distrib.*, vol. 6, iss. 12, pp. 1202-1208, Dec. 2012.

[13] P. Mitra and G. K. Venayagamoorthy, "Wide area control for improving stability of a power system with plug-in electric vehicles," *IET Gen., Transm., Distrib.*, vol. 4, iss. 10, pp. 1151-1163, Oct. 2010.

[14] H. Huang, C. Y. Chung and K. W. Chan, " Quasi-Monte Carlo based probabilistic small signal stability analysis for power systems with plug-in electric vehicle and wind power integration," *IEEE Trans. Power Syst.*, vol. 28, no. 3, pp. 3335-3343, Aug. 2013.

[15] P. Zhang, K. Qian, and C. Zhou, " A methodology for optimization of power systems demand due to electric vehicle charging load," *IEEE Trans. Power Syst.*, vol. 27, no. 3, pp. 1628-1636, Aug. 2012.

[16] A. Rautiainen, S. Repo and P. Jarventausta, " Statistical charging load modeling of PHEVs in electricity distribution networks using National Travel Survey Data," *IEEE Trans. Smart Grid*, vol. 3, no. 4, pp. 1650-1659, Dec. 2012.

[17] S. Acha, K. H. van Dam, and N. Shah, "Modelling spatial and temporal agent travel patterns for optimal charging of electric vehicles in low carbon

networks." *Power and Energy Society General Meeting*, 2012 IEEE

[18] P. Grahn, K. Alvehag and L. Söder, "PHEV utilization model considering type-of-trip and recharging flexibility," *IEEE Trans. Smart Grid*, vol. 5, no. 1, pp. 139-148, Jan. 2014.

[19] L. Zhao, P. Awater and A. Schafer, "Scenario-based evaluation on the impacts of electric vehicle on the municipal energy supply systems," *Power and Energy Society General Meeting*, 2011 IEEE

[20] "2009 National Household Travel Survey," Department of Transportation. [online]. Available: http://nhts.ornl.gov/, Apr. 9, 2009, USA

[21] D. Wu, D. C. Aliprantis and K. Gkritza, "Electric energy and power consumption by light-duty plug-in electric vehicles," *IEEE Trans. Power Syst.*, vol. 26, no. 2, pp. 738-746, May 2011.

[22] M. A. Ortega-Vazquez, F. Bouffard and V. Silva, "Electric vehicle aggregator/system operator coordination for charging scheduling and services procurement," *IEEE Trans. Power Syst.*, vol. 28, no. 2, pp. 738-746, May 2013.

[23] A. Abur and A. G. Expósito, *Power System State Estimation: Theory and Implementation*, CRC Press, Mar. 2004.

[24] F. C. Schweppe and J. Wildes, "Power system static-state estimation, part I: exact model," *IEEE Trans. Power App. Syst.*, vol. PAS-89, no. 1, pp. 120-125, Jan. 1970.

[25] S. Chakrabarti and E. Kyriakides, "PMU measurement uncertainty considerations in WLS state estimation," *IEEE Trans. Power Syst.*, vol. 24, no. 2, pp. 1062-1071, May 2009.

[26] P. Yang, Z. Tan and A. Wiesel, "Power system state estimation using PMUs with imperfect synchronization," *IEEE Trans. Power Syst.*, vol. 28, no. 4, pp. 4162-4172, Nov. 2013.

[27] C. Rakpenthai, S. Uatrongjit and S. Premrudeepreechacharn, "State estimation of power system considering network parameter uncertainty based on parametric interval linear systems," *IEEE Trans. Power Syst.*, vol. 27, no. 1,

pp. 305-313, Feb. 2012.

[28] E. Manitsas, R. Singh and B. C. Pal, “Distribution system state Estimation using an artificial neural network approach for pseudo measurement modeling,” *IEEE Trans. Power Syst.*, vol. 27, no. 4, pp. 1888-1896, Nov. 2012.

[29] R. Singh, B. C. Pal and R. A. Jabr, “Distribution system state estimation through Gaussian mixture model of the load as pseudo-measurement,” *IET Gen., Transm., Distrib.,* vol. 4, iss. 1, pp. 50-59, Jan. 2010.

[30] R. Singh, B. C. Pal and R. B. Vinter, “Measurement placement in distribution system state estimation,” *IEEE Trans. Power Syst.*, vol. 24, no. 2, pp. 668-675, May 2009.

[31] R. A. M. van Amerongen, “On convergence analysis and convergence enhancement of power system least-squares state estimators,” *IEEE Trans. Power Syst*., vol. 10, no. 4, pp. 2038-2044, Nov. 1995.

[32] E. Ghahremani and I. Kamwa, “Dynamic state estimation in power system by applying the extended Kalman filter with unknown inputs to phasor measurements,” *IEEE Trans. Power Syst*., vol. 26, no. 4, pp. 2556-2566, Nov. 2011.

[33] C. Gu and P. Jirutitijaroen, “Dynamic state estimation under communication failure using Kriging based bus load forecasting,” *IEEE Trans. Power Syst.*, vol. 30, no. 6, pp. 2831-2840, Nov. 2015.

[34] Jeu-Min Lin, Shyh-Jier Huang and Kuang-Rong Shih, “Application of sliding surface-enhanced fuzzy control for dynamic state estimation of a power system,” *IEEE Trans. Power Syst.*, vol. 18, no. 2, pp. 570-577, May 2003.

[35] L. Hu, Z. Wang, I. Rahman and X. Liu, “A constrained optimization approach to dynamic state estimation for power systems including PMU and missing measurements," *IEEE Trans. Control Syst. Technol.*, vol. 24, no. 2, pp. 703-710, Mar. 2016.

[36] M. Yazdanian, A. M.-S. and M. Mojiri, “Estimation of electromechanical oscillation parameters using an extended kalman filter," *IEEE Trans. Power*

Syst., vol. 30, no. 6, pp. 2994-3002, Nov. 2015.

[37] E. Ghahremani and I. Kamwa, “Local and wide-area PMU-based decentralized dynamic state estimation in multi-machine power systems," *IEEE Trans. Power Syst.*, vol. 31, no. 1, pp. 547-562, Jan. 2016.

[38] A. K. Singh and B. C. Pal, “Decentralized dynamic state estimation in power systems using unscented transformation,” *IEEE Trans. Power Syst.*, vol. 29, no. 2, pp. 794-804, Mar. 2014.

[39] S. Wang, W. Gao and A. P. S. Meliopoulos, “An alternative method for power system dynamic state estimation based on unscented transform,” *IEEE Trans. Power Syst.*, vol. 27, no. 2, pp. 942-950, May 2012.

[40] G. Valverde and V. Terzija, “Unscented kalman filter for power system dynamic state estimation,” *IET Gen., Transm., Distrib.*, vol. 5, iss. 1, pp. 29-37, Jan. 2011.

[41] A. Rouhani and A. Abur, “Real-Time Dynamic Parameter Estimation for an Exponential Dynamic Load Model," *IEEE Trans. Power Syst.*, vol. 7, no. 3, pp. 1530-1536, May 2016.

[42] G. Anagnostou and B. C. Pal, “Impact of overexcitation limiters on the power system stability margin under stressed conditions," *IEEE Trans. Power Syst.*, vol. 31, no. 3, pp. 547-562, May 2016.

[43] K. Hua, Y. Mishra and G. Ledwich, “Fast unscented transformation-based transient stability margin estimation incorporating uncertainty of wind generation," *IEEE Trans. Sustain. Energy*, vol. 6, no. 4, pp. 1254-1262, Oct. 2015.

[44] M. O. Buygi, G. Balzer, H. M. Shanechi and M. Shahidehpour, “Market-based transmission expansion planning,” *IEEE Trans. Power Syst.*, vol. 19, no. 4, pp. 2060-2067, Nov. 2004.

[45] G. B. Shrestha and P. A. J. Fonseka, “Congestion-driven transmission expansion in competitive power markets,” *IEEE Trans. Power Syst.*, vol. 19, no. 3, pp. 1658-1665, Aug. 2004.

[46] P. Maghouli, H. S. Hosseini, M. O. Buygi and M. Shahidehpour, “A Multi-objective framework for transmission expansion planning in deregulated environments,” *IEEE Trans. Power Syst.*, vol. 24, no. 2, pp. 1051-1061, May 2009.

[47] I. de J Silva, M. J. Rider, R. Romero, A. V. Garcia and C. A. Murari, “Transmission network expansion planning with security constraints,” *IEE Proc.-Gen., Transm., Distrib.*, vol. 152, iss. 6, pp. 828-836, Nov. 2005.

[48] B. Zeng, J. Zhang, X. Yang, J. Wang, J. Dong and Y. Zhang, “Integrated planning for transition to low-carbon distribution system with renewable energy generation and demand response," *IEEE Trans. Power Syst.*, vol. 29, no. 3, pp. 1153-1165, May 2014.

[49] V. Miranda, J. V. Ranito and L. M. Proenca, “Genetic algorithms in optimal multistage distribution network planning," *IEEE Trans. Power Syst.*, vol. 9, no. 4, pp. 1927-1933, Nov. 1994.

[50] M. Lavorato, M. J. Rider, A. V. Garcia and R. Romero, “A Constructive heuristic algorithm for distribution system planning," *IEEE Trans. Power Syst.*, vol. 25, no. 3, pp. 1734-1742, Aug. 2010.

[51] W. El-Khattam, Y. Hegazy and M. Salama, “An integrated distributed generation optimization model for distribution system planning," *IEEE Trans. Power Syst.*, vol. 20, no. 2, pp. 1158-1165, May 2005.

[52] K. Zou, A. P. Agalgaonkar, K. M. Muttaqi and S. Perera, “Distribution system planning with incorporating DG reactive capability and system uncertainties," *IEEE Trans. Sustain. Energy*, vol. 3, no. 1, pp. 112-123, Jan. 2012.

[53] A. S. Bin Humayd and K. Bhattacharya, “Comprehensive multi-year distribution system planning using back-propagation approach,” *IET Gen., Transm., Distrib.*, vol. 7, iss. 12, pp. 1415-1425, Dec. 2013.

[54] Z. Liu, F. Wen and G. Ledwich, “Optimal siting and sizing of distributed generators in distribution systems considering uncertainties," *IEEE Trans. Power Del.*, vol. 26, no. 4, pp. 2541-2551, Oct. 2011.

[55] P. S. Georgilakis and N. D. Hatziargyriou, “Optimal distributed generation placement in power distribution networks: models, methods, and future research," *IEEE Trans. Power Syst.*, vol. 28, no. 3, pp. 3420-3428, Aug. 2013.

[56] V. A. Evangelopoulos and P. S. Georgilakis, “Optimal distributed generation placement under uncertainties based on point estimate method embedded genetic algorithm,” *IET Gen., Transm., Distrib.*, vol. 8, iss. 3, pp. 389-400, Mar. 2014.

[57] A. Khodaei, S. Bahramirad and M. Shahidehpour, “Microgrid planning under uncertainty," *IEEE Trans. Power Syst.*, vol. 30, no. 5, pp. 2417-2425, Sep. 2015.

[58] E. Veldman and R. A. Verzijlbergh, “Distribution grid impacts of smart electric vehicle charging from different perspectives," *IEEE Trans. Smart Grid*, vol. 6, no. 1, pp. 333-342, Jan. 2015.

[59] I. Ziari, G. Ledwich, A. Ghosh and G. Platt, “Integrated Distribution Systems Planning to Improve Reliability Under Load Growth," *IEEE Trans. Power Del.*, vol. 27, no. 2, pp. 757-765, May 2012.

[60] D. T.-C. Wang, L. F. Ochoa and G. P. Harrison, “Modified GA and Data Envelopment Analysis for Multistage Distribution Network Expansion Planning Under Uncertainty," *IEEE Trans. Power Syst.*, vol. 26, no. 2, pp. 897-904, May 2011.

[61] W. Yao, J. Zhao, F. Wen, Z. Dong, Y. Xue, Y. Xu and K. Meng, “A multi-objective collaborative planning strategy for integrated power distribution and electric vehicle charging systems," *IEEE Trans. Power Syst.*, vol. 29, no. 4, pp. 1811-1821, Jul. 2014.

[62] Y. Zheng, Z. Y. Dong, Y. Xu, K. Meng, J. H. Zhao and J. Qiu, “Electric vehicle battery charging/swap stations in distribution systems: Comparison Study and Optimal Planning," *IEEE Trans. Power Syst.*, vol. 29, no. 1, pp. 221-229, Jan. 2014.

[63] Z. Liu, F. Wen and G. Ledwich, “Optimal planning of electric-vehicle charg-

ing stations in distribution systems," *IEEE Trans. Power Del.*, vol. 28, no. 1, pp. 102-110, Jan. 2013.

[64] Y. S. Lam, Y. W. Leung and X. Chu, “Electric vehicle charging station placement: formulation, complexity, and solutions," *IEEE Trans. Smart Grid*, vol. 5, no. 6, pp. 2846-2856, Nov. 2014.

[65] M. A. Rahman, Q. Duan and E. Al-Shaer, "Energy efficient navigation management for hybrid electric vehicles on highways," *Cyber-Physical Systems (ICCPS), 2013 ACM/IEEE International Conference*.

[66] H. Y. Mak, Y. Rong and Z. J. Shen, "Infrastructure planning for electric vehicles with battery swapping," *Management Science*, vol. 59, no. 7, pp. 1557-1575, Jul. 2013.

[67] Q. Dai, T. Cai, S. Duan and F. Zhao, “Stochastic modeling and forecasting of load demand for electric bus battery-swap station," *IEEE Trans. Power Del.*, vol. 29, no. 4, pp. 1909-1917, Aug. 2014.

[68] Q. Kang, J. Wang, M. Zhou and A. C. Ammari, “Centralized charging strategy and scheduling algorithm for electric vehicles under a battery swapping scenario," *IEEE Trans. Intell. Transp. Syst.*, vol. 17, no. 3, pp. 659-669, Mar. 2016.

[69] M. R. Sarker, H. Pandžić and M. A. Ortega-Vazquez, “Optimal operation and services scheduling for an electric vehicle battery swapping station," *IEEE Trans. Power Syst.*, vol. 30, no. 2, pp. 901-910, Mar. 2015.

[70] P. Xie, Y. Li, L. Zhu, D. Shi and X. Duan, “Supplementary automatic generation control using controllable energy storage in electric vehicle battery swapping stations,” *IET Gen., Transm., Distrib.*, vol. 10, iss. 4, pp. 1107-1116, Mar. 2016.

[71] B. Geng, J. K. Mills and D. Sun, “Two-stage charging strategy for plug-in electric vehicles at the residential transformer level," *IEEE Trans. Smart Grid*, vol. 4, no. 3, pp. 1442-1452, Sep. 2013.

[72] W. Yao, J. Zhao, F. Wen, Y. Xue and G. Ledwich, “A hierarchical decom-

position approach for coordinated dispatch of plug-in electric vehicles," *IEEE Trans. Power Syst.*, vol. 28, no. 3, pp. 2768-2778, Aug. 2013.

[73] C. T. Li, C. Ahn, H. Peng and J. Sun, “Synergistic control of plug-in vehicle charging and wind power scheduling," *IEEE Trans. Power Syst.*, vol. 28, no. 2, pp. 1113-1121, May 2013.

[74] T. Wu, Q. Yang, Z. Bao and W. Yan, “Coordinated energy dispatching in microgrid with wind power generation and plug-in electric vehicles," *IEEE Trans. Smart Grid*, vol. 4, no. 3, pp. 1453-1463, Sep. 2014.

[75] P. Richardson, D. Flynn and A. Keane, “Optimal charging of electric vehicles in low-voltage distribution systems," *IEEE Trans. Power Syst.*, vol. 27, no. 1, pp. 268-279, Feb. 2012.

[76] S. Y. Derakhshandeh, A. S. Masoum, S. Deilami, M. A. S. Masoum and M. E. Hamedani Golshan, “Coordination of generation scheduling with PEVs charging in industrial microgrids," *IEEE Trans. Power Syst.*, vol. 28, no. 3, pp. 3451-3461, Aug. 2013.

[77] N. Rotering and M. Ilic, “Optimal charge control of plug-in hybrid electric vehicles in deregulated electricity markets," *IEEE Trans. Power Syst.*, vol. 26, no. 3, pp. 1021-1029, Aug. 2011.

[78] N. Z. Xu and C. Y. Chung, “Reliability evaluation of distribution systems including vehicle-to-home and vehicle-to-grid," *IEEE Trans. Power Syst.*, vol. 31, no. 1, pp. 759-768, Jan. 2016.

[79] Y. He, B. Venkatesh and L. Guan, “Optimal scheduling for charging and discharging of electric vehicles," *IEEE Trans. Smart Grid*, vol. 3, no. 3, pp. 1095-1105, Sep. 2012.

[80] M. González Vayá and G. Andersson, “Optimal bidding strategy of a plug-in electric vehicle aggregator in day-ahead electricity markets under uncertainty," *IEEE Trans. Power Syst.*, vol. 30, no. 5, pp. 2375-2385, Sep. 2015.

[81] W. Yao, C. Y. Chung, F. Wen, M. Qin and Y. Xue, “Scenario-based comprehensive expansion planning for distribution systems considering integra-

tion of plug-in electric vehicles," *IEEE Trans. Power Syst.*, vol. 31, no. 1, pp. 317-328, Jan. 2016.

[82] Q. Cui, X. Wang, X. Wang and Y. Zhang, "Residential appliances direct load control in real-time using cooperative game," *IEEE Trans. Power Syst.*, vol. 31, no. 1, pp. 226-233, Jan. 2016.

[83] P. H. Nguyen, W. L. Kling and P. F. Ribeiro, "A game theory strategy to integrate distributed agent-based functions in smart grids," *IEEE Trans. Smart Grid*, vol. 4, no. 1, pp. 568-576, Mar. 2013.

[84] S. M. Mazhari, H. Monsef and R. Romero, "A multi-objective distribution system expansion planning incorporating customer choices on reliability," *IEEE Trans. Power Syst.*, vol. 31, no. 2, pp. 1330-1340, Mar. 2016.

[85] R. Billinton and W. Li, *Reliability Assessment of Electric Power Systems Using Monte Carlo Methods*. New York, NY, USA: Plenum, 1994.

[86] G. Tollefson, R. Billinton and G. Wacker, "Comprehensive bibliography on reliability worth and electrical service consumer interruption costs: 1980-90," *IEEE Trans. Power Syst.*, vol. 6, no. 4, pp. 1508-1514, Nov. 1991.

[87] K. L. Mak, K. K. Lai and W. C. Ng, "Analysis of optimal opportunistic replenishment policies for inventory systems by using a (s,S) model with a maximum issue quantity restriction," *European Journal of Operational Research*, pp. 385-405, Oct. 2005.

[88] G. Li and X. P. Zhang, "Modeling of plug-in hybrid electric vehicle charging demand in probabilistic power flow calculations," *IEEE Trans. Smart Grid*, vol. 3, no. 1, pp. 492-499, Mar. 2012.

[89] V. G. Kulkarni, " Discrete-time Markov Models," in *Modeling, Analysis, Design, and Control of Stochastic Systems*, Springer, May 1999, pp. 106-109

[90] A. Lojowska, D. Kurowicka and G. Papaefthymiou, "From transportation patterns to power demand: Stochastic modeling of uncontrolled domestic charging of electric vehicles," *Power and Energy Society General Meeting 2011*, San Diego, USA.

[91] SAE electric vehicle and plug-in hybrid electric vehicle conductive charge coupler, SAE Standard J1772, [online]. Available: http://standards.sae.org/j1772_201210/. Jan. 2010.

[92] M. Nejati, N. Amjady and H. Zareipour, “A new stochastic search technique combined with scenario approach for dynamic state estimation of power systems," *IEEE Trans. Power Syst.*, vol. 27, no. 4, pp. 2093-2105, Nov. 2012.

[93] R. Fletcher, “Unconstrained Optimization," in *Practical Methods of Optimization*, 2nd edition, Wiley, 1987.

[94] J. Nocedal and S. J. Wright, “Line Search Methods," in *Numerical Optimization*, 2nd edition, Springer, Jul. 2006.

[95] H. H. Zeineldin, Y. A.-R. I. Mohamed and V. Khadkikar, “A protection coordination index for evaluating distributed generation impacts on protection for meshed distribution systems," *IEEE Trans. Smart Grid*, vol. 4, no. 3, pp. 1523-1532, Sep. 2013.

[96] The New York Independent System Operator (NYISO). [online]. Available: http://www.nyiso.com/public/markets_operations/.

[97] L. Chen, C. Y. Chung, Y. Nie. “Modeling and optimization of electric vehicle charging load in a parking lot.” *The 5th IEEE PES Asia-Pacific Power and Energy Engineering Conference*, Hong Kong, Dec. 2013.

[98] D. S. Allen, "Aggregate dynamics of (S, s) inventory management," *Int. J. Production Economics*, vol. 59, no. 1-3, pp. 231-242, Mar. 1999.

[99] H. M. Yang, C. Y. Chung and J. H. Zhao, “Application of plug-in electric vehicles to frequency regulation based on distributed signal acquisition via limited communication”, *IEEE Trans. Power Syst.*, vol. 28, no. 2 , pp. 1017-1026, May 2013.

[100] M. E. Baran and F. F. Wu, “Network reconfiguration in distribution systems for loss reduction and load balancing," *IEEE Trans. Power Del.*, vol. 4, no. 2, pp. 1401-1407, Apr. 1989.

[101] "Residential Energy Consumption Survey," Energy Information Administration [online]. Available: http://www.eia.gov/consumption/residential/data/2009/, 2009, USA

[102] "Daily Day-Ahead LMP," PJM [online]. Available: http://www.pjm.com/markets-and-operations/energy/day-ahead/lmpda.aspx, USA

[103] R. Carter and A. Cruden, "Optimizing for efficiency or battery life in a battery/supercapacitor electric vehicle," *IEEE Trans. Veh. Technol.,* vol. 61, no. 4, pp. 1526-1533, May 2012.